İSTANBUL TECHNICAL UNIVERSITY ★ INSTITUTE OF SCIENCE AND TECHNOLOGY

ELECTROPOLYMERIZATION AND CHARACTERIZATION OF 1-(4-METHYLPHENYL)-1H-PYRROLE AND 2,2-DIMETHYL-3,4-PROPYLENEDIOXY THIOPHENE

M.Sc. Thesis by

Aslı GENÇTÜRK

Department : Polymer Science and Technology

Programme: Polymer Science and Technology

JANUARY 2007

İSTANBUL TECHNICAL UNIVERSITY ★ INSTITUTE OF SCIENCE AND TECHNOLOGY

ELECTROPOLYMERIZATION AND CHARACTERIZATION OF 1-(4-METHYLPHENYL)-1H-PYRROLE AND 2,2 DIMETHYL-3,4-PROPYLENEDIOXY THIOPHENE

M.Sc. Thesis by

Asli GENÇTÜRK

Date of submission : 25 December 2006

Date of defence examination: 29 January 2007

Supervisor (Chairman): Prof. Dr. A. Sezai SARAÇ

Members of the Examining Committee Assoc. Prof. Dr. Esma SEZER (İ.T.Ü.)

Assoc. Prof. Dr. Yücel ŞAHİN (A.Ü.)

JANUARY 2007

İSTANBUL TEKNİK ÜNİVERSİTESİ ★ FEN BİLİMLERİ ENSTİTÜSÜ

1-4-METİLFENİL-1H-PİROL VE 2,2-DİMETİL-3,4-PROPİLENDİOKSİTİYOFEN' NİN ELEKTROPOLİMERİZASYONU VE KARAKTERİZASYONU

YÜKSEK LİSANS TEZİ

Aslı GENÇTÜRK

Tezin Enstitüye Verildiği Tarih : 25 Aralık 2006
Tezin Savunulduğu Tarih : 29 Ocak 2007

Tez Danışmanı : Prof.Dr. A. Sezai SARAÇ
Diğer Jüri Üyeleri Doç.Dr. Esma SEZER (İ.T.Ü.)
Doç.Dr. Yücel ŞAHİN (A.Ü.)

OCAK 2007

ACKNOWLEDGEMENT

Firstly, I would like to thank my advisor, Prof.Dr. A Sezai SARAÇ, for his encouragement, guidance and discussions in my studies.

I would like to express my grateful and sincerest thanks to Dr. Fevzi Çakmak CEBECİ for his common sense, patience, understanding, and boundless, enthusiasm advices.

I would like to thank Assoc.Prof.Dr. Esma SEZER, Assoc.Prof.Dr. Belkıs USTAMEHMETOĞLU and Dr. Elif Altürk PARLAK for their guidance and advices

I like to thank to my friends Ece AYAZ, Koray YILMAZ, Kerim ÇOBAN, Leyla BAYKAL, Bilge KILIÇ, Sibel SEZGİN and Hülya GEYİK for their support, encouragement and friendship.

I would like to thank to my friends Günay ONUŞ, Gülşah ENGİN, Elif KILIÇ and Gökhan ATALIK for moral support and their patience.

I thank my brother Cem GENÇTÜRK for his special helps during my thesis.

Finally, I would like to thank to my parents to being always with me and supporting my idea.

January 2007 Aslı GENÇTÜRK

TABLE OF CONTENTS

ABBREVIATION

AC : Alternating Current
ATR-FTIR : Attenuated Total Reflectance Fourier Transform Infrared
ACN : Acetonitrile
CP : Conducting Polymer
CV : Cyclic Voltammetry
CF : Carbon Fibre
CFME : Carbon Fibre Microelectrode
CPE : Constant Phase Element
DC : Direct Current
DCM : Dichloromethane
EIS : Electrochemical İmpedance Spectroscopy
EDOT : Ethylenedioxythiophene
FE_SEM : Field Emmision Scannin Electron Microscopy
HOMO : Highly Oriented Molecular Orbitals
IHP : Inner Helmholtz Plane
IRE : İnternal Reflectance Element
ITO : İndium Tin Oxide
MO : Molecular Orbital
PA : Polyacetylene
PPS : Poly(phenylenesulfide)
PEDOT : Poly(3,4-ethylenedioxythiophene)
PAN : Polyacrylonitrile
PEDOT : Poly(3,4-ethylenedioxthiophene)
SEM : Scanning Electron Microscope

LIST OF SYMBOLE

C_1	: Capacitance
C_{dl}	: Double Layer Capacitance
E_g	: Band Gap
E_{eq}	: Equivalant Potential
$E_{1/2}$	: Half wave potential
Q_{dep}	: Deposition Charge
R_p	: Polarization Resistor

LIST OF TABLES

LIST OF FIGURES

ELECTROPOLYMERIZATION and CHARACTERIZATION OF 1-4-METHYLPHENYL-1H-PYRROLE and 2,2-DIMETHYLPROPYLENEDIOXY THIOPHENE

SUMMARY

In 1976, Alan MacDiarmid, Hideki Shirakawa, with a talented group of graduate students and postdoctoral researchers, discovered conducting polymers. Since that discovery, a vast array of other CPs have been synthesized. Electrical conductivity is achieved in the film of conducting polymer by oxidation (p-doping) or reduction (n-doping), followed respectively by the insertion of anionic or cationic species. Due to the double bond alternation in the conjugated polymer backbone, the charged species formed upon doping are able to move along the carbon chain (delocalization) allowing electron transport and thus giving an electronically conductive materials.

Conducting polymers can be prepared via chemical or electrochemical polymerization. Films of electronically conducting polymers are generally obtained onto a support electrode surface by anodic oxidation (electropolymerization) of the corresponding monomer in the presence of an electrolyte solution. The preparation, characterization and application of electrochemically active conducting polymers are stil in the forefront of research activity in electrochemistry.

Carbon fibers have a novel structure, a narrow distribution size, highly accessible surface area, low resistivity, and high stability. Porous carbon is the most frequently selected electrode material which offer large large surface area and very well polarization due to porosity which makes porous carbon is the one of the most promising electrode material for supercapacitor application. CFME shows superior performance in cyclovoltammetric studies due to its micron size cylindrical structure, and its disposable character having a new surface area at each time rather than cleaning the electrode surface which is necessary for Pt or Au electrodes. Generally electrocoating of conjugated polymers on carbon fiber easily allow the characterization of the deposited films by spectroscopic, morphological and electrochemical techniques [36-40]. The comparison of different polymers coated under identical electrochemical conditions gives reliable information [41-44] for the evaluation of the materials in terms of application.

Polypyrrole has been the materials an many investigations. Functional conjugated, PPy and PTh, in which the electronic properties inherent to the π-conjugated systems are associated with new specific properties afforded by covalently attached functional groups, have been the focus of considerable attention during the past decade. Polypyrrole has high mechanical and chemical stability and can be produced continuously as flexible film (thickness 80 μm; trade name: Lutamer, BASF) by electrochemical techniques.

As a class of conducting and electroactive polymers that can exhibit high and quite stable conductivities, a high degree of optical transparency as a conductor, and the ability to be rapidly switched between conducting doped and insulating neutral states, poly (3,4- alkylenedioxythiophene)s (PXDOTs), have attracted attention across academia and industry. Due to their ability to be functionalized at the 2-position of the propylene bridge, ProDOT (Pro=1,3-propylene) monomers and polymers have gained special interest as the polymers that form are regio-symmetric. By increasing the ring size from dioxane (six-membered) to the seven-memnered ring in ProDOT, little change is seen in the electropolymerization and switching behavior of PProDOT relative to PEDOT.

PProDOT-Me_2 is a specific poly(3,4-alkylenedioxythiophene) derivative [53] exhibiting excellent electrochromic properties [54-56] i.e. high contrast ratio, high coloration efficiency, long-term cyclability, and very fast switching speed. It was concluded [57] that the open morphology of the polymer arising from the highly substituted propylene bridge is responsible for facilitated ion movement throughout the whole volume of the material leading to fast doping and dedoping.

The quality of the polymers is greatly influenced by many factors, e.g. impurities, electrode material, pressure, concentrations, temperature, and comonomers. The most decisive, however, are the current density and the electrolyte, particularly the conducting anion X^- because it is incorporated into the polymer as a counterion. [75] By changing reaction conditions, polymers with different surface morphologies, (e.g., an open porous structure) can be obtained

In this study, MPP and ProDOT-Me_2 monomers polymerized with a cyclic voltametry, their characterizarion, spectroelectrochemistry and EIS were investigated.

Electropolymerization was performed on the CFMEs by cyclic voltammetry at a scan rate of at 1.4 V for the monomer using 10 cycles in 0.1 M Bu_4NBF_4/DCM, 0.1 M Bu_4NBF_4/ACN, Bu_4NBF_4/PC, and Bu_4NBF_4/DMF. A thin coating on the CFME was obtained for the 5th cycle, when comparing uncoated and coated fiber (after 5 cycles and 40 cycles) longitudinal striations of carbon fiber can still be seen. But after 40 cycle carbon fiber more than 5 cycles covered with polymer.

Electropolymerization process was performed in 0.1M Bu_4NPF_6 in ACN at various scan rates, cycle numbers and monomer concentration. ACN was chosen as a standard solvent to prepare electrolyte for ProDOT-$(Me)_2$ during this study.

Spectroelectrochemistry of PProDOT-Me_2 film was studied on the potentiodynamically deposited ITO-coated glass slides. Spectroelectrochemistry of PProDOT-Me_2 studies indicate that dark blue color in the reduced form observed at -600 mV and light blue color seen in the oxidized form at 1200 mV. At an applied potential of -600mV, the polymer is in its fully neutral form.

Electrochemical Impedance Spectroscopy (EIS) measurements were performed at open circuit potential in the range of 100 kHz-10 mHz (application of amplitude of 10 mV) for PProDOT$(Me)_2$ electrochemically obtained at different charges (cycles), and at different applied potentials in the range of -0.1 V to 1.3 V with a potential step of 0.1V in parallel to cyclic voltammogram of the PProDOT-Me_2 in monomer free

electrolyte solution where stability of the film exhibit electroactivity without undergoing deformation.

The shape of the plot has a very good agreement with the corresponding CV of the polymer film in monomer free solution. The low capacitance values increase in low potentials, at 0.4 V capacitance values shows a maximum point which converge very well at this potential observed in CV of the ProDOT-Me_2 film for 100 mV/s.

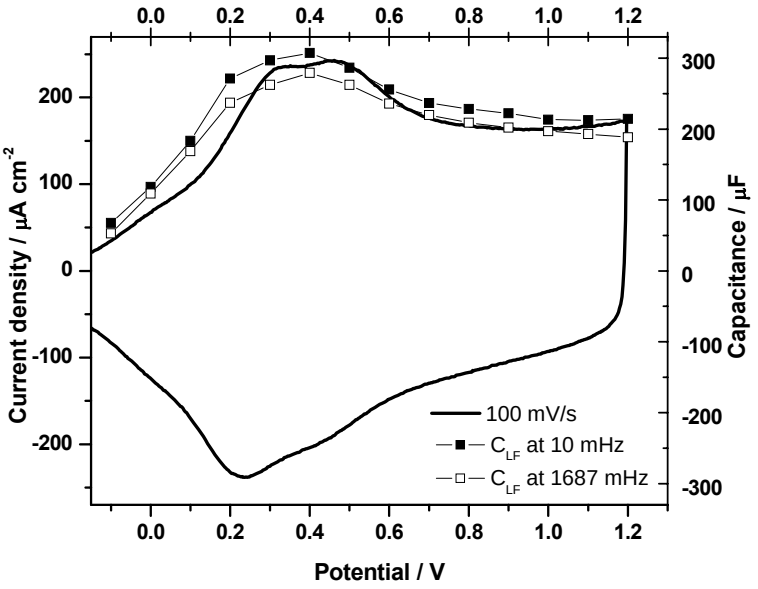

The electrochemical parameters of the CFME/PProDOT-Me_2/Electroyte system were evaluated by employing the ZSimpWin (version 3.10) software from Princeton Applied Research. Two different equivalent electrical circuit model and variation of the solution resistance, double layer capacitance and low frequency capacitance of the PProDOT-Me_2 film, variation of low frequency capacitance values in different electrolyte that solvent was ACN, in different solvents that electrolyte was 0.1 M Bu_4NPF_6 of PProDOT-Me_2 film were investigated in this study.

Morphology of coatings for different applied charge densities and different applied scan rates were studied. The SEM pictures show a pronounced difference in the surface morphology of the two type of different PProDOT-$(Me)_2$ layers. In the beginning, after very thin film formation on CFME, where striations disappear on the whole surface area, at low electropolymerization scan rates coated polymeric layer shows a polymer network with a highly porous structure which might entrap dopant ions.

1-4-METİLFENİL-1H-PYRROLE VE 2,2-DİMETİLPROPİLEN DİOKSİTİYOFEN'NİN ELEKTROPOLİMERİZASYONU VE KARAKTERİZASYONU

ÖZET

1976 da Alan MacDiarmid, Hideki Shirakawa ve bir grup araştırmacı iletken polimerleri keşfetti. Bu keşiften sonra diğer iletken polimerlerin sentezi araştırmacılar tarafından büyük ilgi uyandırmıştır. İletken polimer filmlerde elektriksel iletkenlik anyonik ve katyonik türlerin yüklenmiş olarak yapıya girmesini takip eden yükseltgenme (p-katkılandırma) ve indirgenme (n-katkılandurma) yolu ile gerçekleşmektedir. Konjuge polimerlerin omurgasında çift bağların değişmesi ile katkılandırmadan oluşan yüklenmiş türler yardımıyla karbon zinciri boyunca elektronun taşınması, malzemeye iletkenlik kazandırır.

İletken polimerler kimyasal ve elektrokimyasal olarak oluşturulur.Elektriksel olarak iletken polimerler elektrolit çözeltisi varlığında var olan monomerin anodik yükseltgenmesi (elektrokaplama) ile bir destek elektrot yüzeyinde elde edilir. Elektrokimyasal aktif iletken polimerlerin uygulamaları, hazırlanması ve karakterizasyonu elektrokimyada önemli yer tutmaktadır.

Karbon fiber dar dağılım büyüklüğü, yüksek girilebilir yüzey alanı, düşük dirençlilik, yüksek kararlılık ile mükemmel bir yapıya sahiptir. Gözenekli yapıdaki karbon, geniş yüzey alanı ve iyi polarize olması nedeniyle süperkapasitör uygulamalarda umut vaat eden elektrot malzemelerdir. Karbon fiber mikro elektrot mikron büyüklüğünde silindirik yapısı ve yeni yüzey olması nedeniyle döngülü voltametrik uygulamalarda önem kazanmaktadır. Genelde konjuge polimerlerin karbon fiber mikro elektrot üzerine kaplanması kaplanan filmin spektroskopik, morfolojik ve elektrokimyasal teknikle karakterizasyonunu kolaylaştırır. Belirli elektrokimyasal durumda kaplanan farklı polimerler karşılaştırıldığında uygulama yönünden materyallerin özelliği hakkında bilgi verir.

Polipirol yüksek mekanik, kimyasal kararlılık ve elekrokimyasal teknikle devamlı olarak esnek film elde edilmesi nedeniyle pek çok araştrmada iyi bir maddedir. Fonksiyonellik monomerlere yeni özellikler kazandırmaktadır.

Yüksek ve kararlı iletkenlik sergileyen iletken ve elektroaktif polimerler sınıfına giren poli (3,4- alkilendioksitiyofen)s PXDOTs iletken madde olarak yüksek derecede optik şeffaflık, iletken katkılı ve yalıtkan nötür durum arasında hızlı gidip gelme yeteneği nedeniyle akademi ve endüstri alanında ilgi çekmiştir. Propilen köprüsünün 2 pozisyonundan fonksiyonlanmasının getirdiği özellikten dolayı ProDOT (Pro=1,3-propilen) monomeri ve polimeri özel bir ilgi çekmektedir. ProDOT için halka büyüklüğünün altı üyeliden yedi üyeliye artması

elektrokaplamada ve spektroelektrokimyada PEDOT polimerine göre küçük değişiklik gösterir.

Poli (3,4 alkilendioksitiyofen) türevi olan PProDOT özel elektrokromik özellik (yüksek kolorasyon uygunluğu ve hızkı renk değiştirme gibi) gösterir. Polimerin açık yapısı maddenin tüm hacmine doğru , hızlı katkılandırma ve geri katkılandırma iyon hareketi için cevap vermektedir.

Polimerin niteliği saflık, elektrot özelliği, basınç, konsantrasyon, ve komonomer gibi pekçok faktörden etkilenir. Özellikle akım yoğunluğu ve elektrolit (polimere karşıt iyon olarak giren iletken iyon X^-) önemli olanlardır.

Bu çalışmada MPP ve ProDOT-Me_2 monomerleri döngülü voltametri ile KFME üzerine kaplanmış, polimerlerin karakterizasyonu, spektroelektrokimyası ve elektriksel impedans özellikleri araştırılmıştır.

Elektrokaplama 1.4 V 'da, 50 mV s^{-1} tarama hızında 10 döngü ile 0.1 M Bu_4NBF_4/DCM, 0.1 M Bu_4NBF_4/ACN, Bu_4NBF_4/PC ve Bu_4NBF_4/DMF elektrolit çözeltisi içinde KFME üzerine döngülü voltametri ile kaplanmıştır. 5 ve 40 döngüden sonra KFME üzerinde elde edilen kaplama sonunda kaplanmamış KFME bölgeleri görülmektedir. Fakat 40 döngü sonunda 5 döngüye nazaran daha kalın kaplama elde edilmiştir.

ProDOT-$(Me)_2$ monomeri de 0.1M Bu_4NPF_6/ACN elektroliti içinde farklı tarama sayılarında ve hızlarında ayrıca farklı konsantrasyonda KFME üzerine kaplanmıştır Spektroelektrokimyasal ölçümler ProDOT-Me_2 monomerinin ITO kaplı cam kesit üzerinde potansiyodinamik olarak kaplanması sonucu oluşan film üzerinde yapılmıştır. PProDOT-Me_2 filmde indirgenmiş durumda (nötür durumda) koyu mavi ve oksitlenmiş durumda açık mavi renk gözlenmiştir.

Elektrokimyasal empedans ölçümleri 100kHz-10mHz aralığında açık devre potansiyelinde ve monomer içermeyen elektrolit ortamında döngülü voltametriye paralel olarak polimerin deformasyona uğramadan kararlılık gösterdiği aralıkta (0.1 V artan potansiyel aralıklarla -0.1 V'dan 1.3 V'a farklı potansiyellerde) potansiyel uygulayarak farklı tarama sayılarında elde edilen filmler için gerçekleştirilmiştir.

Grafiğin şekli filmin monomer içermeyen elektrolit ortamında ki döngülü voltametrisine benzer bir eğilim gösterir. Uygulanan potansiyelin artması ile düşük

kapasitans değerleri artar, 0.4 V da maksimum değere ulaşır ve yüksek potansiyeller

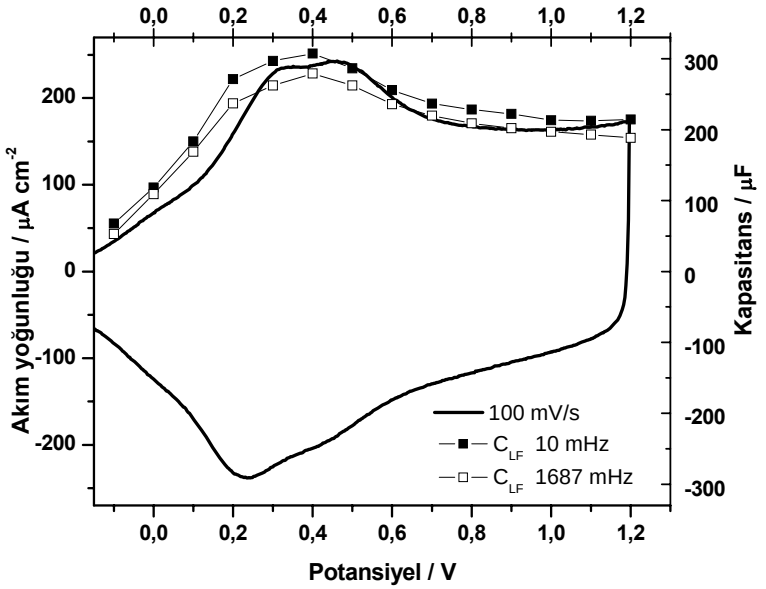

başlar.

KFME/PProDOT-Me_2/Elektrolit sisteminde elektrokimyasal parametreler Princeton Applied Research için uygulanan ZSimpWin (versiyon 3.10) yazılımında gerçekleştirildi. İki farklı eşdeğer devre modeli uygulanmıştır. PProDOT-Me_2 filmin çözelti direncinin çeşitliliği, çift tabaka kapasitans ve düşük frekans kapasitans değerleri farklı elektrolit çözeltilerinde, farklı çözücüler içinde hazırlanan elektrolit çözeltilerinde incelenmiştir.

Farklı tarama hızında ve sayısında kaplamanın görünümü SEM resimleri ile görülmektedir. KFME üzerinde ince film elde edildikten sonra, KFME yüzey alanındaki düz yapılar kaybolmuş ve bazı yüklerde gözenekli yapılar elde edilmiştir.

1 INTRODUCTION

1.1 Conducting Polymers

In 1976, Alan MacDiarmid, Hideki Shirakawa, with a talented group of graduate students and postdoctoral researchers [1], discovered conducting polymers and the ability to dope these polymers over the full range from insulator to metal. This was particulary exciting because it created a new field of research on the boundary between chemistry and condensed matter pyhsics. And because it created a number of opportunities:

- Conducting polymers opened the way to progress in understanding the fundamental chemistry and pyhsics of π-bond-ed macromolecules.

- Conducting polymers provided an opportunity to address questions that had been of fundamental interest to quantum chemistry for decades: Is there bond alternation in long chain polyenes? What is the relative importance of the electron-electron and the electron-lattice interactions in π-bonded macromolecules?

- Conducting polymers provided an opportunity to address fundamental issues of importance to condensed matter physics as well, including, for example, the metal-insulator transition as envisioned by Neville Mott and Philip Anderson and the instability of one-dimensional metals discovered by Rudolph Peierls (the “Peierls Instability”).

- Finally-and perhaps most importantly-conducting polymers offered the promise of achieving a new generation of polymers: materials that exhibit the electrical and optical properties of metals or semiconductors and that retain the attractive mechanical properties and processing advantages of polymers.[2]

Since that discovery, a vast array of other CP_s have been synthesized. The most common of these are shown below in scheme 1.1.

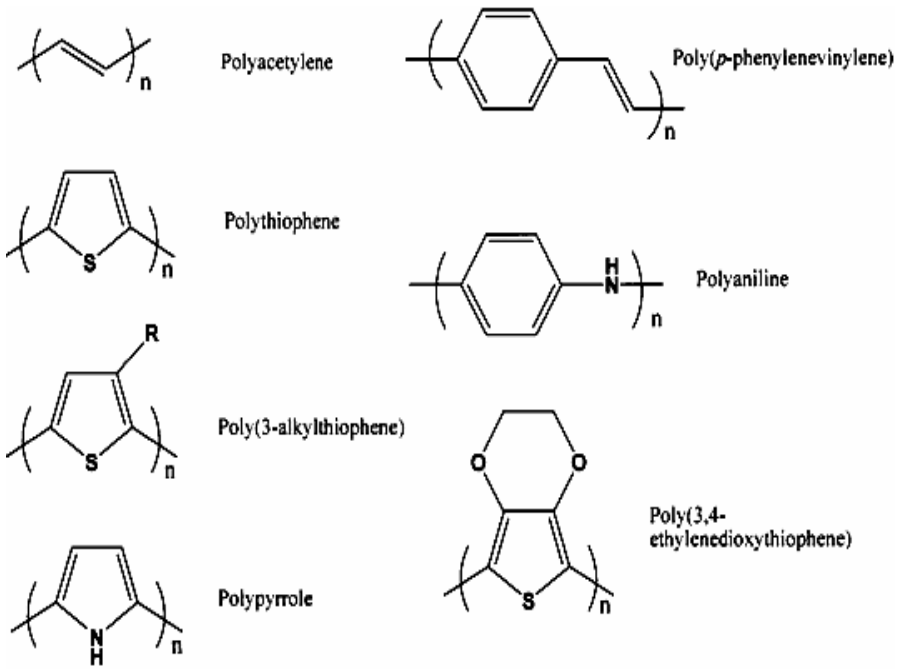

Figure 1.1: Molecular Structure of Several Conjugated Polymers.

All of these systems share one common stucturel feature, namely a rigid nature brought about by sp^2 carbon-based backbone. The utilization of the conjugated constructions affords polymer chains possessing extended π-systems, and it is this feature alone that separates CP_s from their other polymeric counterparts. Using this generic, lowest energy(fully bonding) molecular orbital (MO) represantation as shown by the π-systems model, the picture of primary concern that is generated by these networks consists of a number of π and π* levels (Figure 1.2)

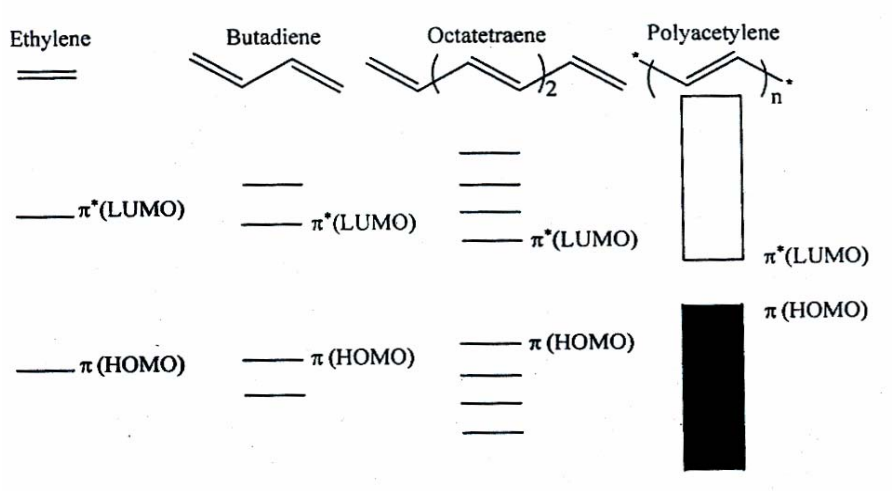

Figure 1.2: Molecular Orbital (MO) Diagram

The electrical properties of any material are a result of the material's electronic structure.The presumption that CP_s form bands through extensive molecular orbital overlap leads to the assumption that their electronic population are the chief determinants of whether or not a material is conductive. Here, materials are classified as one of three types shown in Figure 1.3, being metals, semiconductors, or insulators. Metals are material that possess partially-filled bands, and this characteristic is the key factor leading to the conductive nature of this class of materials. Semiconductors, on the other hand, have filled (valance bands) and unfilled (conduction bands) bands that are seperated by a range of forbidden energies (known as the "band gap"). The conduction band can be populated, at the expense of the valance band, by exciting electrons (thermally and/or photochemically) across this band gap. İnsulators possess a band structure similiar to semiconductors expect here the band gap is much larger and inaccessible under the environmental conditions employed.

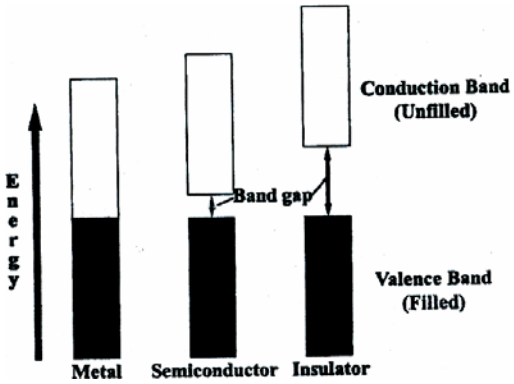

Figure 1.3: Classification of Materials, and Schematic of Valence and Conduction Bands and Band Gap

For electrical conductivity to occur, an electrons must have a vacant place (a hole) to move to and occupy. When bands are completely filled or empty, conduction can not occur. Metals are highly conductive because they possess unfilled bands. Semiconductors possess an energy gap small enough that thermal excitation of electrons from the valence to the conduction bands is sufficient for conductivity however, the band gap in insulators is too large for thermal excition of electron accross the band gap.

1.1.1 Doping and Electrical Conductivity

In the late 1970s Heeger and MacDiarmid found that polyacetylene [$(CH)_n$] produced by Shirikawa's method exhibited a 12 order of magnitude increase in electirical conductivity when exposed to oxidizing agents. So how does this 12 order of magnitude increase in electrical conductivity for polyacetylene occur? The diffuse nature of the extended π-system readily allows electron removal from, or injection, into the polymer. The term "doping" being used to describe polymer oxidation and reduction, respectively. Doping in regards to semiconductors is quite different as it is a very distinct process carried out at low levels (<1%) as compared to CP doping (usually 20-40%). However, the manner by which doping transforms a neutral CP into a conductor remained a mystery for many years.

Electron Paramagnetic Resonanace (EPR) studies have shown that both the neutral and heavily doped CP_s possess no net spin, interpreted as no unpaired electrons, while moderately doped materials were discovered to be paramagnetic in nature. Conductivity experiments showed that it was the "spin-less", heavily-doped form

that is the most conductive for a given CP. Such behavior marks an abrupt departure from simple band theory, which centers around spin-containing charge carriers.

Polyacteylene turns out to be a special case when considering its neutral and doped forms. Comparison of the two neutral forms, reveals them to be structurally identical, and thus, their ground states are degenerate in energy. Two successive oxidation on one chain could yield radical cations that, upon radical coupling, become non-associated charges termed positive "solutions".

In contrast to polyacetylene, the other CP_s shown in Figure 1.1 have non-degenerate ground states (i.e. they do not possess two equivalent resonance forms, and thus, do not show evidence of solutions formations. In this instance, the oxidation of the CP is believed to result in the destabilization (raising of the energy) of the orbital from which the electron is removed. This orbital's energy is increased and can be found in the energy region of the band gap as shown. Initially, if only one electron per level is removed a radical cation is formed and is known as a "polaron". Further oxidation removes this unpaired electron yielding a dicationic species termed a "bipolaron". High dopant concentrations create a bipolaron- "rich" material and evetually leads to band formation of bipolaron levels. Such a theoretical treatment, thereby, explains the appearance, and subsequent disappearance, of the EPR signal of a CP with increased doping as the neutral polymer transitions the polaronic form and subsequently to the spinless bipolaronic state.

Contrary to polyacetylene's independent charges, the bipolaron unit remains infact and the entire entity propagates along the polymer chain. In the case of unsubstitued polythiophene, the bipolaronic unit is believed to be spread over six to eight rings. This "bipolaron lenght" is by no means an absolute number as different polymer backbone and substituent types yield various lenghts.

While this general model of charge carrier generations has developed over the years, it is not without conjecture. As one alternate possibility, the presence of diamagnetic π-dimers, resulting from the combination of cation radicals, has been proposed. Much of the basis of these theories comes from investigations into the structural and electronic proparties of small conjugated molecules.

1.1.2 Optical Properties

Doping also brings about radical changes in a CPs optical properties. For instance, neutral polythiophene films are red in color, while doped polythiophene in blue in color. A broad variety of color changes that can be structurally controlled have been observed for the CPs in changing between their respective redox state. These optical changes are a consequence of polaronic levels and bipolaron bands residing in the band gap. While the neutral polymer only has its charcteristic π-π^* transition, several new transitions are possible to the orbitals in the bipolaronic state. The energies of these new transitions are necessarily lower and result in the polymer having red-shifted absorptions. While the altering of a CPs optical properties can be readily accomplished via chemical means, electrochemical doping is attractive from an applications standpoint, and these polymers provide a new family of electrochromic materials.

1.1.3 Pyrrole

The first reported polymerization of pyrrole was in 1916. Polypyrrole was prepared by the chemical oxidation of pyrrole using hydrogen peroxide. An amorphous black powder known as 'pyrrole black' was obtained, which was insoluble in common organic solvents. Polypyrrole was shown to be a conducting polymer in 1968. Dall'Olie et al [3] prepared it by oxidation of pyrrole in sulfuric acid as a black powder with room temperature conductivity of 8 S cm^{-1}. A fairly long period elapsed before this organic π-system attracted general interest and was found to be electrically conductive. Conductive polypyrrole films are obtained directly by anodic polymerization of pyrrole in aqueous or organic electrolytes (acetonitrile). They are black and under suitable reaction conditions, can be detached from the anode in the form of self-supporting films (minimum thickness ca. 30μm). Some of the conducting salt used in the electrolyte solution is incorporated in the film as a counterian.

In contrast to polyacetylene, polypyrrole has high mechanical and chemical stability and can be produced continuously as flexible film (thickness 80 μm; trade name: Lutamer, BASF) by electrochemical techniques.

The quality of the polymers is greatly influenced by many factors, e.g. impurities, electrode material, pressure, concentrations, temperature, and comonomers. The most decisive, however, are the current density and the electrolyte, particularly the conducting anion X^- because it is incorporated into the polymer as a counterion. [4] By changing reaction conditions, polymers with different surface morphologies, (e.g., an open porous structure) can be obtained. Variation of the monomers and their substituents yields polymers with conductivities between 10^2 and 10^{-4}S/cm. Alkyl substituents also increase the solubility of the polymers with the results that electrically conducting polymers can be applied as coating from solution.

Polypyrrole has been the materials an many investigations. Functional conjugated, PPy and PTh, in which the electronic properties inherent to the p-conjugated systems are associated with new specific properties afforded by covalently attached functional groups, have been the focus of considerable attention during the past decade. [5]

1.1.4 PXDOT Derivatives

Due to its high oxidation potential, thiophene itself is difficult to polymerize electrochemically. However, upon alkyl substitution the monomer oxidation potential is lowered to an easily accessible range, which has resulted in the extensive study of poly(3-methylthiophene) and other poly(3-alkylthiophene). [6]

Substition at the 3- and 4- positions of thiophene prevents the occurence of α-β and β-β coupling during electropolymerization, yielding more ordered polymers with longer conjugation lengths. Initially, the synthesis of 3,4-disubstituted polythiophenes was carried out with the goal of stabilizing the oxidized form, as well as providing solubility and processability. [7]

While these substituents do lower the oxidation potential and stabilize the oxidized form of the polymers to nucleophilic attack, they also lead to severe steric interactions that distort the π-conjugated system [8] decreasing the degree of cunjugation and lowering the conductivity. To overcome this drawback, poly(3,4-cycloalkylthiophenes) were synthesized, and it was demonstrated that carbocycles at the 3- and 4- positions reduced the steric hindrance, espacially in the case of poly(3,4-cycloalkylthiophenes). This strategy was taken a step further and the

methylene adjacent to the heterocycle was replaced by a heteroatom making the oxidized form even more stable with less steric distortion. As a result, polythiophenes carrying 3,4-dialkoxy and 3,4-alkylenedioxy substituents exhibit the most pronounced stability.

Jonas et al. [9] were the first to anodically polymerize a member of the 3,4-alkylenedioxythiophene family, 3,4-ethylenedioxythiophene. The most intensive research has focused on the PEDOT parent as it has been successfully commercialized by AGFA-Gevaert N.V. and Bayer AG. Using EDOT as the core linkage, materials have been prepared in which the conductivity ranges from less than 10^{-1} S cm^{-1}. Furthermore, their optical properties can be varied over a broad range as evidenced by the electronic bandgap, which ranges from less than 1.0 e V to 2.4 e V.

The alkyl-substitued PEDOTs derived from 20 have been compared to the parent PEDOT. [10-13] The solvent and electrolyte dependence of EDOT-C_8H_{17} and EDOT-$C_{14}H_{29}$ was studied by Sankaran and Reynolds. [14] By repetitive scanning, electroactive polymer films were deposited onto electrodes. Compared to the parent EDOT monomer, the alkyl derivatives oxidize at lower potential.

As a class of conducting and electroactive polymers that can exhibit high and quite stable conductivities, a high degree of optical transparency as a conductor, and the ability to be rapidly switched between conducting doped and insulating neutral states, poly (3,4- alkylenedioxythiophene)s (PXDOTs) (Scheme 1.2), have attracted attention across academia and industry.

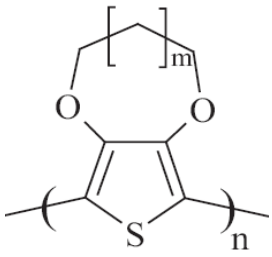

Figure 1.4: Poly (3,4- alkylenedioxythiophene)s (PXDOTs)

Since both chemically and electrochemically prepared PXDOT is insoluble and unprocessible, intensive research has been carried out to synthesize PXDOT derivatives that would overcome this problem.

Due to their ability to be functionalized at the 2-position of the propylene bridge, ProDOT (Pro=1,3-propylene) monomers and polymers have gained special interest as the polymers that form are regio-symmetric. By increasing the ring size from dioxane (six-membered) to the seven-memnered ring in ProDOT, little change is seen in the electropolymerization and switching behavior of PProDOT relative to PEDOT. There are distinct changes in the physical properties of the monomers as EDOT is a liquid at room temperature, while ProDOT is a solid. This makes purification by recrystallization and access to highly pure ProDOT monomers quite facile. There are large changes observed when comparing the optical properties of the substitued PProDOTs, especially the dimethyl and diethyl derivatives that exhibit enhanced electrochromic contrasts throughout the visible region. [15] This will be addressed further later. In addition, by appending long chains at the 2-position of the propylene bridge, soluble and peocessible PProDots are accessible, which are not only electroactive but are also highly fluorescent (deep-red emission) in solution. [16]

Turning to the eight-membered ring-containing species. BuDOT (e.g., 24; Bu=butylene), again little change is observed in electropolymerizability and switching relative to PEDOT or PProDOT. It should be noted that pentylene functionallized derivative, which might gain the acronym PenDOT, has not been synthesized to date due to the difficulty in closing nine-membered rings, and remains elusive.

1.2 Electropolymerization

Electrochemical synthesis utilizes the ability of a monomer to be self-coupled upon irreversible oxidation (anodic polymerization) or reduction (cathodic polymerization). While this method does not always produce materials with well-defined structures (as do the three other polymerization methods to be discussed), electropolymerization, nonetheless, is a rather convenient alternative, avoiding the need for polymer isolation and purificition.

In an electrochemical polymerization, the monomer, dissolved in an appropriate solvent containing the desired anionc doping salts, is oxidized at the surface of an electrode by application of an anodic potential (oxidation). The choice of the solvent

and electroyte is of particular importance in electrochemistry since both solvent and electrolyte should be stable at the oxidation potential of the monomer and provide an ionically conductive medium. [17] As a results of the initial oxidation, the rdical cation of the monomer is formed and reacts with other monomers present in solution to form oligomeric products and than the polymer. The extended conjugation in the polymer results in a lowering of the oxidation potential compared to the monomer. Therefore, the synthesis and doping of the polymer are generally done simultaneously. The anion is incorporated into the polymer to ensure the electrical neutrality of the film and, at the end of the reaction, a polymeric film of controllable thickness is formed at the anode. The anode can be made of a variety of materials including platinum, carbon fiber, gold, glassy carbon and indium tin oxide (ITO) coated glass. The electropolymerization is generally achieved by potentiostatic (constant potential) or galvanostatic (constant-current) methods. Potentiodynamic techniques such as cyclic voltametry corresponds to a repetitive triangular potential waveform applied at the surface of the electrode. [18]

1.3 Carbon Fiber Microelectrodes

Carbon fibers exhibit truly outstanding properties. Their strength, competes with the strongest steels; they can have stiffness, E, greater than any metal, ceramic or polymer; and they can exhibit thermal and electrical conductivities that greatly exceed those of competing materials. If the strength or stiffness values are divided by the low density, 1800-2100 kg m^{-3}, then their huge specific properties make this class of materials quite unique.

Polyacrylonitrile (PAN) type carbon fiber, produced by carbonization of PAN precursor, having high tensile strength and high elastic modulus, extensively applied for structural material composites in aerospace and industrial field and sporting / recreational goods. PAN based fibers are produced from a solubilized mixture that is wet or dry spun to produce a fiber, ostensibly for use in the textile industry. This fiber is stabilized and carbonized to produce a carbon fiber. Aerospace grade material can be obtained in tows that contain between 3000 and 12000 fibers. Lower performance materials are usually formed using larger tows that contain up to 320 000 fibers. PAN based carbon fibers are cheaper when produced from larger tows.

Pitch type of the fiber, produced by carbonization of oil/coal pitch precursor, having extensive properties from low elastic modulus to ultra high elastic modulus. Fibers with ultra high elastic modulus are extensively adopted in high stiffness components and various uses as utilizing high thermal conductivity and / or electric conductivity. Pitch fibers are melt spun products obtained in small tow sizes varying from 2000 to 4000 fibers. They are usually larger diameter (10-15 pm) than fibers formed from PAN. The most important mechanical and physical properties exhibited by carbon fibers are the elastic modulus, tensile strength, electrical and thermal conductivities.

Carbon fibers are used in fiber-reinforced composites, which consist of fiber and resin. Original large-scale applications were in the reinforcement of polymers. As the technology of textile reinforced composites expanded, a growing demand from the aerospace industry for composite materials with superior properties emerged. In particular, materials with higher specific strength, higher specific modulus and low density were required. Other desirable properties were good fatigue resistance and dimensional stability. Although carbon fibers meet these demands, it is necessary to improve interfacial properties between reinforcing (carbon) fibers and the polymeric matrix. The electrochemical deposition of conducting polymers on carbon substrates has been studied with the goal of improving the mechanical properties of conducting polymers, so as to use them as electrodes in different applications: electrochromic displays, batteries, sensors, capacitors.

Electropolymerization onto carbon fiber microelectrodes was performed by Sarac et al. Surface characterizations of thin film coating of random poly(N-vinylcarbazole-co-vinylbenzenesulfonic acid), [19, 20] copolymer on carbon fiber was performed. Copolymer films of pyrrole and 3,4 ethylenedioxythiophene (EDOT) were synthesized electrochemically on the carbon fiber microelectrodes (CFME). Deposition conditions on the carbon fiber and influence of the monomer concentrations to the copolymerization as well as the electrochemistry of the resulting polymers and copolymers were studied using cyclic voltametry, in-situ spectroelectrochemistry, FTIR-ATR and scanning electron microscopy. [21]

Thin film electro-coated poly(N-vinylcarbazole-co-vinylbenzene sulfonic acid) [22,23] p(NVCzVBSA) , poly(carbazole-co-methylthiophene), (p(CzMeTh) and

polycarbazole (p(Cz)) carbon fibre microelectrodes (CFMEs) were characterized by scanning electron microscopy (SEM) and FTIR-ATR spectroscopy.

1.4 Electrochemical Impedance Spectroscopy

Electrical resistance is the ability of a circuit element to resist the flow of electrical current. Ohm's law (Equation 1-1) defines resistance in terms of the ratio between voltage E and current I.

$$R = \frac{E}{I} \tag{1.1}$$

While this is a well known relationship, it's use is limited to only one circuit element the ideal resistor. An ideal resistor has several simplifying properties:

· It follows Ohm's Law at all current and voltage levels.

· It's resistance value is independent of frequency.

· AC current and voltage signals though a resistor are in phase with each other.

The real world contains circuit elements that exhibit much more complex behavior. These elements force us to abandon the simple concept of resistance. In its place we use impedance, which is a more general circuit parameter.

Impedance is a totally complex resistance encountered when a current flows through a circuit made of resistors, capacitors, or inductors, or any combination of these. Depending on how the electronic components are configured, both the magnitude and the phase shift of an ac can be determined. Because an inductive effect is not usually encountered in electrochemistry, we consider only the simple equivalent circuit shown in Figure 1.6 in which no inductor is present.

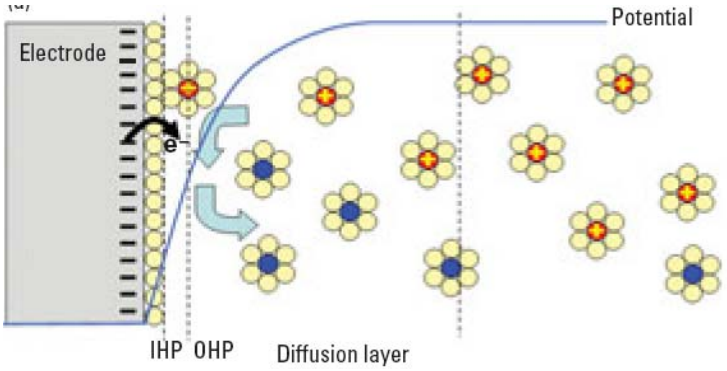

Figure 1.5: A simple electrified interface, in which the vertical dotted lines in **(a)** are represented by the electronic components in **(b). (a)** The oxidants (red) with a positive charge diffuse toward the negatively charged electrode, accept electrons from the electrode at the interface, become the reductants (blue), and diffuse to the bulk of the solution. The oxidant is also a counterion to the electrode. No specific adsorption is considered at the interface. IHP and OHP are the inner and outer Helmholtz planes, respectively.

However, first consider an experiment in which a series of increasing dc potentials (a ramp) are applied to a working electrode in an electrochemical cell containing an electroactive species. A current– potential curve (Figure 1.6) is obtained, which is described by the Butler–Volmer equation (solid line)

$$i = i_0 \left[e^{\frac{-\alpha n F}{RT}\eta} - e^{\frac{(1-\alpha) n F}{RT}\eta} \right] \qquad \textbf{(1-1)}$$

in which η is the overpotential defined as $E - E$eq, with E and Eeq representing the applied and equilibrium potentials, respectively; i_o is the exchange current at η= 0; n is the number of electrons transferred; F is the Faraday constant; R is the gas constant; T is the absolute temperature; and α is the transfer coefficient for electron transfer. The faradaic current i is limited by the mass transport (dashed line curving to the right) when the rate of electron transfer becomes large enough. At a given overpotential ηbias, the slope of the curves, di/dηbias, is 1/Rp, in which Rp is the polarization resistance.

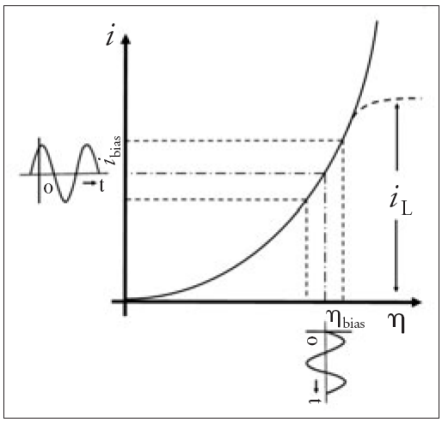

Figure 1.6: The dc plotted as a function of overpotential according to the Butler-Volmer equation (solid line), which is limited by mass transport at large overpotentials (dashed line curving to the right), an ac voltage (broken line) superimposed on the dc bias potential, _bias (dot-dashed line), shown on the *i* axis [ηbias + ηsin(ωt)], and the resulting ac superimposed on the dc on the *i* axis [*i*bias + _*i*sin(ωt +Ø)]. *R*p is obtained by taking _η/_*i*, in which *i* is obtained after applying the ac voltage wave at a given η.

When a small ac voltage wave of frequency ω at ηbias (Figure 1.4) is superimposed, the ac of the same frequency will be flowing on top of the dc. Because the interface has resistors and a capacitor (Figure 1b), the flowing ac will experience a phase shift, expressed as ibias, caused by the ac wave perturbation. For an equivalent circuit (Figure 1b), a straightforward impedance expression can be derived by applying Ohm's law to two components connected in parallel. One of these is Rp, and the other is 1/(jωCd), in which Cd is the double-layer capacitance.

$$Z(\omega) = R_s + \frac{R_p}{1 + j\omega R_p C_d} =$$

$$R_s + \frac{R_p}{1 + \omega^2 R_p^2 C_d^2} - \frac{j\omega R_p^2 C_d}{1 + \omega^2 R_p^2 C_d^2} = Z' + jZ'' \qquad \textbf{(1-2)}$$

To make the derivation of the equation and its interpretation straightforward, we neglected the contribution of the Warburg component. Thus, the impedance of the interface consists of two parts, a real number Z' and an imaginary number Z'' with a complex representation, $Z(\omega) = Z'(\omega) + jZ''(\omega)$ with Ø(the phase angle) = $\tan^{-1}$ $[Z''(\omega)/Z'(\omega)]$. Although the capacitance is relatively constant over the potential at a given electrode, the *R*p varies as a function of ηbias applied to the electrode. At a given dc bias potential, a series of $Z(\omega)$ data are obtained in a range of frequencies, typically 100 kHz^{-1} to 10^{-4} Hz. The impedance varies, depending on frequencies, and

is often plotted in different ways as a function of frequency (making it a spectroscopic technique), hence, the name EIS [24-29].

By treating the impedance data in such a frequency range, system characteristics for an electrochemical reaction (i.e., *R*s, *R*p, and *C*d) can be obtained. *R*p is a function of potential; however, at $\eta = 0$, it becomes the charge-transfer resistance R_{CT}. Two convenient ways of treating the impedance data are the Nyquist plot, (Figure1.5a) in which imaginary numbers $Z''(\omega)$ are plotted against real numbers $Z'(\omega)$, and the Bode plot, (Figure 1.5b) in which absolute values of impedance or phase angle are plotted against the frequency. Extraction of the system characteristics requires interpreting the Nyquist plot according to Equation (1.3).

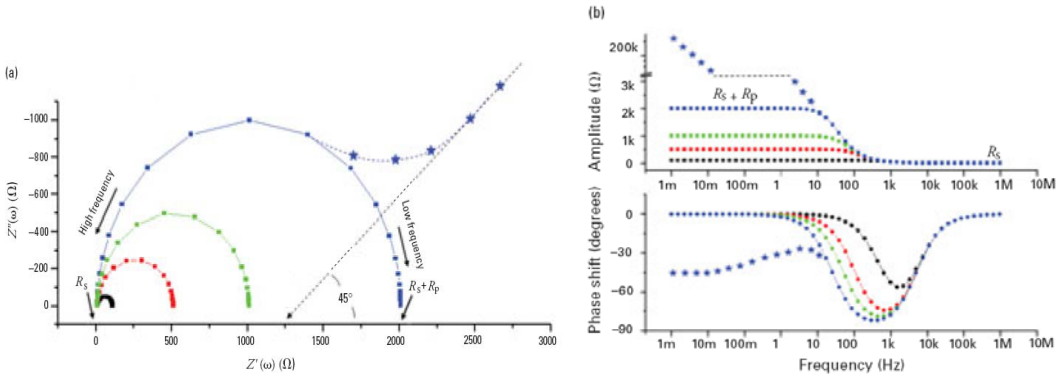

Figure 1.7: (a) Nyquist plot **(b)** Bode magnitude of Z and Bode phase angle

At high frequencies, the frequency dependent term of Equation 1.3 vanishes, resulting in $Z(\omega) = Z'(\omega) = R$s, which is an intercept on the $Z'(\omega)$ axis on the high frequency side ($\emptyset = 0$ or $Z''(\omega) = 0$). For $\omega \rightarrow 0$, Equation 1.3 becomes $Z(\omega) = R$s + *R*p, which is an intercept on the $Z'(\omega)$ axis on the lowfrequency side. At the frequency where a maximum $Z''(\omega)$ is observed, the straightforward relationship $R_p.C_d = 1/\omega_{max} = 1/(2\pi f_{max}) = \zeta_{rxn}$, which is the time constant of the electrochemical reaction, can be shown and indicates how fast the reaction takes place. Also, if $R_p.C_d$ is known, C_d can be obtained because R_p is already known from the low-frequency intercept on the $Z'(\omega)$ axis. The Nyquist plot gives all the necessary information about the electrode–electrolyte interface and the reaction. Similar information is obtained by examining the Bode diagram using Equation 1.3. Log R_s and log (R_p+R_s) are obtained straight forwardly from the $Z(\omega)$ versus logω plot at high and low frequencies from the same argument as the Nyquist plot. In the intermediate

frequency region, an almost straight line with a slope of ~ –1.0 can be seen. The equation for this line is obtained by ignoring the frequency-independent terms, R_s and 1 in the denominator, of Equation 1.3 to yield

$$Z(\omega) = R_s + \frac{R_p}{1 + j\omega R_p C_d} \quad \textbf{(1-3)}$$

Taking the logarithm on both sides of the resulting equation yields log $Z(\omega)$ = –log ω – log C_d, which says that log $|Z(\omega)|$ versus log ω would have a slope of –1, and C_d can be obtained from the intercept of this line with the $Z(\omega)$ axis when –log ω = 0 at ω = 1. Thus, the Bode plot provides the same information as the Nyquist plot. The Ø versus log ω plot shows that the impedance responses are resistive primarily at high and low frequencies as indicated by practically no phase shifts, whereas at intermediate frequencies, they are mostly capacitive as their phase shifts get closer to 90^o.

Thus far, we have discussed the equivalent circuit without considering the effect of the Warburg impedance; however, its contribution can be important at low frequencies because the mass transport of the electroactive species may limit the electron- transfer process. The Warburg impedance [30] is imparted by mass transfer.

Measuring impedance principle shown in Figure 2 is the basis on which impedance is measured: A small ac wave, typically 5–10 mV (peak-to-peak) of a given frequency, is superimposed on the dc ηbias, and the resulting ac and its phase shift ibias are measured. These measurements may be made in various ways [31-33]; however, the frequency response analyzer (FRA; Figure 4) has become the industry standard in electrochemical instrumentation in recent years. The reference ac wave of frequency _ super imposed on a given dc bias potential is applied to a working electrode in the electrochemical cell. The ac signal S(t) obtained from the cell is then multiplied by the reference sine or cosine wave and integrated to obtain.

1.4.1 Equivalent Circuit Elements

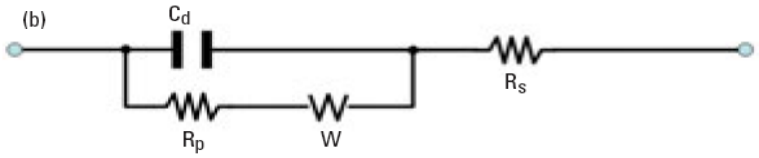

Figure 1.8: An equivalent circuit representing each component at the interface and in the solution during an electrochemical reaction is shown for comparison with the physical components. C_d, double layer capacitor; R_p, polarization resistor; W, Warburg resistor; R_s, solution resistor.

Electrolyte Resistance

Solution resistance is often a significant factor in the impedance of an electrochemical cell. A modern 3 electrode potentiostat compensates for the solution resistance between the counter and reference electrodes. However, any solution resistance between the reference electrode and the working electrode must be considered when you model your cell.

The resistance of an ionic solution depends on the ionic concentration, type of ions, temperature and the geometry of the area in which current is carried. In a bounded area with area A and length l carrying a uniform current the resistance is defined as:

$$R = \rho\frac{l}{A} \tag{1-4}$$

where r is the solution resistivity. The conductivity of the solution, k , is more commonly used in solution resistance calculations. Its relationship with solution resistance is:

$$R = \frac{1}{\kappa}\cdot\frac{l}{A} \Rightarrow \kappa = \frac{l}{RA} \tag{1-5}$$

Standard chemical handbooks list k values for specific solutions. For other solutions, you can calculate k from specific ion conductances. The units for k are siemens per meter (S/m). The siemens is the reciprocal of the ohm, so 1 S = 1/ohm.The value of the double layer capacitance depends on many variables including electrode potential, temperature, ionic concentrations, types of ions, oxide layers, electrode roughness, impurity adsorption, etc.

Double Layer Capacitance

A electrical double layer exists at the interface between an electrode and its surrounding electrolyte. This double layer is formed as ions from the solution "stick on" the electrode surface. Charges in the electrode are separated from the charges of these ions. The separation is very small, on the order of angstroms.

Polarization Resistance

Whenever the potential of an electrode is forced away from it' s value at open circuit, that is referred to as polarizing the electrode. When an electrode is polarized, it can cause current to flow via electrochemical reactions that occur at the electrode surface. The amount of current is controlled by the kinetics of the reactions and the diffusion of reactants both towards and away from the electrode.

In cells where an electrode undergoes uniform corrosion at open circuit, the open circuit potential is controlled by the equilibrium between two different electrochemical reactions. One of the reactions generates cathodic current and the other anodic current. The open circuit potential ends up at the potential where the cathodic and anodic currents are equal. It is referred to as a mixed potential. The value of the current for either of the reactions is known as the corrosion current.a new parameter, R_p, the polarization resistance. As you might guess from its name, the polarization resistance behaves like a resistor

Diffusion

Diffusion can create an impedance known as the Warburg impedance. This impedance depends on the frequency of the potential perturbation. At high frequencies the Warburg impedance is small since diffusing reactants don't have to move very far. At low frequencies the reactants have to diffuse farther, thereby increasing the Warburg impedance.

The equation for the "infinite" Warburg impedance is:

$$Z = \sigma(\omega)^{-1/2} (1-j) \qquad \textbf{(1-6)}$$

On a Nyquist plot the infinite Warburg impedance appears as a diagonal line with a slope of 0.5. On a Bode plot, the Warburg impedance exhibits a phase shift of 45°.

Constant Phase Element

Capacitors in EIS experiments often do not behave ideally. Instead, they act like a constant phase element (CPE) as defined below.

The impedance of a capacitor has the form:

$$Z = A(j\omega)^{-\alpha} \tag{1-7}$$

When this equation describes a capacitor, the constant A = 1/C (the inverse of the capacitance) and the exponent a = 1. For a constant phase element, the exponent is less than one.

The "double layer capacitor" on real cells often behaves like a CPE instead of like like a capacitor. Several theories have been proposed to account for the non-ideal behavior of the double layer but none has been universally accepted. In most cases, you can safely treat a as an empirical constant and not worry about its physical basis.

1.5 Characterizations

1.5.1 Attenuated Total Reflection Fourier Transform Infrared Spectroscopy

Attenuated Total Reflectance (ATR) spectroscopy, known as internal reflection spectroscopy or multiple internal reflectance (MIR), is a versatile, nondestructive technique for obtaining the infrared spectrum of the surface of material or the spectrum of materials either too thick or too strongly absorbing to be analyzed by standart transmission spectroscopy.

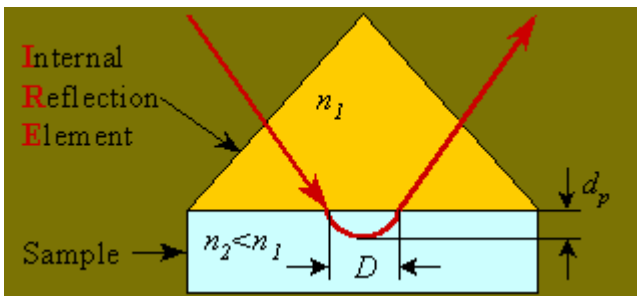

Figure 1.9: Schematic representation of path of a ray of light for total internal reflection (Single reflection). The ray penetrates a fraction of a wavelength (d_p) beyond the reflecting surface into the rarer medium of refractive index n_2 and there is

a certain displacement (*D*) upon reflection, n_1 is refractive index of the interval reflection elements

Attenuated Total Reflectance (ATR) FTIR is widely used by researchers to examine a variety of sample types including solids, powders, pastes and liquids for food analysis, biomedical applications, polymers, and thin films. In addition to the identification of functional groups during more routine analysis, ATR-FTIR spectroscopy is useful for mechanistic studies of vapor-solid interactions during chemical vapor deposition or heterogeneous catalysis by *in situ* real time monitoring of surface species[1]. These experiments typically require the IR beam to exit the spectrometer, pass through a vacuum system or pressure reactor containing the ATR crystal and gas phase molecules of interest via IR transparent windows, and finally to return to the spectrometer for detection.

1.5.2 Spectroelectrochemistry

Experimentally, the band gap is related to the wavelength of the first absorbsion band band in the electronic spectrum of the substance. Thus a photon with λ (wavelength) can exite an electron from HOMO to LUMO level $\pi \rightarrow \pi^*$ if the energy condition is fulfilled.

$$\Delta E = E(LUMO)-E(HOMO)$$

$$\Delta E = h\nu = h(c/\lambda) \quad \textbf{(1-8)}$$

ΔE = The band gap (Energy gap)

There are no partially filled band, conducting polymer are typically semiconductors. Because E_g depends on the molecular structure of repeat unit.

1.5.3 Scanning Electron Microscope (SEM)

The scanning electron microscope (SEM) is a type of electron microscope capable of producing high resolution images of a sample surface. SEM images have a characteristic three-dimensional appearance and are useful for judging the surface structure of the sample.

In a typical SEM electrons are thermionically emitted from a tungsten or lanthanum hexaboride (LaB_6) cathode and are accelerated towards an anode; alternatively electrons can be emitted via field emission (FE). Tungsten is used because it has the highest melting point and lowest vapour pressure of all metals, thereby allowing it to be heated for electron emission. The electron beam, which typically has an energy ranging from a few hundred eV to 50 keV, is focused by one or two condenser lenses into a beam with a very fine focal spot sized 1 nm to 5 nm. The beam passes through pairs of scanning coils in the objective lens, which deflect the beam in a raster fashion over a rectangular area of the sample surface. Through these scattering events, the primary electron beam effectively spreads and fills a teardrop-shaped volume, known as the interaction volume, extending from less than 100 nm to around 5 μm into the surface. Interactions in this region lead to the subsequent emission of electrons which are then detected to produce an image. X-rays, which are also produced by the interaction of electrons with the sample, may also be detected in an SEM equipped for energy-dispersive X-ray spectroscopy or wavelength dispersive X-ray spectroscopy.

The nature of the SEM's probe, energetic electrons, makes it uniquely suited to examining the optical and electronic properties of semiconductor materials. The high-energy electrons from the SEM beam will inject charge carriers into the semiconductor. Thus, beam electrons lose energy by promoting electrons from the valence band into the conduction band, leaving behind holes.

In a direct bandgap material, recombination of these electron-hole pairs will result in cathodoluminescence; if the sample contains an internal electric field, such as is present at a p-n junction, the SEM beam injection of carriers will cause electron beam induced current (EBIC) to flow.

2 EXPERIMENTAL

2.1 Chemicals

Monomer 1-(4-Methylphenyl)-1H-pyrrole was used from Aldrich Chemicals with a purity of %97. Electrolytes, tetrabutylammonium hexafluorophosphate (Bu_4NPF_6), tetraethylammonium hexafluorophosphate (Et_4NPF_6), tetraethylammonium tetrafluoroborate (Et_4NBF_4), tetrabutylammonium tetrafluoroborate (Bu_4NBF_4)were used from Fluka chemicals after drying in vacuum oven without further purification with a ratio of %99 purity. Dichloromethane (DCM) was used as receieved from Merck, acetonitrile (ACN), propylene carbonate (PC) from Riedel de Haen Chemical without further purification. Tetrahydrofuran (THF) was received from Sigma-Aldrich.

2.2 Preparation of carbon Fiber Microelectrode (CFMEs)

SGL SIGRAFIL C 320 B (A high strength and high modulus of elasticity coupled with high electrical conductivity carbon fibers) (SGL Carbon Group) were used as working electrodes. All of the electrodes were prepared by using 3 cm of the CFME (with average diameter of around 7 μm) attached to a copper wire with a Teflon tape. Generally 20-30 carbon fibers was used. Roughly 1 cm of the CFME was dipped into the solution to keep the electrode area constant ($4.4x10^{-2}$) and the rest of the electrode was covered with the Teflon type. The CFMEs were firstly cleaned with acetone and then dried up with an air-dryer before the experiments.

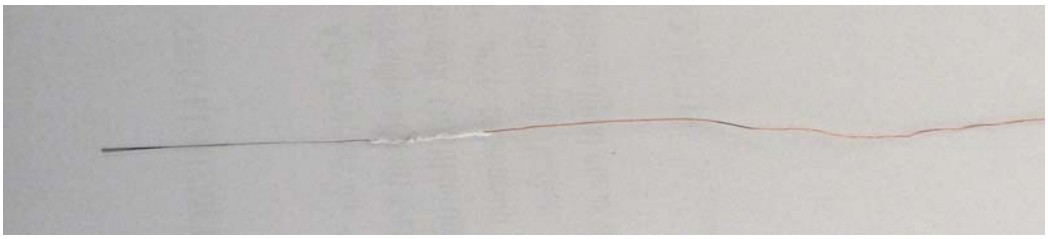

Figure 2.1 : Carbon Fiber Micro Electrode

2.3 Electropolymerization and Characterization of the Monomers

2.3.1 Electropolymerization

Electropolymerization were performed with different electrolyte system 0.1 M Bu_4NBF_4, 0.1M Bu_4NPF_6 , 0.1M Et_4NPF_6, 0.1M Et_4NBF_4 in different solvents such as ACN, DCM, PC, DMF, different monomer concentrations, scan rates, scan number. Princeton Applied Research, Parstat 2263 model potentiostat which is a self contained unit that combines potentiostat circuitry with phase-sensitive detection (Faraday cage that Bass Cell Stand C3) was used for cyclic voltametry (CV). Electropolymerization was performed three- electrode system with a CFME as a working electrode, platinium (Pt) wire as a counter and silver (Ag) wire as a pseudo reference electrode. The three electrodes were then dipped into the cell which was a conical shape cell with an radius of 1.7 cm in bottom, and heigh of 6 cm with radius of 2.5 cm in top with a volume of 5 mL solution. Those electrode system consist of CFME, reference electrode (Ag (wire)) and counter electrode (Pt (wire)) which have a distance of about 1 cm to each other. Those electrode system consist of CFME, reference electrode (Ag (wire)) and counter electrode (Pt (wire)) which have a distance of about 1 cm to each other.

Figure 2.2: Cell Which Is Used At The Electropolymerization

2.3.2 Electrochemical Impedance Spectroscopy (EIS):

EIS measurements were taken at room temperature (25^{o}C) using a conventional three electrode cell configuration. The electrochemical cell was connected to a Potentiostat (PARSTAT 2263) with interfaced to a computer described above. An electrochemical impedance software PowerSine was used to carried out impedance measurements between 10 mHz and 16 kHz. The AC amplitude voltage used for the experiments was 10 mHz and DC potentials. The impedance spectra were analyzed using ZSimpWin V3.10.

2.3.3 Spectroelectrochemical Spectroscopy

For spectroelectrochemical studies, polymer films were synthesized on indium tin oxide (ITO) coated glass slides from a 10mM solution of ProDOT-Me_2 in 0.1M Bu_4NPF_6/ACN using potentiodynamic deposition at a constant potential of 1.6V. The film washed before studying the spectroelectrochemical properties with ACN solution and a series of UV-Vis spectra were obtained at various potentials. Spectroelectrochemical measurements were carried out using Perkin Elmer Lambda 45 UV-Vis spectrometer connected to a computer. A three electrode cell was used. The working electrode was an ITO coated glass slides (8 mm x 50 mm x1.1 mm , 30mm of the ITO electrode immersed into the solution to keep electrode area constant at 2.4 cm^2, $R_s \leq 10\Omega$ provided from Colorado Concept Coatings LLC) the counter was a platinum wire and silver wire as the pseudo reference electrode. The potentials were applied using Princeton Applied Research Potentiostat model 2263 as previously described. Data were recorded with UV Winlab for spectral data.

2.3.4 FT-IR ATR Spectroscopy

Carbon fiber surface coated with polymer by electrochemical polymerization were analyzed by FT-IR reflectance spectrophotometer. (Perkin Elmer, Spectrum One; with a Universal ATR attachment with a diamond and ZnSe crystal C70951).

2.3.5 Scanning Electron Microscopy

The morphological studies were analyzed using a SEM. The morphological features of the coated carbon fiber electrodes were performed by field emission scanning electron microscopy (FE-SEM) by Jörg Nissen (Zentraleinrichtung für Elektronenmikroskopie)

3 RESULTS AND DISCUSSION

3.1 Electropolymerization and Characterizations of poly (1-(4-Methylphenyl)-1H-pyrrole) on Carbon Fiber Microelectrode

Poly(1-(4-Methylphenyl)-1H-pyrrole) films were synthesized electrochemically on carbon fiber microelectrodes (CFME). Deposition conditions on the carbon fiber and the influence of solvent on the polymerization, as well as the electrochemistry of the resulting polymers were studied. Structural studies of the polymers were conducted using different techniques such as cyclic voltammetry, reflectance FTIR (FTIR-ATR) and scanning electron microscopy.

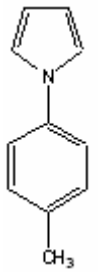

Figure 3.1: 1-(4-Methylphenyl)-1H-pyrrole

3.1.1 Redox Parameters of Me-PhPy In Different Solvents During The Electrochemical Growth Process

Electropolymerization was performed for the monomer using multiple cycles in 0.1 M Bu_4NBF_4/DCM and 10 cycles in 0.1 M Bu_4NBF_4/ACN, Bu_4NBF_4/PC, Bu_4NBF_4/DMF. The electrodeposition of P(MPP) on the CFMEs by cyclic voltammetry at a scan rate of 50 mV s^{-1} at 1.4 V for Bu_4NBF_4/DCM shown in Figure 3.2. The monomer concentration was 10^{-2} M. The oxidation potentials of the monomer were determined from the first cycles as shown in Table 3.1.

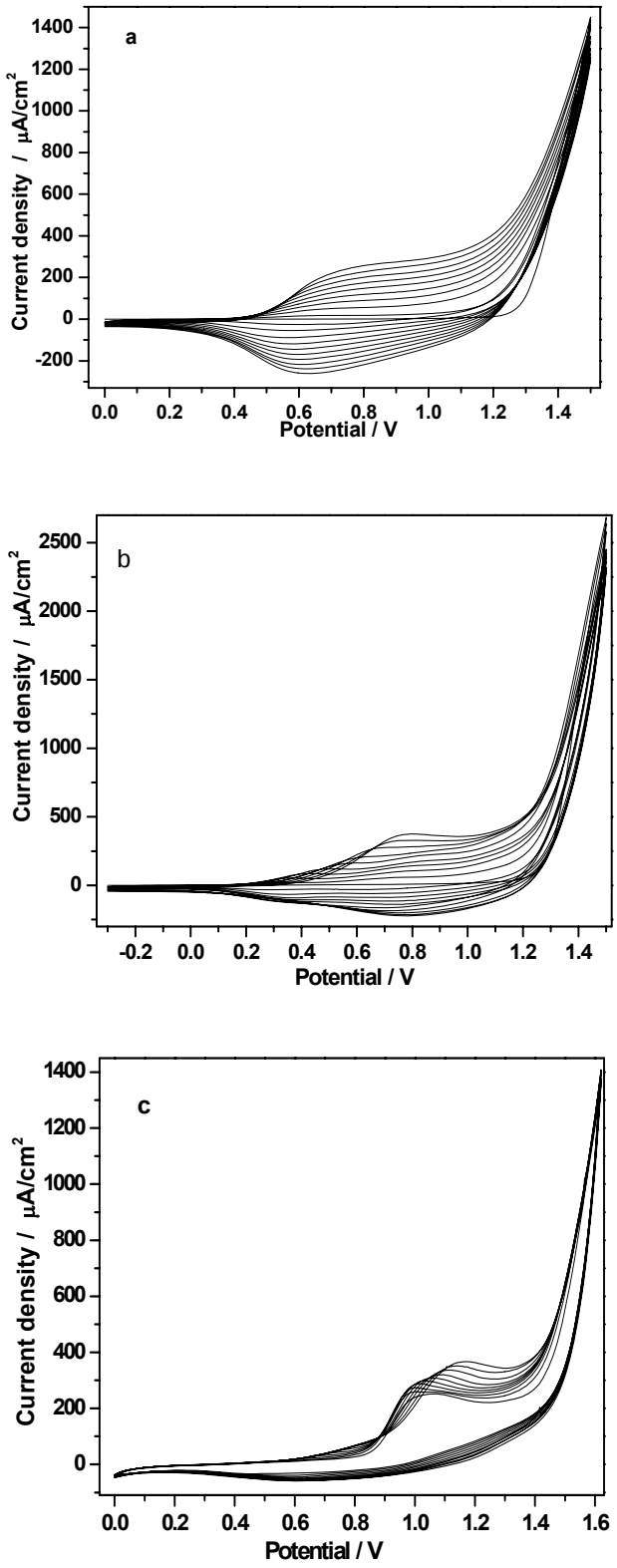

Figure 3.2: Electrodeposition of P(MPP) by potential scanning from a 10^{-2} M solution of monomer in a) 0.1 M Bu_4NBF_4/DCM b) 0.1 M Bu_4NBF_4/ACN c) 0.1 M Bu_4NBF_4/PC

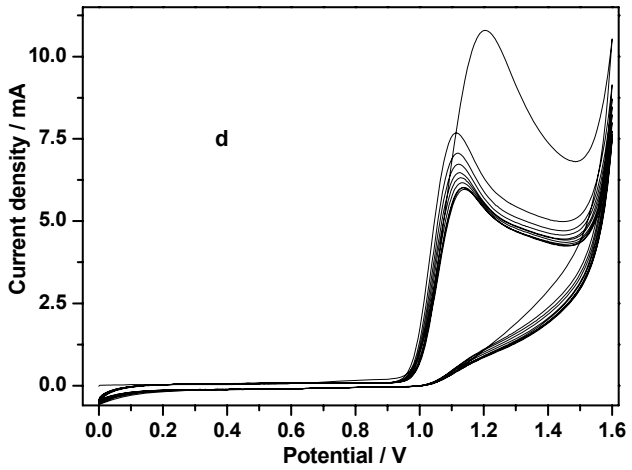

Figure 3.2: Electrodeposition of P(MPP) by potential scanning from a 10^{-2} M solution of monomer in d) 0.1 M Bu_4NBF_4/DMF at 50 mV s^{-1} 10 cycle on the carbon fibre micro-electrodes.

Table 3.1: Redox parameters of MPP in different solvents during the electrochemical growth process (10th cycle)

Solvents	E_a / V	E_c / V	ΔE / V	I_a/I_c	I_a / μA	Ic / μA
DCM	0.82	0.63	0.19	0.98	256	261
ACN	0.76	0.80	0.04	0.69	358	247
PC	1.16	0.66	0.5	0.20	358	72
DMF	1.11	-	-	-	150	-

Figure 3.3 represents the cyclic voltammogram of thin films of P(MPP) on the CFME at scan rates of 20, 50, 100, 150, 200, 250, 300 mV s^{-1} in 0.1 M Bu_4NBF_4/DCM. The films were grown by cyclic voltammetry at 50 mV s^{-1}. Polymer present well defined and reversible redox processes in DCM, and ACN containing Bu_4NBF_4. 0.1 M Bu_4NBF_4/DMF does not present reversible redox processes, not any cathodic peak was obtained in monomer free. The half wave oxidation potentials of the polymers ($E_{1/2}$) are observed at about 0.75 V in DCM. The scan rate dependence of the anodic and cathodic peak currents shows a linear dependence on scan rate as illustrated in Figure 3.4.

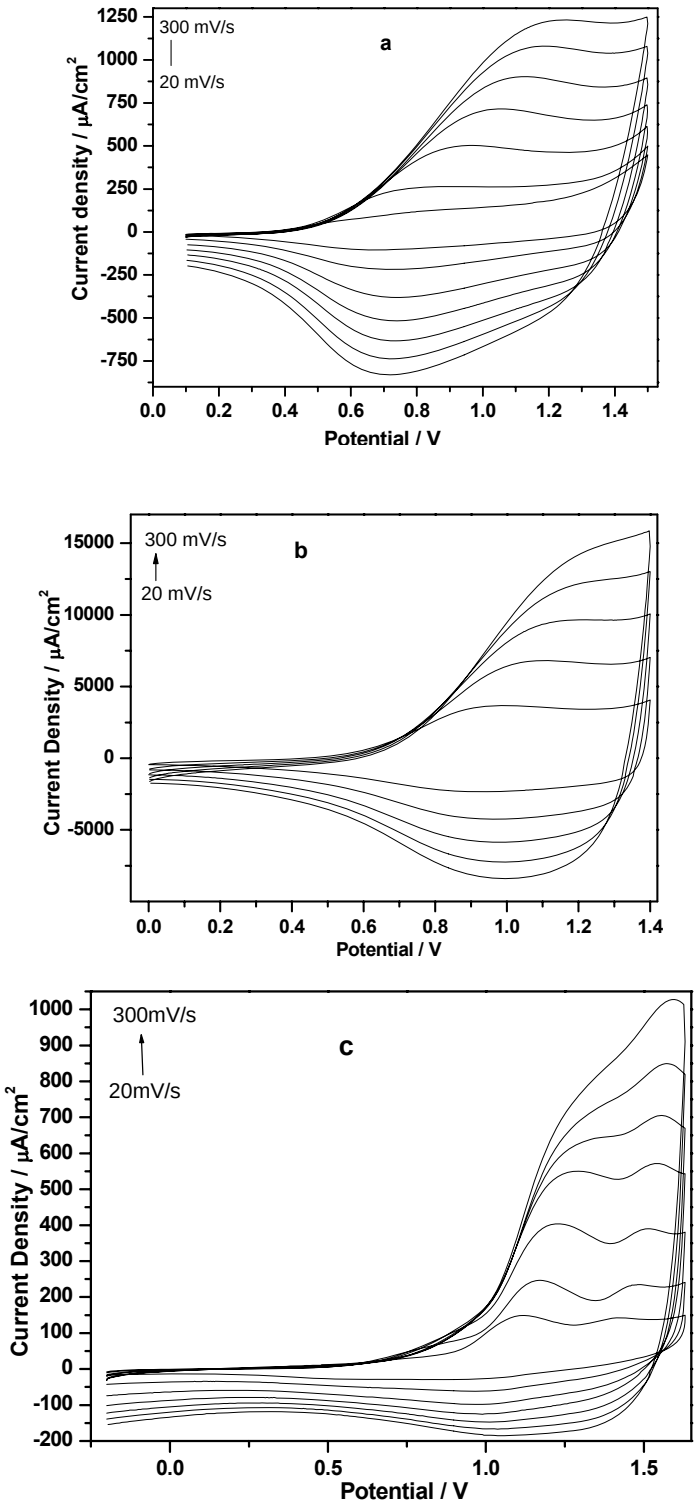

Figure 3.3: Cyclic voltammogram of P(MPP) in monomer free solution of a) 0.1 M Bu_4NBF_4/DCM b) 0.1 M Bu_4NBF_4/ACN c) 0.1 M Bu_4NBF_4/PC at a scan rate of (a) 20, (b) 50, (c) 100 (d) 150 (e) 200 (f) 250 (d) 300 mV s^{-1}

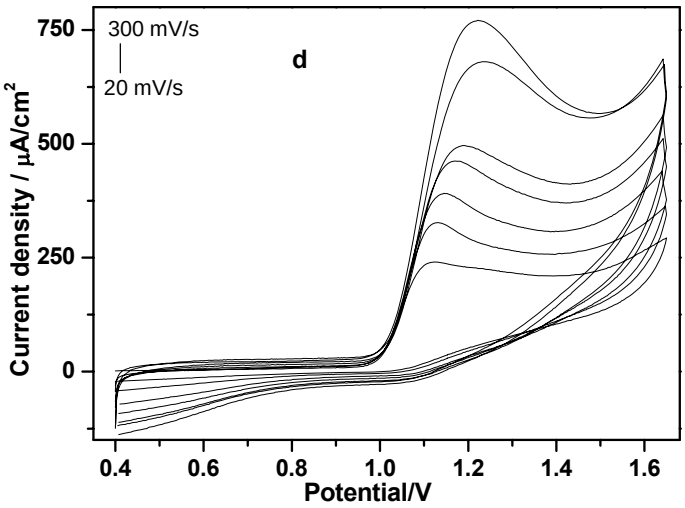

Figure 3.3: Cyclic voltammogram of P(MPP) in monomer free solution of d) 0.1 M Bu_4NBF_4/DMF at a scan rate of (a) 20, (b) 50, (c) 100 (d) 150 (e) 200 (f) 250 (d) 300 mV s^{-1}

Table 3.2: Redox parameters of P(MPP) in different solvents during the monomer free.

Solvent	E_a,V	E_c,V	ΔE,V	$E_{1\backslash 2}$	i_a/i_c	i_a,μA	i_c,μA
DCM	0.79	0.72	0.07	0.75	0.82	53.5	44.3
ACN	1.06	0.99	0.07	1.02	0.50	150	75
PC	1.15	1.04	0.11	1.09	0.25	48	12.3
DMF	1.13	-	-	-	-	64.7	-

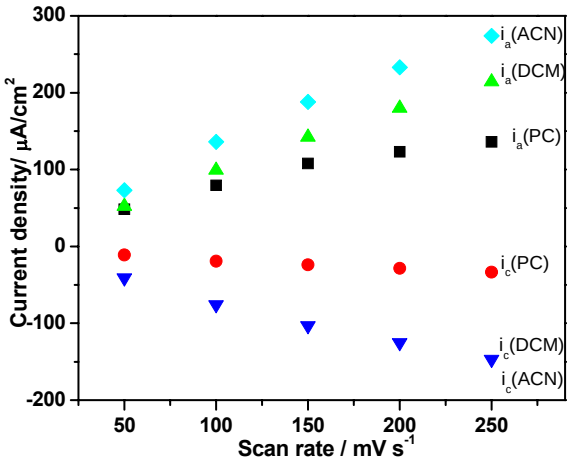

Figure 3.4: Current density vs. scan rate dependency plot obtained from Figure 3.2.

Table 3.3: Peak current, onset potential of polymeric thin film electrocoated onto CFME and dielectric and viscosity of solvents (measured in this work). (i_a and E_{onset} data obtained during polymer growth 10.cycle)

Solvent	i_a, µA	$E_{onset,V}$	Dielectric constant	Kinematic Vis. / mm^2/s
ACN	150	1.25	36.0	0.31
DCM	53.5	1.14	10.2	0.44
PC	48.0	1.33	69.2	1.38
DMF	64.7	0.99	39.2	0.74

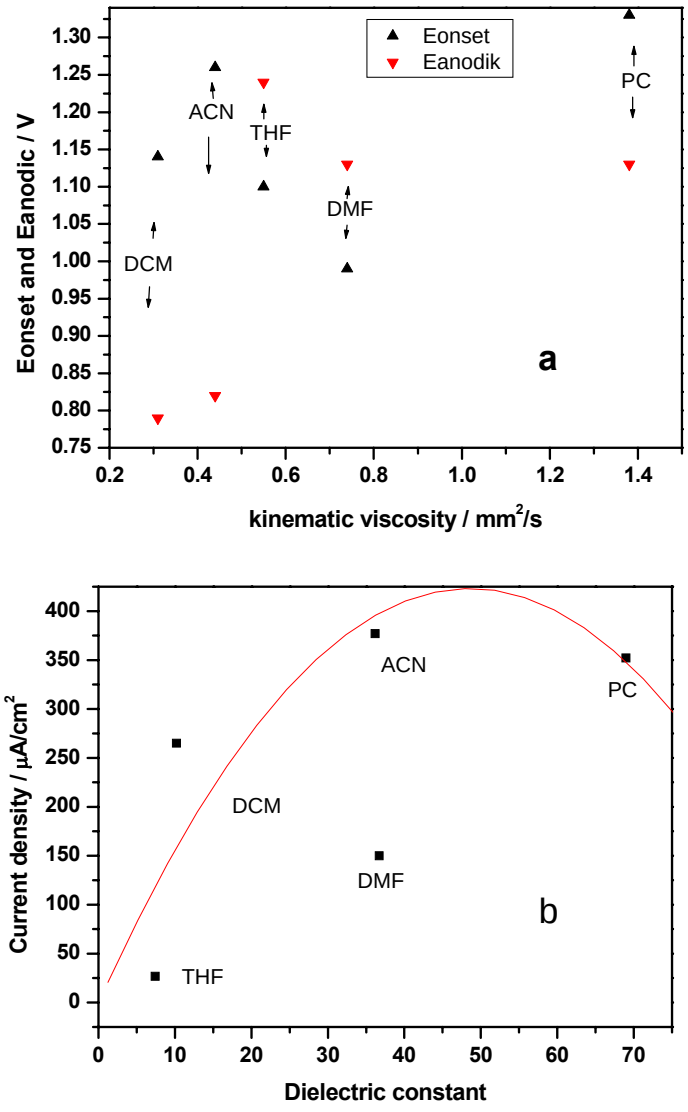

Figure 3.5: (a) The effect of kinetic viscosity of the solvent on to onset potential and peak potential obtained during the electropolymerization (b) The effect of dielectric constant of the solvent on to current density obtained during the polymerization.

E_{onset} of polymer increases with viscosity and current density increases with dielectric constant seen in Figure 3.5. A decrease in PC was observed this might be due to the very high viscosity of the PC compared to the other studied solvents. Because of increasing viscosity with increasing electrophoretic effect, polymerization or oxidation is difficult.

3.1.2 FTIR Reflectance-Spectra (ATR-FTIR)

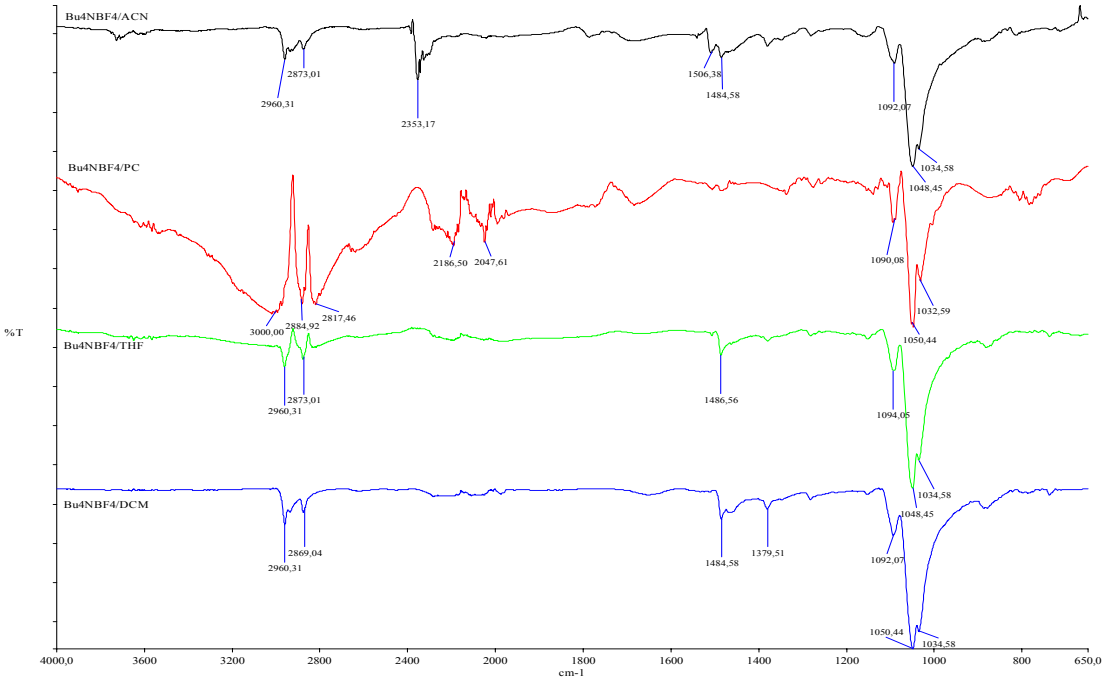

Figure 3.6: FTIR-ATR spectrum of P(MPP), the electrodeposition of P(MPP) on the CFMEs by cyclic voltammetry at different solvent containing electrolyte 0.1 M Bu_4NBF_4

It is shown in FTIR-ATR spectrum results electropolymerization in PC containing Bu_4NBF_4 does not show the same electropolymerization in the other solvents. New peaks are obtained and characteristics peaks shifted. Doping peak at 1048 cm^{-1} slightly shifts to 1044 cm^{-1}.

Table 3.4: ATR-FTIR absorbsion bands and peak assignment of the P(MPP), obtained at the electrodeposition of P(MPP) on the CFMEs by cyclic voltammetry at a scan rate of 100 mV s^{-1} at 1.4 V in 0,1 M Bu_4NBF_4/DCM

Peak / cm^{-1}	Fragment	Intensity / Comment
2954	Phenyl	=C-H (aromatic)
2873	$C\text{-}CH_3$	C-H Stretching vibration
1482	Pyrrole	C=C Stretch
1382	Pyrrole	-C-N Stretching vibration
1046	Bu_4NBF_4	Dopant ion

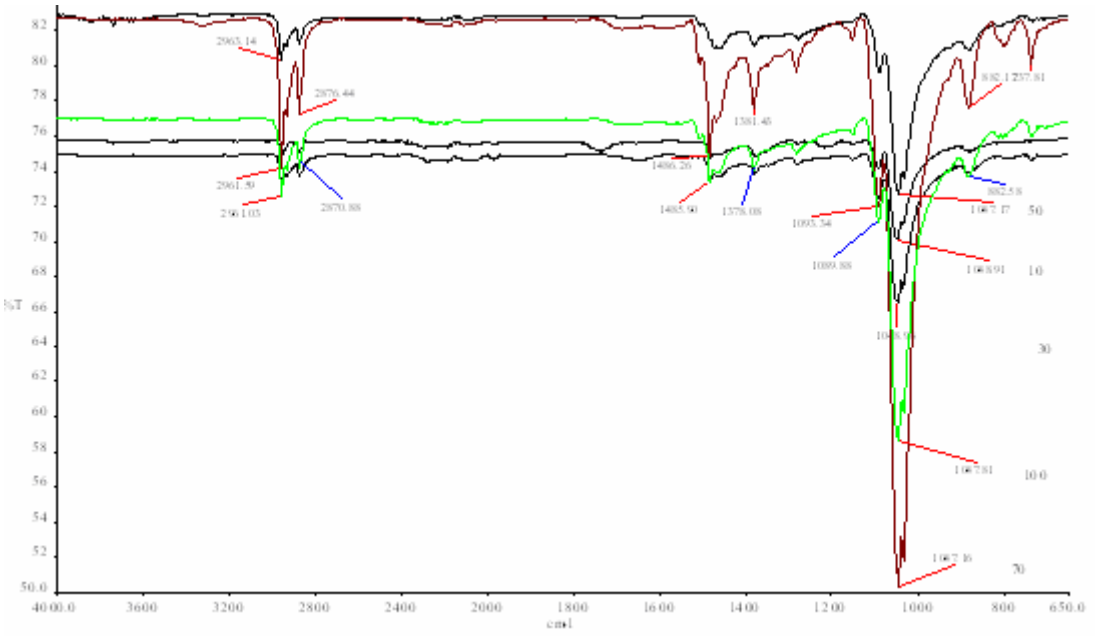

Figure 3.7: FTIR-ATR spectrum of P(MPP), for the film obtained by the electrodeposition of P(MPP) on the CFMEs by cyclic voltammetry at a scan rate of 100 mV s^{-1} at 1.4 V in 0,1 M Bu_4NBF_4/DCM

The peak at about 2873 cm^{-1} is due to the C-CH_3 stretch of the methyl units. The peak at 1048 cm^{-1} and 1380 cm^{-1} may correspond to BF_4^- dopant ion and C-N stretching peak, respectivelly. Those peaks occurring at 879, 882 cm^{-1} are due to the C-H out-of-plane deformation of the methylphenylpyrrole units.

3.1.3 Morphology of the MPP coated CFMEs

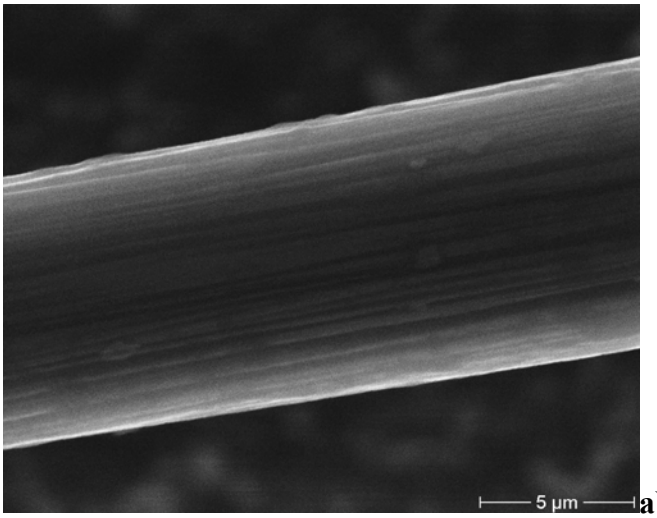

a)

Figure 3.8: SEM of (a),uncoated carbon fiber

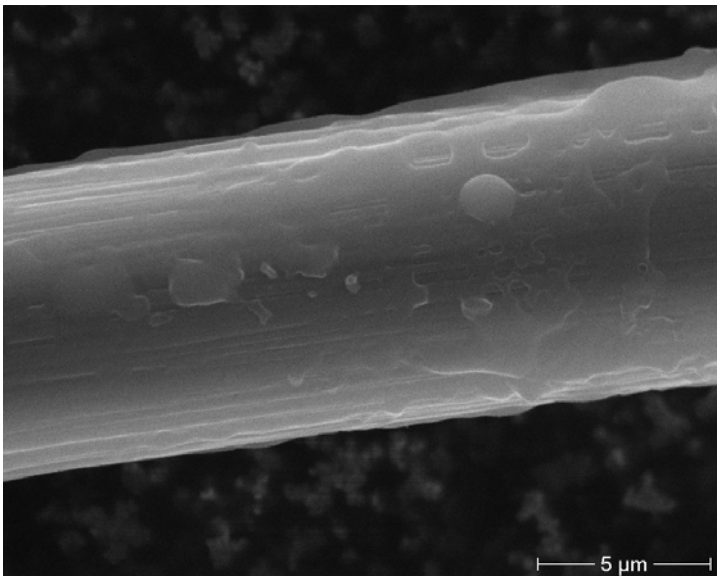

b)

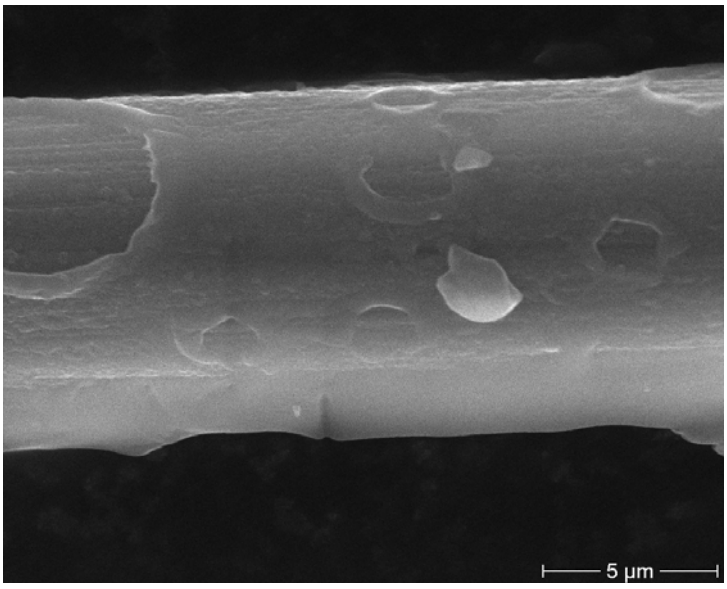

c)

Figure 3.8: SEM of (b) 5th cycle coating and 40th cycle coating (c)

The polymers of MPP on the CFME were grown under different scan number by potentiodynamic depositions, from the solution of 0,1 M Bu_4NBF4/DCM containing 0.01M MPP .

The morphologies of thin MPP coatings on CFMEs were investigated comparatively by scanning electron microscopy (SEM). A thin coating on the CFME was obtained for the 5th cycle, when comparing uncoated and coated fiber (after 5 cycles and 40 cycles) longitudinal striations of carbon fiber can still be seen Figure 3.8 but after 40 cycle carbon fiber more than 5 cycles covered with polymer.

3.2 Electrochemical Polymerization and Characterization of 2,2-Dimethyl-3,4-propylenedioxythiophene

Alkoxy-substituted polythiophenes, such as PEDOT, and its derivatives PProDOT, have been investigated due to their ease of synthesis, a low oxidation potential, high chemical stabilities in the oxidatively doped state, good electrochemical properties. In addition to high conductivity and stability PEDOT is found to be highly transparent in thin, oxidized films. As a result PEDOT derivatives are now utilized in several industrial applications including antistatic coatings for photographic films, electrode material in solid state capacitors, substrates for electroless metal deposition in printed circuit boards, indium tin oxide (ITO) electrode- replacement material in organic electroluminescent lamps. [34]

The ProDOT-Me_2 monomer has been synthesized in three steps from commercially available starting materials using Mitsunobu conditions [35] followed by alkaline hydrolysis [36] and decarboxylation [37] of the resulting precursor. Monomer is a crystalline solid and could be easily obtained, stored and handled in a highly pure state whereas EDOT is a liquid at room temperature. ProDOT-Me_2 exhibited the greatest maximum in-situ conductivity, because of its structure; it can be symmetrically di-substituted on the central carbon of the propylene bridge. Whereas PEDOT shows an electrochromic contrast ratio Δ%T of only 45%, in poly(3,4-propylenedioxythiophene) (PProDOT) this value is enhanced to 62% in order to reach 78% in poly(2,2-dimethyl-propylenedioxythiophene) (PProDOT-Me_2) [47].

Electrochomic properties and the synthesis of 2,2-Dimethyl-3,4-propylenedioxythiophene [ProDOT-$(Me)_2$] were reported in literature by comparison with other poly(3,4-propylenedioxythophene) derivatives for looking contrast ratios on ITO glass working electrode [38]. Tetrahedral substitution pattern of PProDOT-$(Me)_2$, causes the alkyl groups to be positioned above and below the plane of the π-conjugated chain, can allow high doping levels and inhibit π-stacking [39].

The optical properties of and its coloration efficiency have been investigated by colorimetric analysis [40]. As a result of its outstanding behaviour and its rapid switching was tested as a promising candidate in different types of electrochromic

devices [41-42]. The quaternary central carbon of the propylene bridge of should cause structural conditions which can favour high charge capacitance.

Electrochemical impedance spectroscopy (EIS) is an effective tool to validate the presence of the capacitance. The well-developed theoretical background and established experimental procedures make EIS as a convenient and readily available technique for obtaining important electrochemical information, such as electrolyte resistance, charge transfer resistance, double layer capacitance, faradaic capacitance etc. [43]

Comparative study of EDOT and 3,4-Trimethylenedioxythiophene was electropolymerized on Pt, and the qualities of the films obtained by electropolymerization found to be dependent on applied potential (for EDOT) [44]

3.2.1 Electropolymerization of 2,2-Dimethyl-3,4-propylenedioxythiophene on Carbon Fibre Micro Electrode

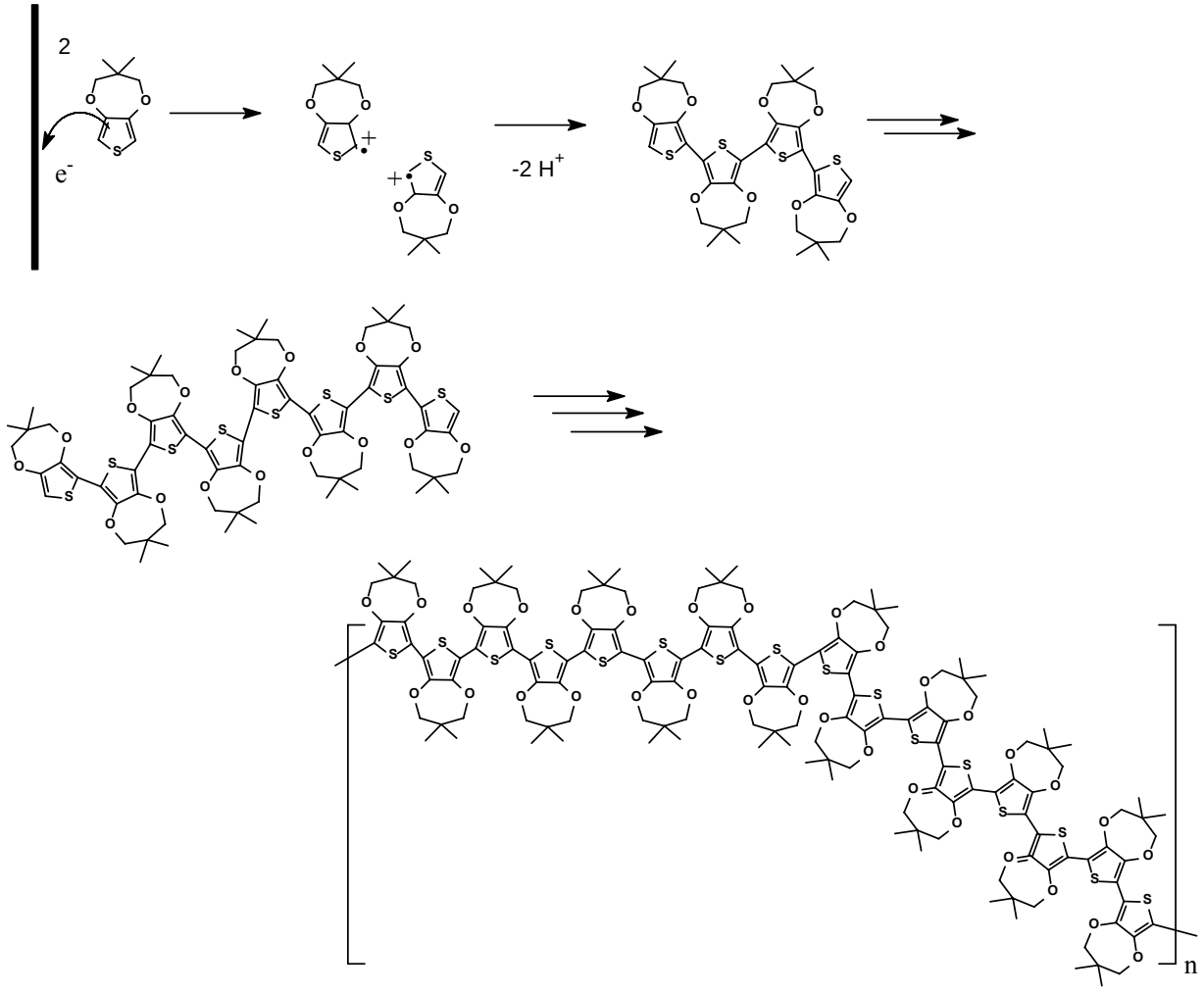

Figure 3.9: Tentative electropolymerization mechanism of ProDOT-$(Me)_2$

Electropolymerization process was performed in 0.1M Bu_4NPF_6 in ACN at various scan rates, cycle numbers and monomer concentration. ACN was chosen as a standard solvent to prepare electrolyte for ProDOT-$(Me)_2$ during this study. Electropolymerization of ProDOT-Me_2 on carbon fiber microelectrode (CFME) was first achieved by cyclic voltammetry from 0.1M Bu_4NPF_6 in ACN electrolyte solution containing 0.01 M ProDOT-$(Me)_2$ between 0-1.6V at a scan rate of 100mV/s given in Figure 3.10. The onset potential of ProDOT-$(Me)_2$ was about 1.4V. The current increases with the cycle number, indicates insoluble polymer film was coated on CFME Figure 3.11). Multisweep cyclic voltammogram of 10 mM ProDOT$(Me)_2$ in 0,1 M Bu_4NPF6/ACN on CFME show an increasing current density with each cycle (E_{pa1} = 0.373V, E_{pa2} = 0.524V, E_{pc1} = 0.291V, E_{pc2} = 0.484V at 20th

cycle), resulting in the formation of thin film of conducting polymer on CFME at 100 mV/s scan rate and 20 cycle (charge density Q=63.00 mC/cm^2).

CFMEs were washed thoroughly with ACN after electropolymerization and the scan rate dependence of polymer film was investigated. Figure 3.11b shows electroactivity of the polymer film on the CFME in monomer free solution. The cyclic voltammogram of a polymer coated CFME in monomer free solution with different scan rates (0,1 M Bu_4NPF6/ACN) shows two oxidation peaks (E_{pa1} = 0.360 V, E_{pa2} = 0.483 V) and corresponding reduction peaks [E_{pc1} = 0184V, E_{pc2} = 0.389 V (weak)] (Figure 3.11b). Scan rate dependencies of the oxidation and reduction peaks of the polymer were calculated using current density values with respect to square root of the scan rate. Correlation coefficient of the oxidation 1 and 2 peaks, reduction 1 and 2 peaks were calculated as 0.9997 and -0.9998, 0.9999 and -0.9998 respectively.

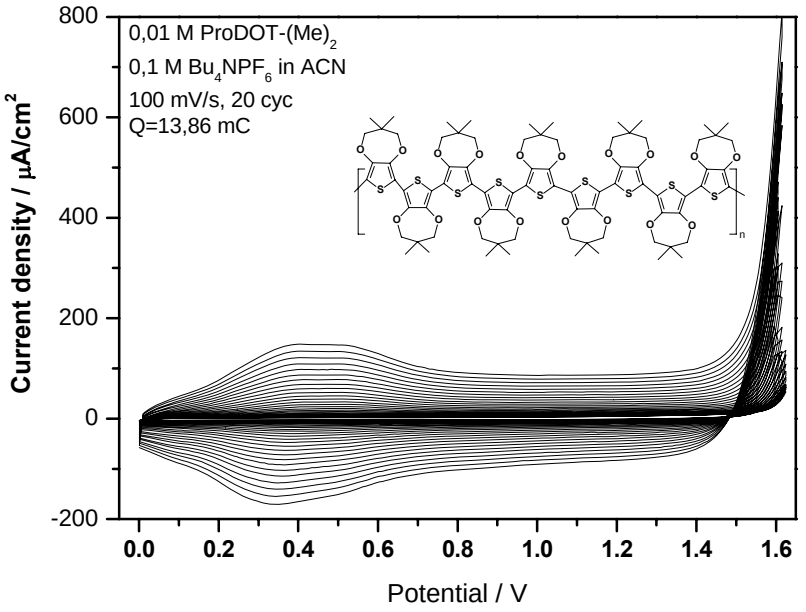

Figure 3.10: Cyclic voltametry of 0.01 M ProDOT-$(Me)_2$ deposition in 0.1 M Bu_4NPF_6/ACN at 100 mV/s, 20 cycle on CFME Q_{dep}=13.86 mC

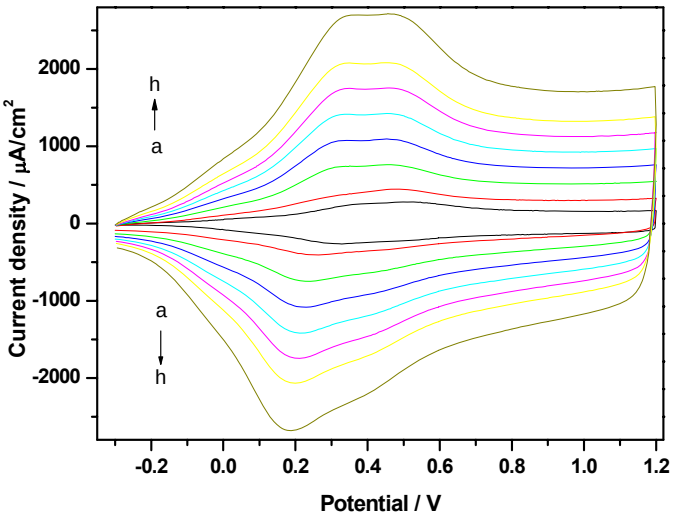

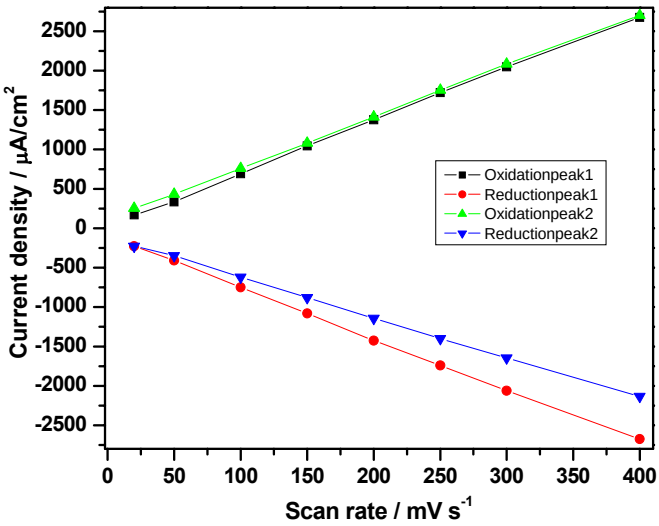

Figure 3.11: a) Polymer PProDOT-Me_2 obtained under condition Figure 3.8 in a monomer free electrolyte solution scanned at (a) 20, (b) 50, (c) 100, (d) 150, (e) 200, (f) 250, (g) 300, (h) 400 mV/s. **b)** Scan rate dependence of the cyclic voltammogram which is given in Figure 3.9a

3.2.2 Spectroelectrochemistry of 2,2-Dimethyl-3,4-propylenedioxythiophene

Spectroelectrochemistry of PProDOT-Me2 film was studied on the potentiodynamically deposited ITO-coated glass slides, as shown in Figure 3.12.

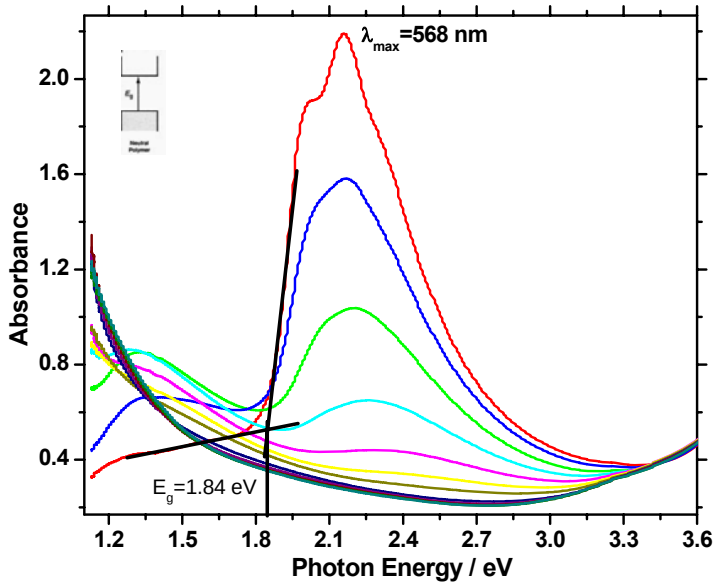

Figure 3.12: In-situ spectroelectrochemistry in 0,1 M Bu_4NPF6/ACN for PProDOT-Me_2 potentiostatically deposited at 1.6V on a ITO coated glass slide, a) -600mV, b) 0 c) 100mV, d) 200mV, e) 300mV f) 400mV g) 500mV h) 700mV j) 800mV k) 900mV l) 1000mV m)1100mV n) 1200mV

Spectroelectrochemistry of PProDOT-Me_2 studies indicate that dark blue color in the reduced form observed at -600 mV and light blue color seen in the oxidized form at 1200 mV. At an applied potential of -600mV, the polymer is in its fully neutral form, band gap of the polymer (E_g) was calculated from onset for the π to π^* transition as 1.85 eV. PProDOT-Me_2 shows very little difference in color relative to PEDOT (E_g = 1.6 eV) as PEDOT is cathodically coloring polymer that is dark opaque blue in its reduced form, and a very transmissive light blue in its oxidized form.[45]

PProDOT-Me_2 shows good contrast in the visible region. This higher contrast is due to its higher percentage of transmittance in the oxidized form. To investigate the switching time of these polymers and stability of their electrochromic changes, double potential pulse switching experiments were performed between -0.6V and 1.2V. The polymer exhibited effectively fast switching time since the time between coloration and bleaching processes was about 0.5 s. And also working shows that substituted PXDOTs have especially fast switching properties when compared to the unsubstituted parents. [46]

3.2.3 ATR-FTIR Characterization of PProDOT-$(Me)_2$

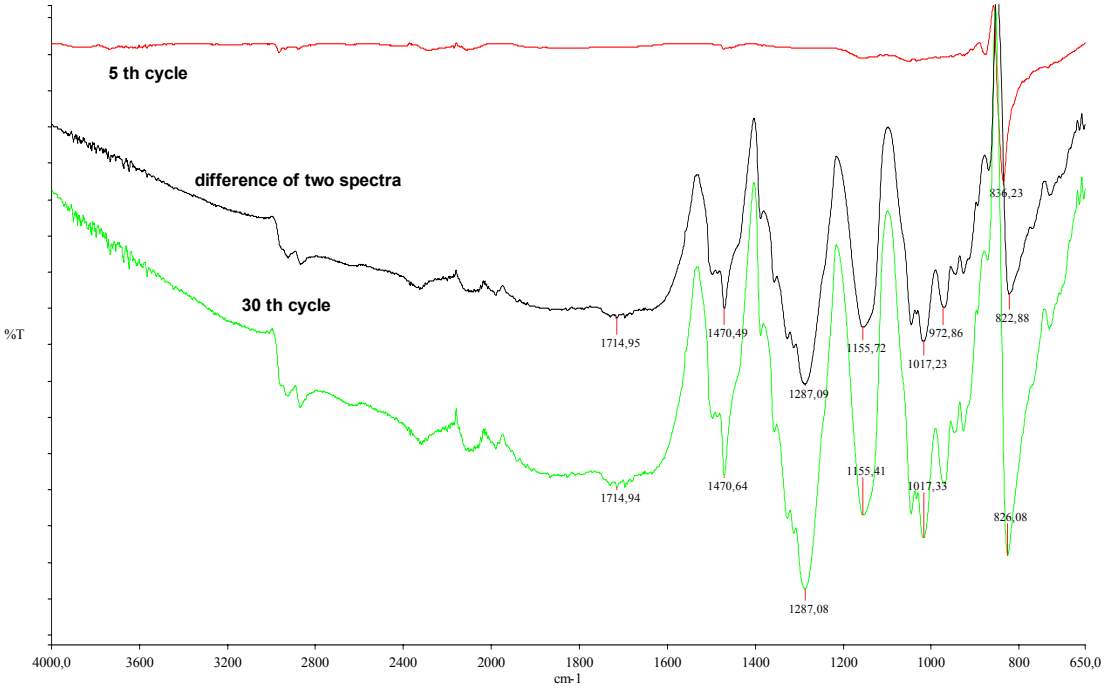

Figure 3.13: Ex-situ FTIR-ATR spectrum of CFMEs potentiodynamically coated by 10 mM ProDOT$(Me)_2$ at 100mV/s scan rate by the application of two different charge densities during the electrogrowth (5.26 mC/cm^2 and 18.53 mC/cm^2 for the 5th and 30th cycle, respectively).

Table 3.5: ATR-FTIR absorbsion bands and peak assignment of the PProDOT-$(Me)_2$ obtained by cyclic voltammetry at a scan rate of 100 mV s^{-1} at 1.6 V in 0,1 M Bu_4NPF_6/ACN

Peak / cm^{-1}	Fragment	Intensity / Comment
1470	Polythiophene	C=C aromatic stretching vibration
1287	Polythiophene	C-H plane deformation vibration
833-825	Polythiophene	C-S- stretching vibration
1048	Bu_4NPF_6	PF^{6-}

FTIR-ATR of PProDOT-$(Me)_2$ coated CFME shows the corresponding spectra between 4000 and 650 cm^{-1}. A pattern of five main bands (1470, 1287, 1155, doublet at 1017 and 826 cm^{-1}) was observed for a PProDOT$(Me)_2$ film coated on CFME Figure 3.13.

The band at 1470 cm^{-1} (aromatic stretching of C=C bond) and a peak at 1287 cm^{-1} (in plane deformation of C-H bond at β position) are known to be characteristic

vibrational peaks of polythiophene. Vibrations at 1469-1470 cm^{-1}, 1295, 1286 cm^{-1} and 1160-1155 cm^{-1} originate from the stretching of C-C and C= C bonds in the thiophene ring.

Further vibrations from the C-S bond in the thiophene ring can be seen at 833-825 cm^{-1} assigned to ν(C-S) [C-S- stretching]. Vibrations at 1017-1048 cm^{-1} are assigned to stretching in the alkylenedioxy group [50]

When the cycle number increased, the appearance of characteristic peaks of PProDOT$(Me)_2$ was observed. The peak intensities increased with increase in charge what confirms the film formation of PProDOT$(Me)_2$ on CFME. PF^{6-} absorbs at 1048-1017 cm^{-1}.

The pattern of three main bands (1319, 1195, doublet at 1090 and 1060 cm^{-1}) observed during p-doping of PEDOT. Additional bands at 1513 and 980 cm^{-1} at p-doping was related to the oxygen containing substitution of the PEDOT rings.

The presence of a strong absorption band at 1048-1017 cm^{-1} in higher charges indicates that these films are highly doped with PF^{6-}.

3.3 Electrochemical Impedance Spectroscopy (EIS)

Electrochemical Impedance Spectroscopy (EIS) measurements were performed at open circuit potential in the range of 100 kHz-10 mHz (application of amplitude of 10mV) for PProDOT$(Me)_2$ electrochemically obtained at different charges (cycles), 100mV/s.

3.3.1 Cycle Effects on ProDOT-Me_2 coated CFMEs; An EIS Investigation at Open Circuit Potential

Figure 3.12 shows the Bode magnitude and Figure 3.13 shows the Bode phase angle of PProDOT-Me_2 film prepared under with different charges by application of different scan numbers during the electropolymerization. (In the 1.157 mC to 2.157 mC region) with all plots showing a high capacitance (high Bode phase angle about 90^o)

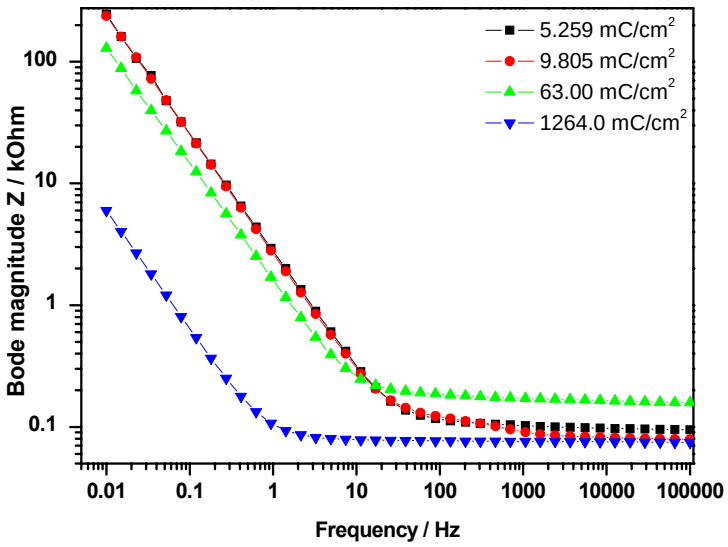

Figure 3.14: EIS of PProDOT-Me_2 by variation of cycle numbers (5, 10, 30 and 40 cycles) (charge density) Bode Z Magnitude plot [Monomer: 10mM ProDOT-Me_2 Range 100 kHz-10 mHz (application of amplitude of 10mV)

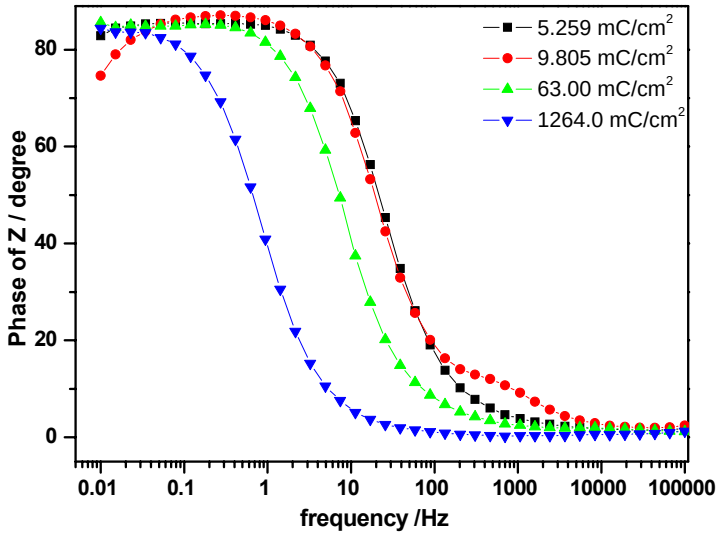

Figure 3.15: EIS of PProDOT-Me_2 by variation of cycle numbers (5-40 cycles) (polymerization charge) Bode phase plot [Monomer: 10 mM ProDOT-Me_2 Electrolyte: 0.1 M Bu_4NPF_6/ACN, Referans Electrode: Ag (wire) Working Electrode: CFME, Counter Electrode: Pt(wire)] Range 100 kHz-10 mHz (application of amplitude of 10mV)

Small charge densities (5.259 mC/cm^2 and 9.805 mC/cm^2) have shown maximum at higher frequencies than for the charges applied as (63.00 mC/cm^2, 1264.09 mC/cm^2 max at lower frequencies).

Comparison with PEDOT we have found similar trend, by the increase of charge applied (during electropolymerization) Bode phase curve shifts (and peak) to lower frequencies which this change is in parallel line with PEDOT case.

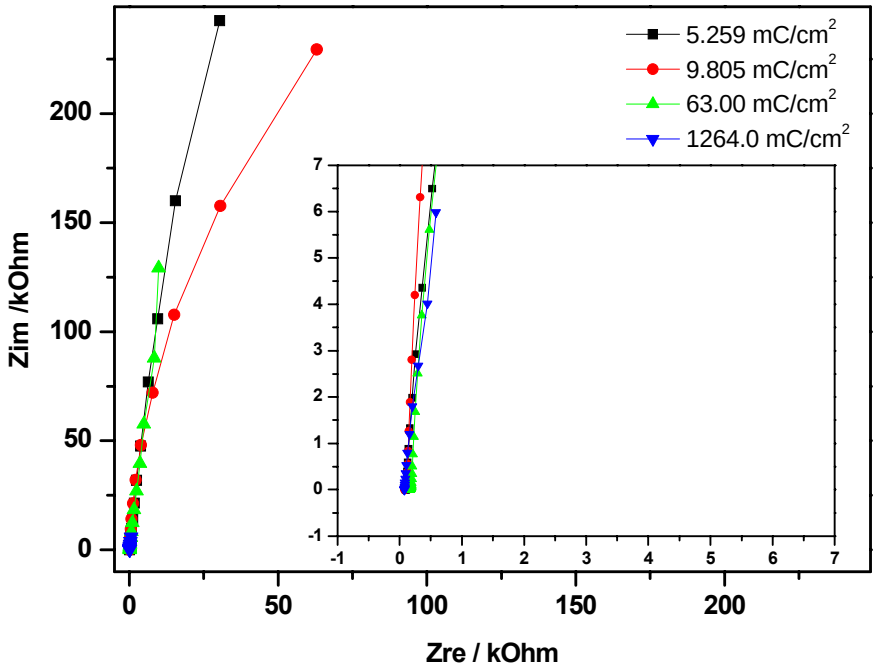

Figure 3.16: Nyquist plot of PProDOT-$(Me)_2$/CFME by the application of different charges during the electrocoating process (polymerization charges obtained during the cyclovoltammetric coating, 5-40 cycles) Range 100 kHz-10 mHz (with a.c. amplitude of 10mV)

In addition to the Nyquist plot steepnes (Figure 3.16), the ideal supercapacitor behavior, was also observed with a phase of angle of about 90º (from Bode phase plot) (Figure 3.15) The absence of semicircle at high frequencies indicates a fast electron transfer between PProDOT-Me_2 film at carbon fiber electrode. Thus,the rate-limiting step is mainly the diffusion of ions within the polymer film [5].

Low frequency capacitance (C_{LF}) are 65.10 µF, 69.40 µF, 123.2 µF, 2.659 mF for 5, 10, 30, 40 cycle respectively.

3.3.2 Electrochemical Impedance Spectroscopy (EIS) Measurement with Applying Potential on ProDOT-Me_2 coated CFMEs

Electrochemical Impedance Spectroscopy (EIS) measurements were performed at different applied potentials in the range of -0.1 V to 1.3 V with a potential step of

0.1V in parallel to cyclic voltammogram of the PProDOT-Me_2 in monomer free electrolyte solution where stability of the film exhibit electroactivity without undergoing deformation.

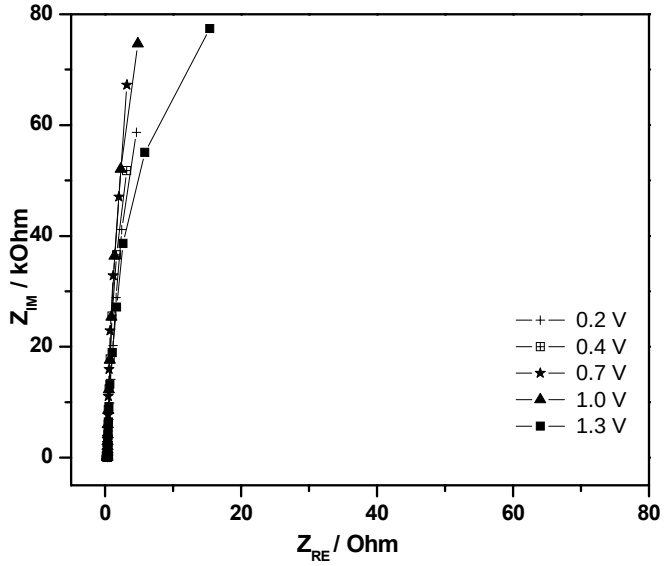

Figure 3.17: Nyquist plots at 0.2 V to 1.3 V for a PProDOT-Me_2 film deposited at 100 mV/s, 20cycle in 0.1 M Bu_4NPF_6/ACN solution

Resuts of the EIS measurements are given in Figure 3.17 as Nyquist and Bode plot at different potentials for ProDOT-Me_2 film. The complex plane impedance plots demonstrate a vertical line with a phase angle very close to -90^o. Impedance behavior of the film similar in the range of 0.2 V to 1.3 V.

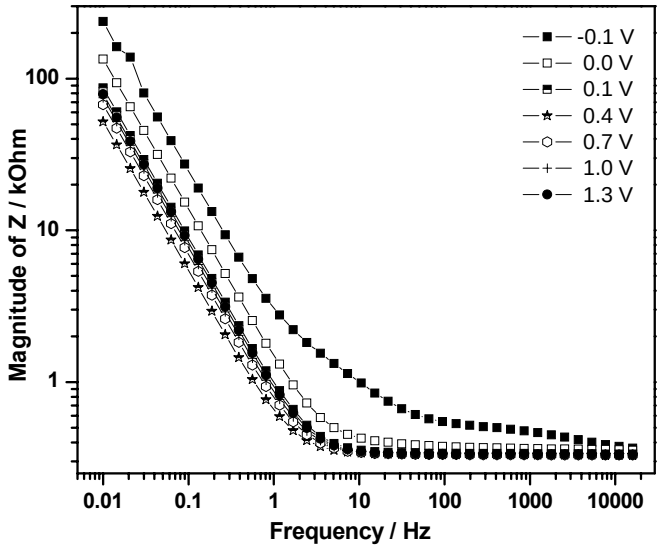

Figure 3.18: Bode magnitude of Z at -0.1 V to 1.3 V for a PProDOT-Me_2 film deposited at 100 mV/s, 20 cycle in 0.1 M Bu_4NPF_6/ACN solution

Bode plots shown in Figure 3.18 and 3.19 can be divided into a high frequency component (bended at -45^o) and a low frequency component (near vertical) with the transition between the two regions. The resistive and capacitive impedances are equal at the transition i.e. -45^o.

Figure 3.19 shows the variation of the Bode phase angle plots of the CFME/PProDOT-Me_2 film deposited at 100 mV/s, 20cycle in 0.1 M Bu_4NPF_6/ACN solution at different DC potentials.

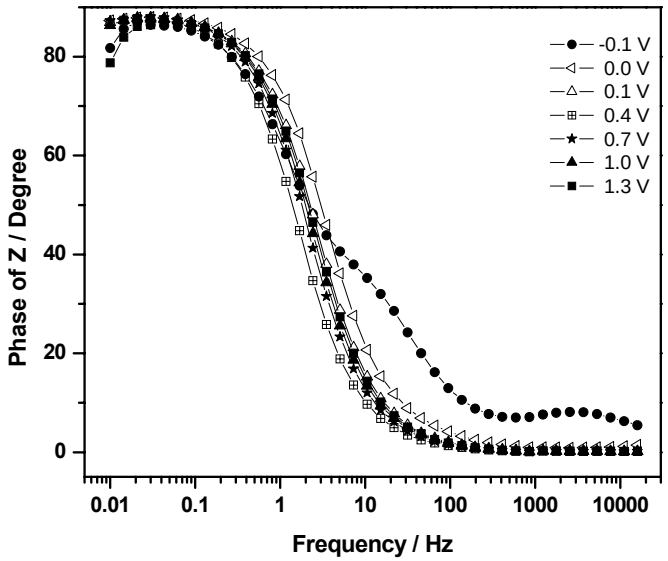

Figure 3.19: Bode phase angle plots at -0.1 V to 1.3 V for a PProDOT-Me_2 film deposited at 100 mV/s, 20 cycle in 0.1 M Bu_4NPF_6/ACN solution and CV at 100 mV/s

The low frequency capacitance values from impedance spectroscopy were obtained from the slope of a plot of the imaginary component (Z_{IM}) of the impedance at low frequencies versus inverse of the reciprocal frequency (f) using following equation [44].

$$C_{LF} = (2\pi f Z_{IM})^{-1} \qquad \textbf{(3-1)}$$

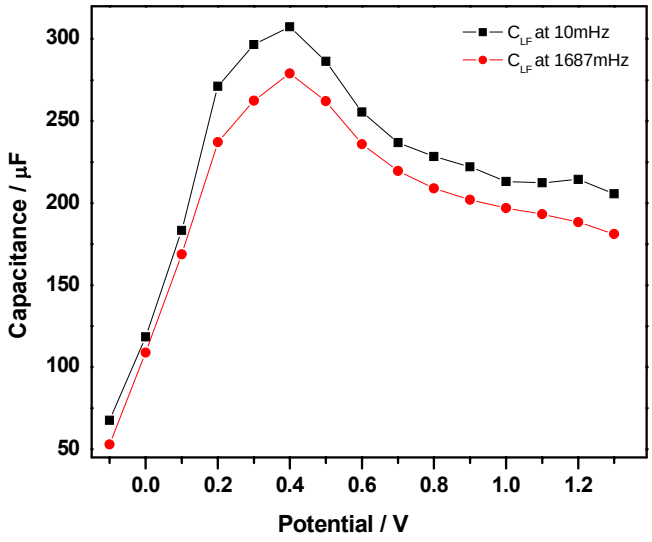

Figure 3.20: Variation of the low frequency capacitance values of the electrochemically polymerized PProDOT-Me_2 film deposited at 100 mV/s, 20 cycle in 0.1 M Bu_4NPF_6/ACN solution and

Figure 3.18 illustrates the variation in the specific capacitance values of PProDOT-Me_2 film deposited electrochemically 5mM ProDOT-Me_2 monomer at 100 mV/s, 20 cycle in 0.1M Bu_4NPF_6/ACN solution at 10 mHz and 1687 mHz at DC potential -0.1 and 1.3V. The shape of the plot has a very good agreement with the corresponding CV of the polymer film in monomer free solution. The low capacitance values increase in low potentials, at 0.4V capacitance values shows a maximum point which converge very well at this potential observed in CV of the ProDOT-Me_2 film for 100mV/s. In the range of 0.4V and 1.3V the low capacitance values decreases little by little.

$$Ccv = j/v \qquad \textbf{(3-2)}$$

j: current density (A)

v: scan rate (V/s)

Capacitance value from the CV (Equation 3.2) was found 2 mF. C_{LF} calculated from the EIS, which is slightly smaller than the value computed from its CV curve.

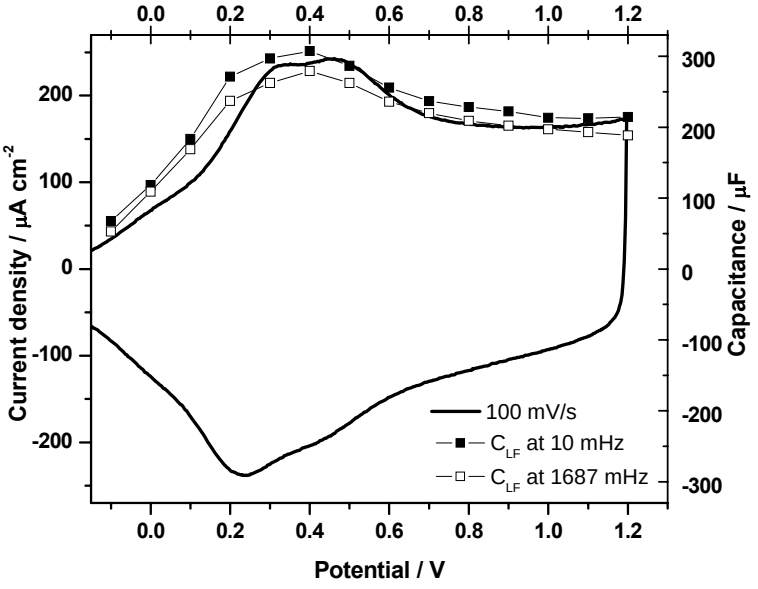

Figure 3.21: Variation of the low frequency capacitance values of the electrochemically polymerized ProDOT-Me_2 film deposited at 100 mV/s, 20 cycle in 0.1 M Bu_4NPF_6/ACN solution and CV at 100 mV/s.

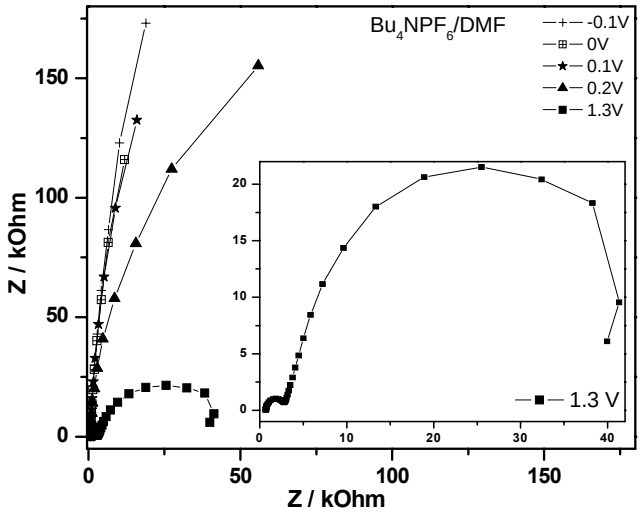

Figure 3.22: Nyquist plot at -0.1V to 1.3V for a PProDOT-Me_2 film deposited at 100 mV/s, 20 cycle in 0.1 M Bu_4NPF_6/ACN solution and EIS measurements were performed in 0.1 M Bu_4NPF_6/DMF solution

Figure 3.23 shows Bode phase angle and magnitude of Z plots in which the frequency dependence of the system is clearer compared to Nyquist plots. In the potential region as the frequency increase from 10 mHz to 10 Hz magnitude of impedance exhibits a large drop, in the case of higher electrode potentials drop in magnitude is a narrow frequency window 10 mHz to 1000 Hz. From these observations we can conclude that the most capacitive potential range in terms of

magnitude of the impedance by frequency is 0.7 V. Bode phase angle of the films was given in Figure 3.23a. We can separated into three frequency regions namely low, medium and high frequency regions. Low frequency region is from 10 mHz to 1 Hz, in this regions all potential except 1.3 V polymer film shows a maximum at 100 mHz with a phase angle of (-87^o), starting from this frequency phase angle decreases and drops to (-45^o) where the electrode behaves in the low frequency region of 100 to 200 mHz, at 1.3 V two peak observed at 200 mHz (-55^o) and 400 Hz (-35^o)

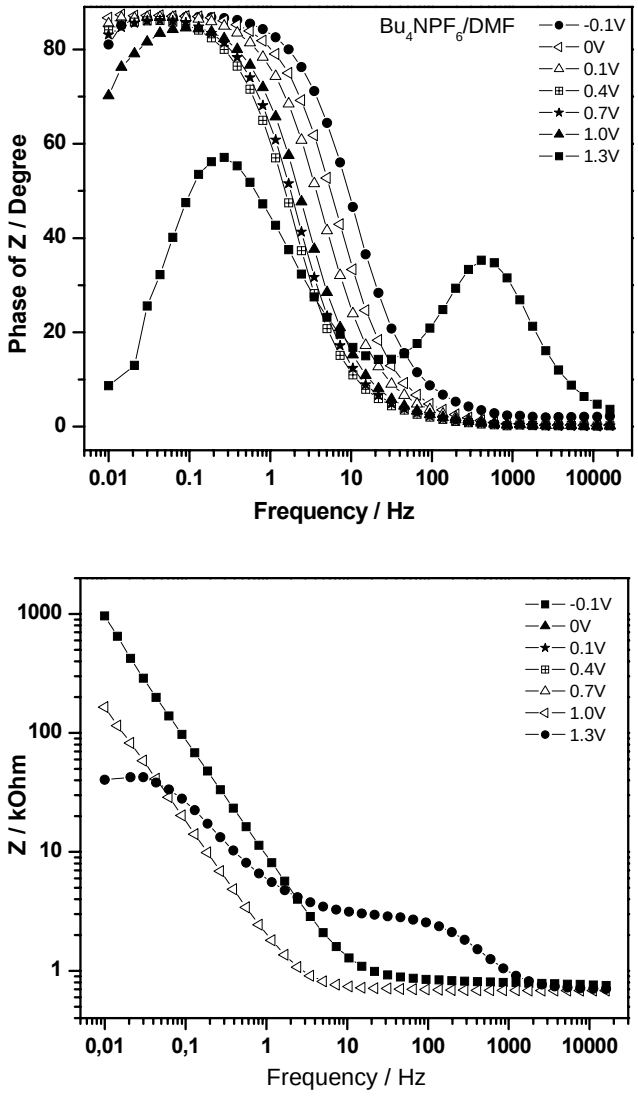

Figure 3.23: (a) Bode phase angle and **(b)** Bode magnitude of Z at -0.1V to 1.3V for a PProDOT-Me_2 film deposited at 100 mV/s, 20cycle in 0.1 M Bu_4NPF_6/ACN solution and EIS measurements were performed in 0.1 M Bu_4NPF_6/DMF solution

3.3.3 Electrical Equivalent Circuit

The electrochemical parameters of the CFME/PProDOT-Me_2/Electroyte system were evaluated by employing The ZSimpWin (version 3.10) software from Princeton

Applied Research. We observed excellent agreement between experimental results and the parameters obtained from the best fitting electrical equivalent circuit model, if the chi-squared (χ^2) minimized below 10^{-4}. χ^2 is the function defined as the sum of the squares of the residuals.

Two electrical equivalent circuits were used in simulation of the impedance behaviour of the film from the experimentally obtained impedance data. First model (see Figure 3.24) was built using series components; the first one is the bulk solution resistance of the polymer and the electrolyte, R_S, second one the parallel combination of the double layer capacitance, C_{dl}, and, R_1 is the resistance of the electrolyte. A series connection to R_1 made up using CPE in parallel with R_2 and W, R_2 is the charge transfer, and W is the Warburg impedance of the polymer. The last component a capacitor element (C_{CF}) is introduced in parallel with a charge transfer resistor (R_{CF}) corresponding to the carbon fiber microelectrode polymer coating. Simulation results are given Table 3.6 show that this electrical equivalent circuit was successfully applied to the experimental data to explain the interface between the carbon fiber microelectrode, the polymer film and electroyte in this potential region.

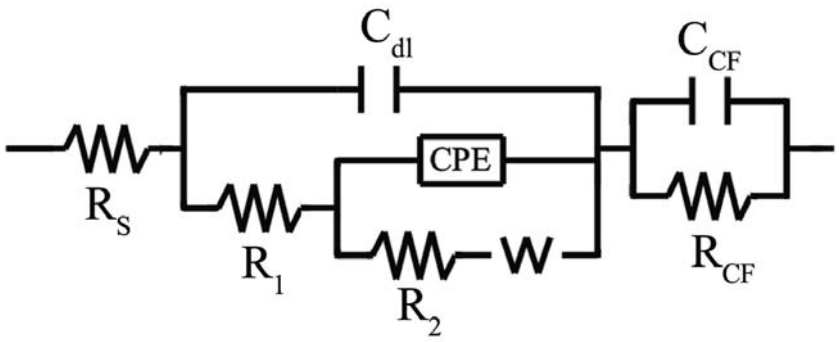

Figure 3.24: Equivalent Electrical Circuit (Model 1) Used in Simulation.

Table 3.6: Potential dependence of the parameters calculated from the Model 1 which is given Figure 3.20. (5mM ProDOT-Me_2 monomer deposited by electrochemically at 100 mV/s, 10cycle in 0.1 M Bu_4NPF_6/ACN solution)

	E=0.2V	E=0.4V	E=0.7V	E=1.0V	E=1.3V
R_s / Ohm	1850	1852	1851	1851	1860
C_{dl} / F	$9.782x10^{-5}$	$1.115x10^{-4}$	$1.039x10^{-4}$	$6.932x10^{-5}$	$9.617x10^{-18}$
R_1 / Ohm	2964	3449	14860	390.2	1.083
Q / Y_o/ S s^{-n}	$1.501x10^{-5}$	$6.497x10^{-5}$	$5.057x\ 10^{-6}$	$2.548x10^{-5}$	$8.891x10^{-5}$
n	0.8932	0.96	1	1	0.9818
R_2 / Ohm	723000	$9.356x\ 10^{6}$	9.998	98990	$1.296x10^{6}$
W / Y_o/ S s^{-n}	$2.532x10^{-6}$	$1.222x\ 10^{-16}$	$2.966x\ 10^{-6}$	$2.942x10^{-6}$	$9.046x10^{-6}$
C_{CF} / F	$2.052x10^{-4}$	0.0011	$2.866x10^{-4}$	0.0025	$2.404x10^{-4}$
R_{CF} / Ohm	20.9	25360	28.11	44.15	26.24
Chi Squared (χ^2)	$3.57x10^{-5}$	$4.87x\ 10^{-5}$	$3.81x10^{-5}$	$3.66x10^{-5}$	$5.09x10^{-5}$

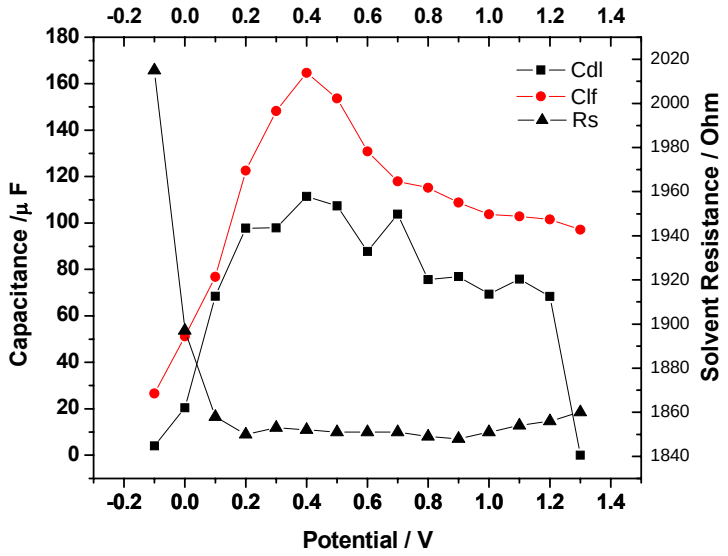

Figure 3.25: Variation of the solution resistance, double layer capacitance and low frequency capacitance of the PProDOT-Me_2 film deposited electrochemically 5mM ProDOT-Me_2 monomer at 100 mV/s, 10cycle in 0.1 M Bu_4NPF_6/ACN solution.

shows variation of the solution resistance, double layer capacitance and low frequency capacitance of the PProDOT-Me_2 film deposited electrochemically 5mM ProDOT-Me_2 monomer at 100 mV/s, 10cycle in 0.1 M Bu_4NPF_6/ACN solution**.**

Equivalent electrical circuit (Model 2 see Figure 3.26) was constructed without the last component a capacitor element (C_{CF}) and transfer resistor (R_{CF}). Numerical results of the Model 2 are shown in Table 3.7.

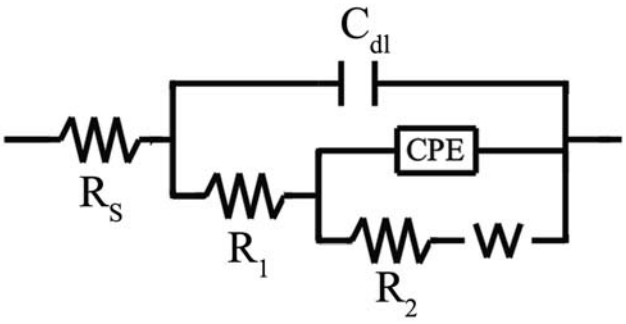

Figure 3.26: Equivalent Eelectrical Ccircuit (Model 2) Used in Simulation.

Table 3.7: Potential dependence of the parameters calculated from the Model 2 which is given Figure 3.22. (5mM ProDOT-Me_2 monomer deposited by electrochemically at 100 mV/s, 10 cycle in 0.1 M Bu_4NPF_6/ACN solution)

	E=0.2V	E=0.4V	E=0.7V	E=1.0V	E=1.3V
R_s / Ohm	1851	1852	1851	1851	1861
C_{dl} / F	$7.381x10^{-5}$	$1.026x10^{-4}$	$7.885x10^{-5}$	$6.798x10^{-5}$	$5.775x10^{-5}$
R_1 / Ohm	3659	47170	502.1	440.3	2901
Q / Y_o/ S s^{-n}	$3.88x10^{-5}$	$4.824x10^{-5}$	$3.167x10^{-5}$	$2.875x10^{-5}$	$3.126x10^{-5}$
n	0.9491	0.9664	0.9619	0.9595	0.9495
R_2 / Ohm	$1.041x10^{6}$	631800	$1.077x10^{6}$	$1.117x10^{6}$	$1.342x10^{6}$
W / Y_o/ S s^{-n}	$2.771x10^{-6}$	$5.434x10^{-6}$	$2.987x10^{-6}$	$2.941x10^{-6}$	$9.237x10^{-6}$
Chi Squared (χ^2)	$3.49x10^{-5}$	$5.38x10^{-5}$	$3.71x10^{-5}$	$3.60x10^{-5}$	$4.74x10^{-5}$

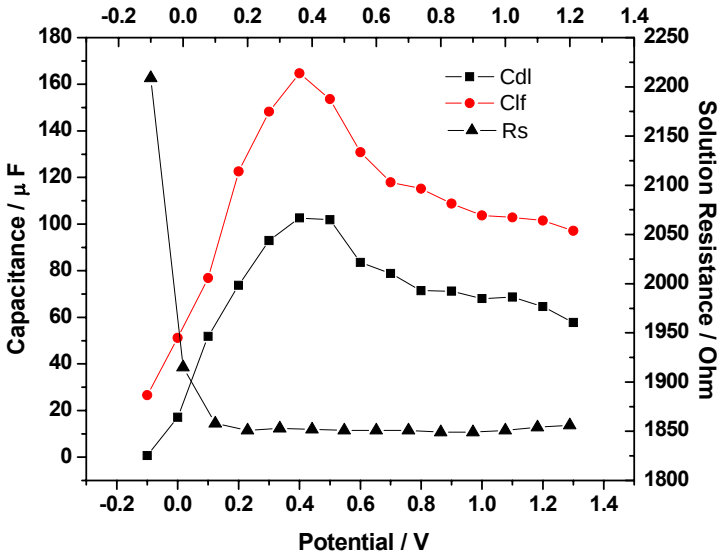

Figure 3.27: Variation of the solution resistance, double layer capacitance and low frequency capacitance of the PProDOT-Me_2 film deposited electrochemically 5mM ProDOT-Me_2 monomer at 100 mV/s, 10 cycles in 0.1 M Bu_4NPF_6/ACN solution.

Figure 3.27 shows variation of solution resistance, double layer capacitance and low frequency capacitance of the PProDOT-Me_2 film. Rs is almost constant and it is independent of Edc. The values of Rs, Edc between -0.1 V and 1.3 V are as follows about 1852 Ω. The solution resistance Rs was found to be inversely proportional to the concentration of the supporting electrolyte for PEDOT. Furthermore, Rs is practically independent of film thickness and Edc. These experimental results allow us to describe Rs as the solution resistance.

3.3.4 Electrolyte and Solvent Effects on ProDOT-Me_2 coated CFMEs; An EIS Investigation

Figure 3.28 shows variation of low frequency capacitance values in different electrolyte that solvent was ACN of PProDOT-Me_2 film. CFME/ PProDOT-Me_2 film has capacitance values higher in tetrabuthylammoniumhexafluorophosphate (Bu_4NPF_6) and tetrabuthylammoniumtetrafluoroborate (Bu_4NBF_4) compared to tetraethylammonium hexafluorophosphate (Et_4NPF_6) and tetraethylammoniumtetrafluoroborate (Et_4NBF_4).

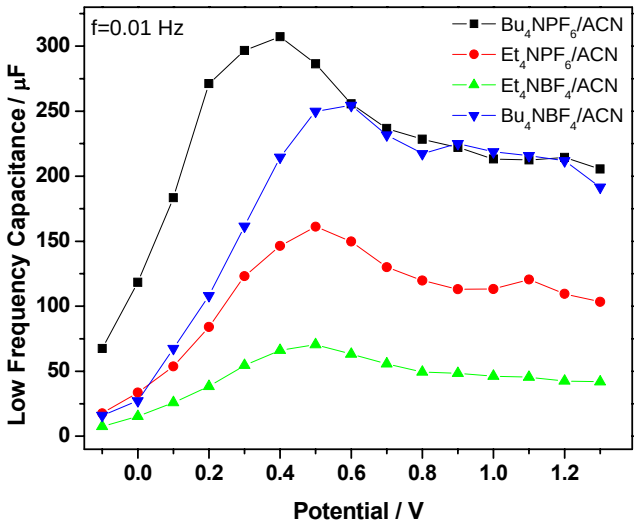

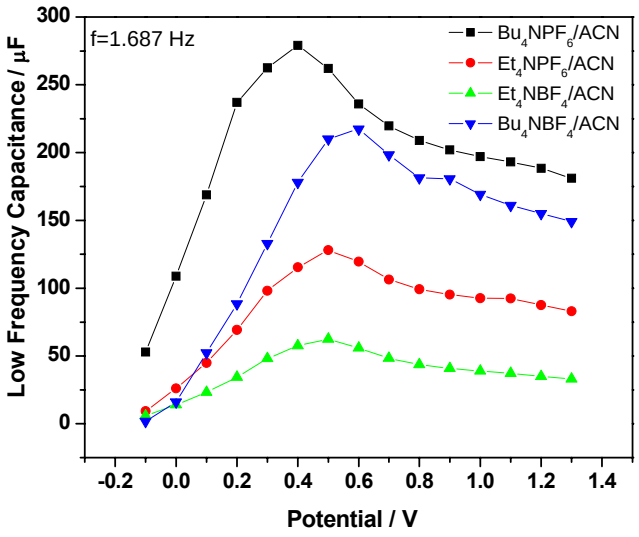

Figure 3.28: Variation of low frequency capacitance of the PProDOT-Me_2 film in **a)** 10 mHz **b)** 1687 mHz deposited electrochemically 5mM ProDOT-Me_2 monomer at 100 mV/s, 20 cycle in Bu_4NPF_6/ACN, Et_4NPF_6/ACN, Bu_4NBF_4/ACN, Et_4NBF_4/ACN solutions.

Figure 3.29 shows variation of low frequency capacitance values in different solvents of PProDOT-Me_2 film. CFME/ PProDOT-Me_2 film has capacitance values higher in asetonitrile (ACN) compared to propylene (PC) and dimethyl formamide (DMF). Shape of the capacitance curves at various potentials in ACN, PC and DMF exhibits similar fashion. The peak which is observed at around 0.4V in ACN, PC and DMF solvents exhibits higher specific capacitance at corresponding to the oxidation peak of the polymer (see Figure 3.9).

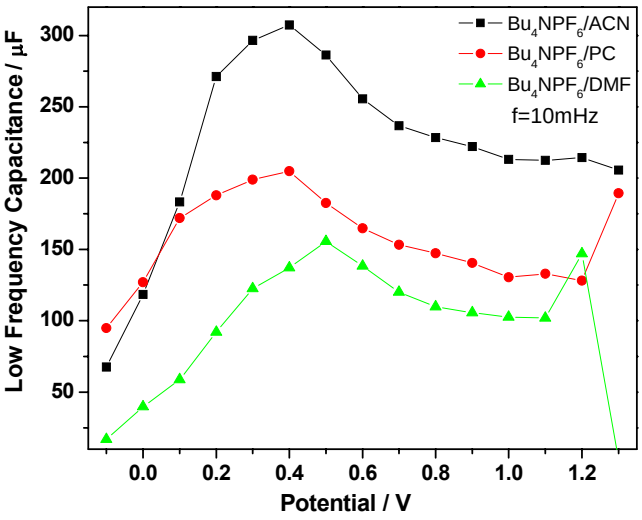

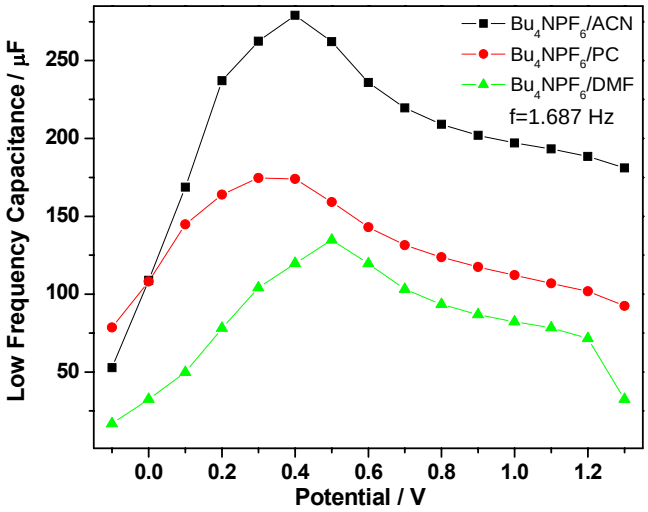

Figure 3.29: Variation of low frequency capacitance of the PProDOT-Me_2 film in **a)**10 mHz, **b)** 1687 Hz deposited electrochemically 5mM ProDOT-Me_2 monomer at 100 mV/s, 20 cycle in 0.1 M Bu_4NPF_6/ACN

3.3.5 Cycle Effects on ProDOT-Me_2 coated CFMEs; An EIS Investigation

Figure 3.30 shows the Nyquist plot at 0.4V for a PProDOT-Me_2 film deposited at 100 mV/s, in 0.1 M Bu_4NPF_6/ACN solution and Figure 3.31 shows the Bode phase angle of PProDOT-Me_2 film prepared under with different charges by application of different scan numbers during the electropolymerization. (5, 10, 20, 30 cycle) with all plots showing a high capacitance (high Bode phase angle about 90^o). Figure 3.29 shows the Bode magnitudeof Z, capacitance behavior increase with the increasing applied charges in the low frequencies.

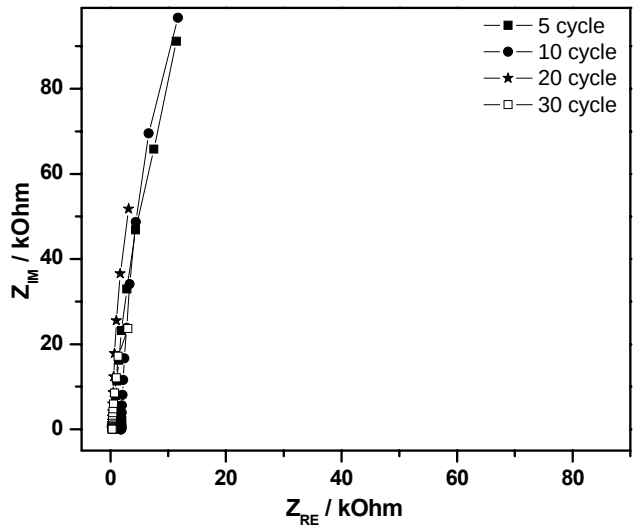

Figure 3.30: Nyquist plots at 0.4 V for a PProDOT-Me_2 film deposited at 100 mV/s, in 0.1 M Bu_4NPF_6/ACN solution

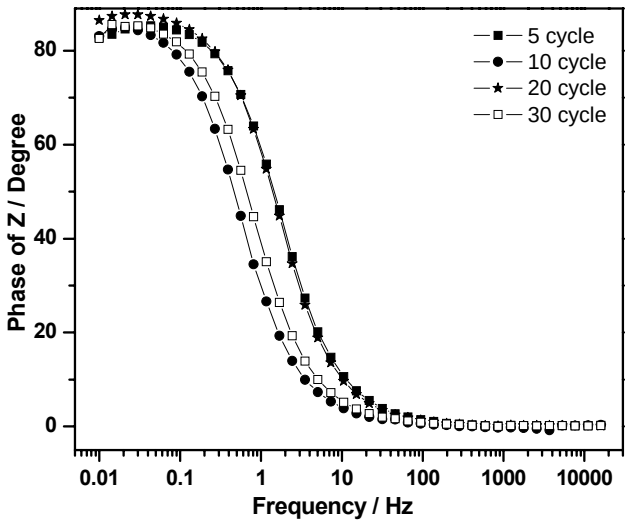

Figure 3.31: Bode phase angle at 0.4 V for a PProDOT-Me_2 film deposited at 100 mV/s, in 0.1 M Bu_4NPF_6/ACN solution

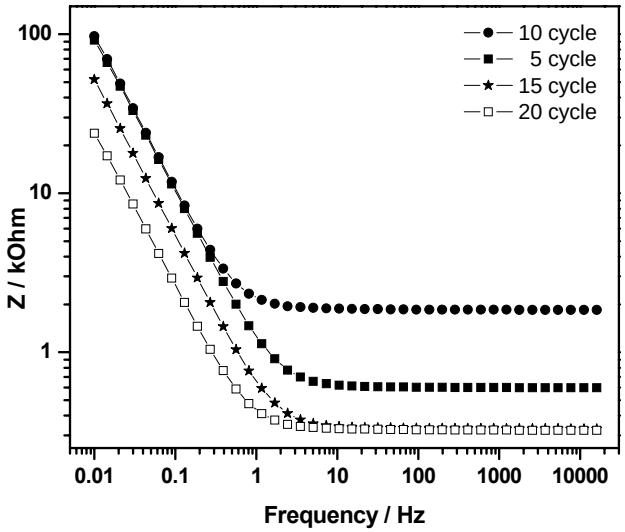

Figure 3.32: Bode magnitude of Z at 0.4 V for a PProDOT-Me_2 film deposited at 100 mV/s, in 0.1 M Bu_4NPF_6/ACN solution

Table 3.8: Deposition charge dependence calculated for PProDOT-Me_2 film 5mM ProDOT-Me_2 in 0,1M Bu4NPF6/ACN monomer free solution (0.4V DC potential) (Model 2 was performed)

	5 Cycle Q=2.080mC	10 Cycle Q=2.457mC	15 Cycle Q=2.496mC	20 Cycle Q=5.540mC	25Cycle Q=6.350mC	30 Cycle Q=13.56mC
R_s / Ohm	599.8	1852	1281	330.6	521.2	323.8
C_{dl} / F	$1.192x10^{-4}$	$1.026x10^{-4}$	$1.117x10^{-4}$	$2.22x10^{-4}$	$1.066x10^{-4}$	$3.448x10^{-4}$
R_1 / Ohm	46.43	47170	739.4	106.9	43	39.28
Q / Y_o/S s^{-n}	$3.374x10^{-5}$	$4.824x10^{-5}$	$3.343x10^{-5}$	$6.993x10^{-5}$	$8.998x10^{-5}$	$2.587x10^{-4}$
n	0.923	0.9664	0.8	0.9532	0.9648	0.9665
R_2/ Ohm	353000	631800	576300	1.411x106	514900	163600
W / Y_o/S s^{-n}	$6.07x10^{-6}$	$5.434x10^{-6}$	$4.458x10^{-6}$	$5.558x10^{-6}$	$9.961x10^{-6}$	$2.118x10^{-5}$
Chi Squared (χ^2)	$4.66x10^{-5}$	$5.37x10^{-5}$	$3.5x10^{-5}$	$4.14x10^{-5}$	$5.50x10^{-5}$	$9.48x10^{-5}$

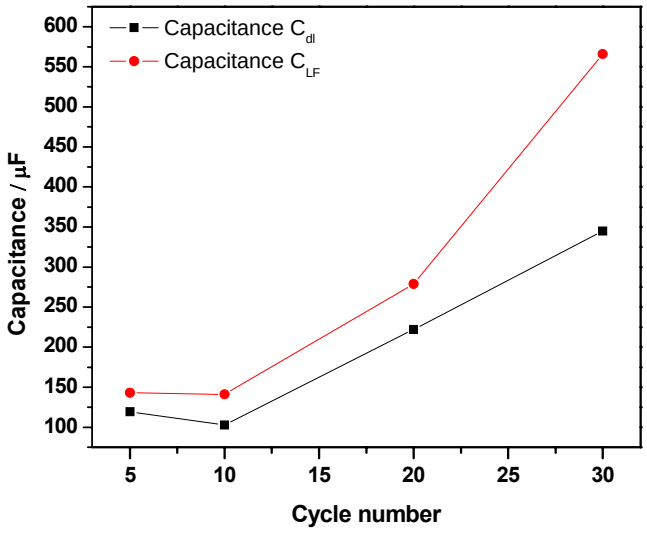

Figure 3.33: Variation of the double layer capacitance and low frequency capacitance of the PProDOT-Me_2 film deposited electrochemically 5mM ProDOT-Me_2 monomer at 100 mV/s, in 0.1 M Bu_4NPF_6/ACN solution in different cycle.

Figure 3.33 shows the variation of the double layer capacitance and low frequency capacitance of the PProDOT-Me_2 film obtained in different cycle. At maximum low capacitance value observed in 30 cycle is about 570 µF.

3.4 Morphology of Coatings

3.4.1 Morphology of coatings for different applied charge densities

The polymers of ProDOT-$(Me)_2$ on the CFME were grown under different scan parameters by potentiodynamic depositions, from the solution of 0,1 M Bu_4NPF_6/ACN containing 0.01M ProDOT-$(Me)_2$. The morphologies of thin P ProDOT-$(Me)_2$ coatings on CFMEs were investigated comparatively by scanning electron microscopy (SEM) (Figure 3.34).

A thin coating on the CFME was obtained for the 5th cycle, when comparing uncoated and coated fiber (after 5 cycles) longitudinal striations of carbon fiber can still be seen (Figure 3.34 and 3.35).

Porous and thicker polymer coatings can be observed after higher charge applications (20th cycle) (Figure 3.35).

Applying higher charges (more scan numbers) does not lead to increase in the diameter linearly but empty spaces of nanospheroidal (even nanooctameroidal) fibrous polymeric chain network starts to fill with more compact polymeric material.(Figure 3.36)

A porous structure resulting from a three dimensional nucleation growth is observed. The SEM picture of PProDOT-$(Me)_2$ films shows clusters of globules or pores with avoid space between.

The SEM pictures show a pronounced difference in the surface morphology of the two type of different PProDOT-$(Me)_2$ layers. In the beginning, after very thin film formation on CFME, where striations disappear on the whole surface area, at low electropolymerization scan rates coated polymeric layer shows a polymer network with a highly porous structure which might entrap dopant ions and/or immobilizing agents (for biosensor applications).

The porous thin layer obtained under the small electropolymerization charges has shown almost an octamer shaped structure with a size of ~ 100 nm. Such porous structure was followed by filling with more compact material at high scan rates where polymer build up continuous inside the porous structure.

Formation of thin films of PProDOT-Me_2 on Carbon fiber gives the property of flexibility of chains. A more open, or less dense, polymer morphology will allow more dopant ions to be accommodated within the film resulting highly charged state.

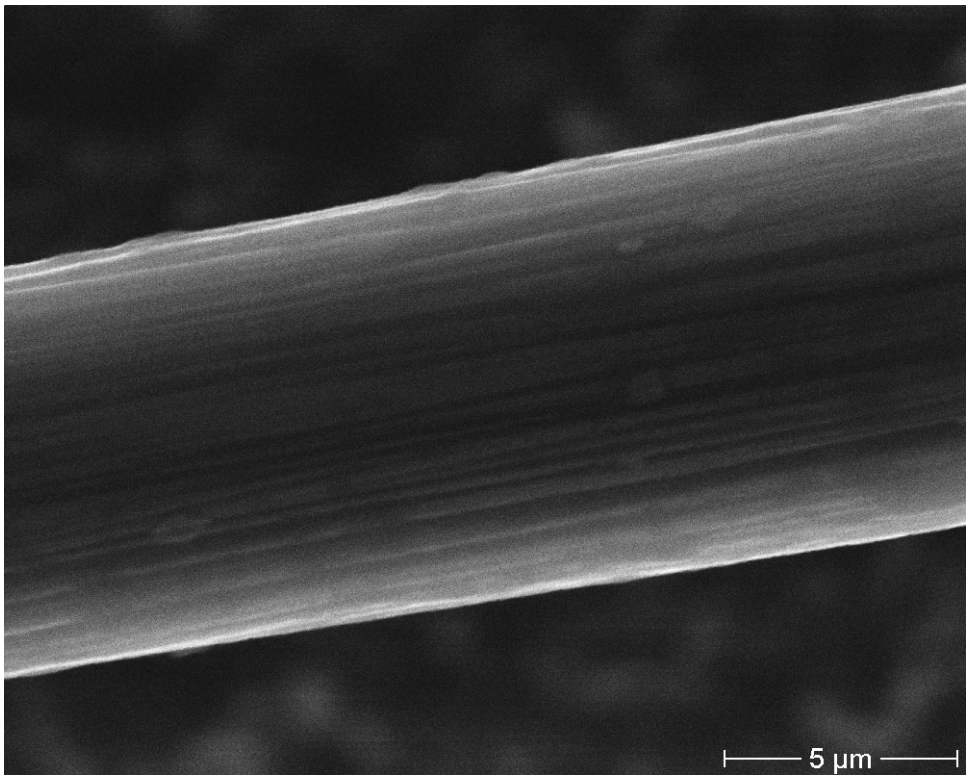

Figure 3.34: SEM picture of an uncoated carbon fiber microelectrode.

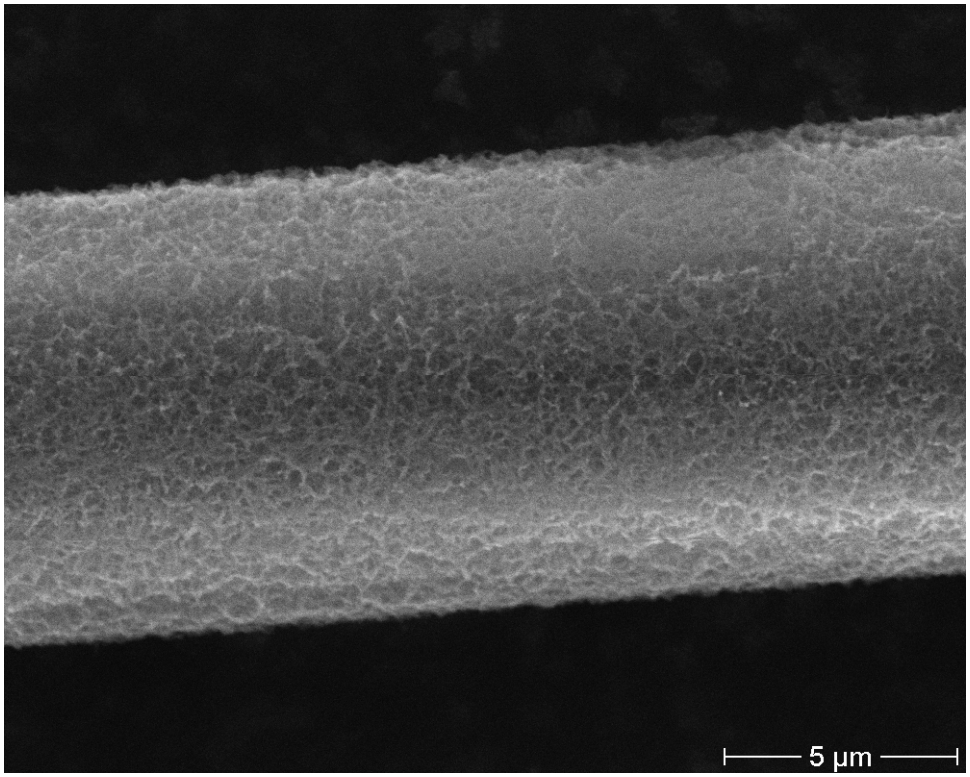

Figure 3.35: SEM of 20th cycle coated CFME.

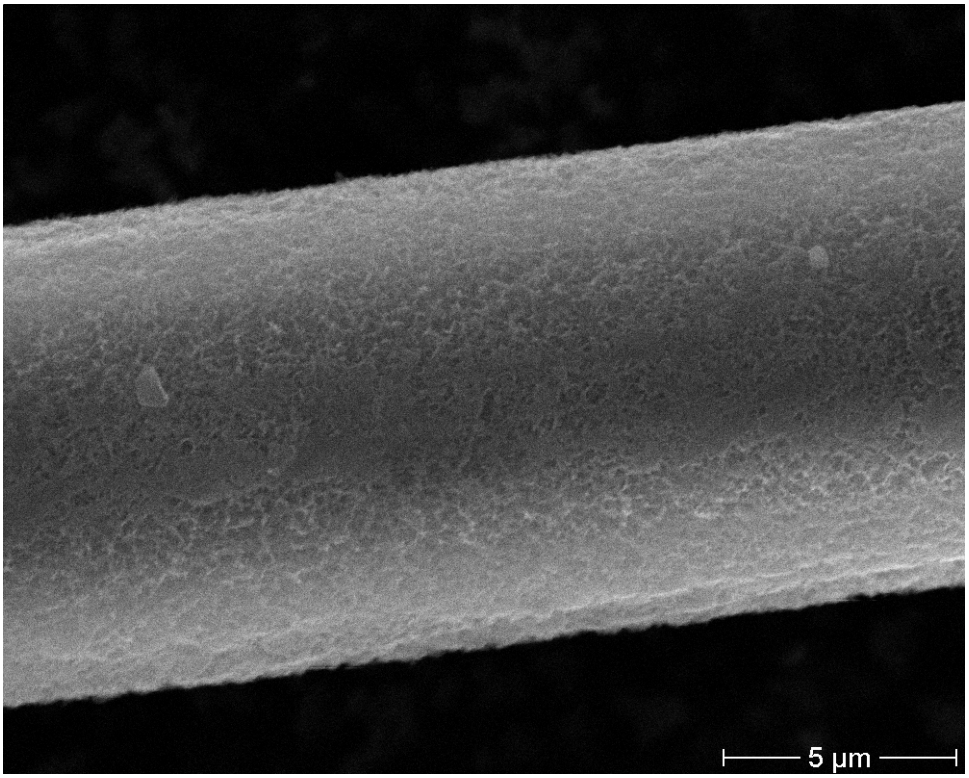

(a)

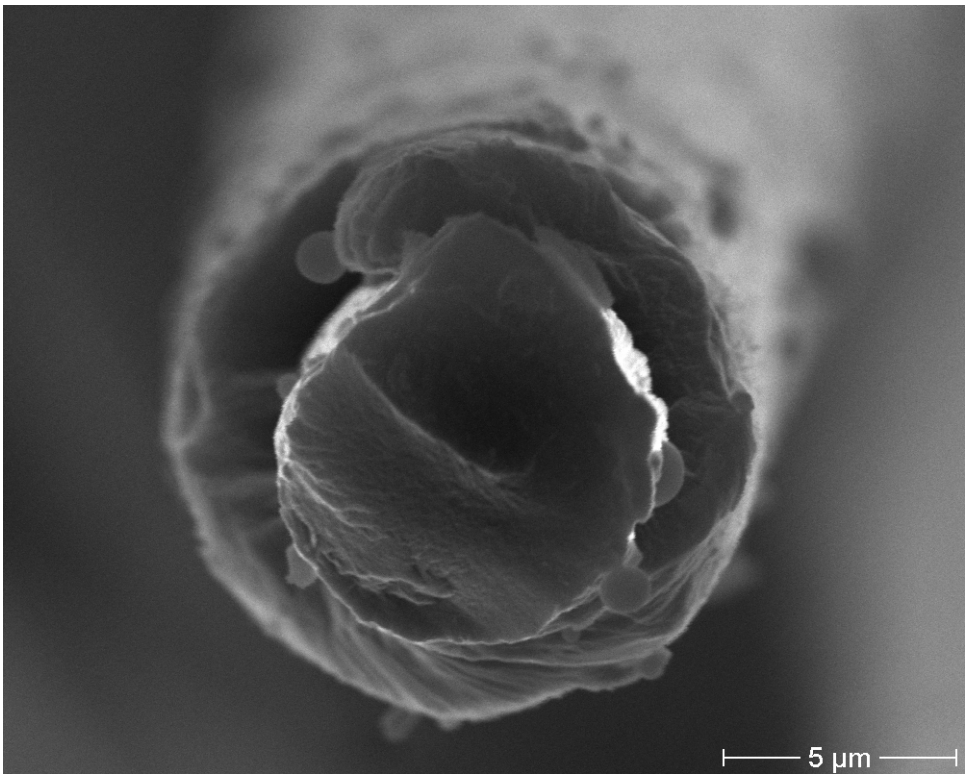

(b)

Figure 3.36 : SEM of (a) 40th cycle coating, and (b) cross section of 40th cycle

EDX examination of PProDOT-Me_2/ CFME coated at 40th cycle (results not shown here) clearly indicates the presence of S in PProDOT-Me_2 on the carbon fiber

surface, during the electrocoating process, a further oxidation of polymer film leads to positively charged polaron and bipolarons. Depending on the extent of PProDOT-Me_2 film oxidation, these sites will be doped by the anion of supporting electrolyte (PF_6^-). The presence of phosphorous and fluorine in the coated fiber surfaces supports this idea.

3.4.2 Morphology of coatings and EDX results for different scan rates

PProDOT-Me_2 coated CFMEs for SEM were prepared by Cyclovoltametric electropolymerisation under different scan rates at the same potential range 0-1.6 V. keeping the working electrode surface area constant. The SEM pictures (Figure 3.37) show a pronounced difference in the surface morphology of the two different P ProDOT-$(Me)_2$ layers at low electropolymerization scan rates, coated polymeric layer shows a polymer network with a highly porous structure which might entrap dopant ions and/or immobilizing agents (for biosensor applications).

For different rates under conditions applied in this work, only 20mV/s scan rate showed a porous structure and at higher scan rates thin coatings were obtained with a decreasing thickness. But at 10 mV/s the rate of electron transfer was slow, so first porous and than bulky island coating was obtained on the surface and inside of the pores, In contrast to high scan rates, (at 20 mV/s) the porous thin layer obtained under the small electropolymerization charges has shown almost an octamer shaped structure with a size of ~ 100 nm. Such porous structure was followed by filling with more compact material at high scan rates where polymer build up continious inside the porous structure.In the beginning ,after very thin film formation on CFME, where striations disappear on the whole surface area. These observations supports our suggestion for the role of the use and activation on PProDOT-$(Me)_2$ layers synthesised under certain cycle numbers, scan rates and other conditions .It is interesting to note that the polymerisation of this porous polymer network in the case of certain electropolymerization charge could still be described by a simple model for instantaneous ‘nucleation’ and 3D growth as a porous structure, i.e., at 20 mV/s scan rates.

The presence alkylenedioxy group and tetrahedral substitution pattern of PProDOT-$(Me)_2$ by causing the methyl groups to be positioned above and below the plane of

the π-conjugated chain which can allow high doping levels and inhibit π-stacking.[50]

Formation of thin films of PProDOT-Me_2 on Carbon fiber gives the property of flexibility of chains. A more open, or less dense, polymer morphology will allow more dopant ions to be accommodated within the film resulting highly charged state.

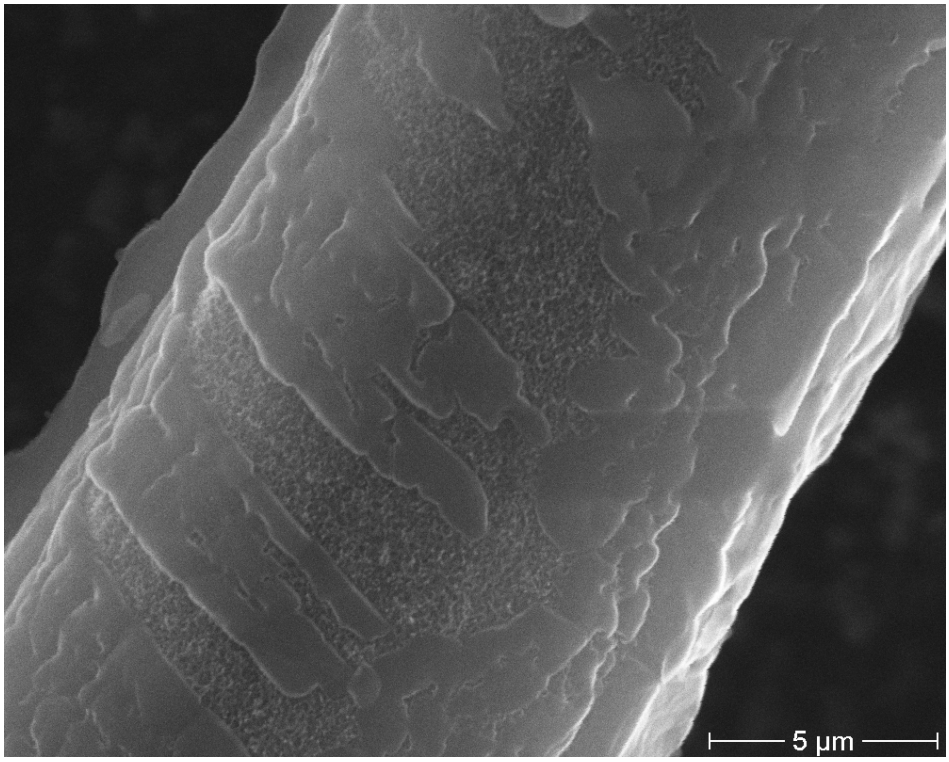

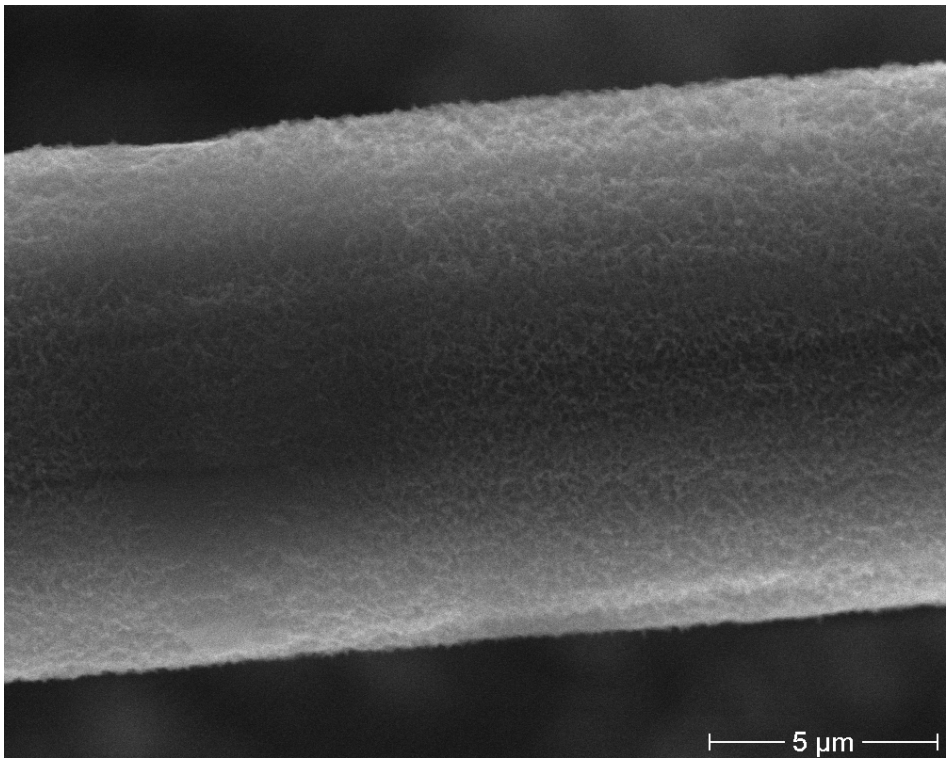

Figure 3.37: SEM picture of 10mV/s (a), 20 mV/s (b)

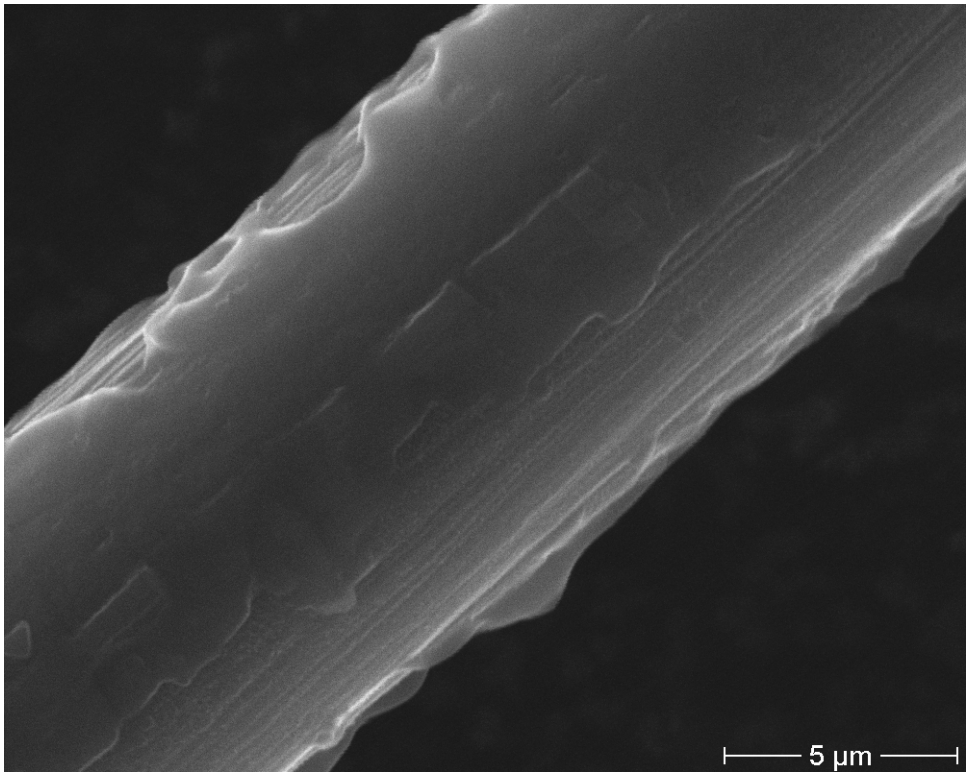

Figure 3.38: SEM picture of 50 mV/s (c) 400 mV/s (d)

4 CONCLUSIONS

This thesis 1-(4-Methylphenyl)-1H-pyrrole and 2,2-Dimethyl-3,4-propylenedioxythiophene monomers were performed onto carbon fiber micro electrode by electrochemical polymerization and electrochemical characterizations and morpholological studies. Testing the polymer film in the use electrochromic device construction and polymer electrode on CFME as an active electrode material in supercapacitor applications are the final step in my thesis.

Firstly electrochemical polymerizations of 1-(4-Methylphenyl)-1H-pyrrole and 2,2-Dimethyl-3,4-propylenedioxythiophene monomers were succesfully carried out. Effect of electrolyte at the polymerization was investigated in 1-(4-Methylphenyl)-1H-pyrrole monomer.

Electrochemical Impedance Spectroscopy is a powerful tool for the analysis of electrochemical system. This technique was used to explained electrochemical characteristics of the polymer electrodes like resistance, capacitance and impedance. Two electrical equivalent circuits corresponding to the polymer electrodes and calculated values of the each component of these circuit using a simulation program which found aggrements with experimental and calculation data.

Device properties based on PProDOT-Me_2 were checked with the spectroelectrochemical measurements. Typical CV of the polymeric film exhibits very well-defined and reversible redox processes. The impedance study on specific capacitance values observed.

Two equivalent circuits were used in simulation of the impedance behavior of the polymer films from the experimentally obtained impedance data. The model 2 was used in the electroactive region. These electrical equivalent circuit was succesfully applied to the experimental data to explain interface between carbon fiber microelectrode the polymer and the electrolyte in potential region.

Morphology of the resulting polymer shows that thickness of the polymer film is a function of number of cycles and increases with the number of deposition charge during the electropolymerization.

REFERENCES

[1] **Shirakawa, H., Louis, E. J., Macdiarmid, A.G., Chiang, C. K. and Heeger, A.J.,** Synthesis of Electrically Conducting Organic Polymer- Halogen Derivatives of Polyacetelene, (Ch.X),

[2] **Jean Roncali**, 1999 Electrogenerated Functional Conjugated Polymers as Advanced Electrode Materials. *Journal of Materials Chemistry* 9 (9): 1875-1893

[3] **Dall'Olio, A., Dascola, Y., Varacco, V. and Bocchi, C. R.,** 1968. CRC Seances Acad. Sci. Ser. C, 466.

[4] **Schnoller, M., Wersing, W. and Naarman, H.,** 1987. Intrinsically Conductive Organic Polymers as Electrode Material for Functional Ceramics in Electronics, *Makromolekulare Chemie-Macromolecular Symposia*, **8**, 83-95

[5] **J. Roncali**, 1992, Conjugated Poly(thiophenes) Synthesis, Functionalization, and Applications C*hemical. Reviews***. 92**, (4) 711-738.

[6] **M. Leclerc, G. Daoust, J. Chem.oc**.1990 Desing of New Conducting 3,4-Disubstitited Polythiophenes *Journal of the Chemical Society-Chemical Communications*. 3, 273

[7] **L. B. Groenendal, F. Jonas, D. Freitag, H. Pielartzik, J. R. Reynolds,** 2000 *Advanced Materials***.** Poly(3,4-ethylenedioxythiophene) and Its Derivatives **12** 481;

[8] **G. Tourillon, F. Garnier,** 1984. *Journal of Electroanalytical. Chemistry* 161 1 51-58

[9] d) **M. Dietrich, J. Heinze, G. Heywang, F. Jonas**, 1994 Electrochemical and Spectroscopic Characterization of Polyacetylenedioxythiophenes *Journal* of *Electroanalitical Chemistry*. 369, 87.

[10] **S. A. Sapp, G. A. Sotzing, J. R. Reynolds,** 1998. High contrast ratio and fast-switching dual polymer electrochromic devices *Chemistry of. Materials*. *10*, 2101

[11] **A.Kumar, D. M. Welsh, M. C. Morvant, F. Piroux, K. A. Abboud, J. R. Reynolds,** 1998**.** Conducting poly(3,4-alkylenedioxythiophene) derivatives as fast electrochromics with high-contrast ratios *Chemistry of Materials*. 10, 896

[12] **E. Havinga, C. M. Mutsaers, L. W. Jenneskens, 1996.** Absorption Properties of Alkoxy-Substituted Thienylene-Vinylene Oligomers as a Function of the Doping Level *Chemistry of. Materials*. 8, 769.

[13] **L. Groenendaal, G. Zotti, F. Jonas**, 2001. Optical, conductive and magnetic properties of electrochemically prepared alkylated poly(3,4-ethylenedioxythiophene)s, *Synthetic Metals***.** 118, 105.

[14] **B. Sankaran, J. R. Reynolds,** 1997. High-Contrast Electrochromic Polymers from Alkyl-Derivatized Poly(3,4-ethylenedioxythiophenes) *Macromolecules*, 30, 2582.

[15] **C. L. Gaupp, D. M. Welsh, J. R. Reynolds,** 2002. Poly(ProDOT-Et_2): A High-Contrast, High-Coloration Efficiency Electrochromic Polymer *Macromoleculer Rapid Communications*. 23, 885.

[16] **D. M. Welsh, L. J. Kloeppner, L. Madrigal, M. R. Pinto, K. S. Schanze, K. A. Abboud, D. Powell, J. R. Reynolds**, 2002. Regiosymmetric Dibutyl-Substituted Poly(3,4-propylenedioxythiophene)s as Highly Electron-Rich Electroactive and Luminescent Polymers *Macromolecules*, 35, 6517.

[17] **Bard, A. J. and Faulkner, L. R.,** 2001. Electrochemical methods**:** fundamentals and applications, John Wiley, New York

[18] **Lyons, M. E. G.,** 1997. *Advances in Chemical Physics*, Polymeric Systems, John Wiley&Sons New York

[19] **Sarac, A. S., Serantoni, M., Tofail, S. A. M. and Cunnane, V. J**., 2004 Morphologial and spectroscopic analyses of poly [N-Vinylcarbazole-co-vinylbenzenesulfonic acid] copolymer electrografted on carbon fiber: the effect of current density, *Applied Surface Science*, 229, 13, 18

[20] **Sarac, A. S., Serantoni , M., Tofail, S. A. M. and Cunnane, V. and Mcmonagle, J, B.,** Characterization of nanosize thin films of electrografted N-vinylcarbazole copolymers (P[NVCz-co-VBSA] and P[NVCz-co-3-MhTh]) onto carbon fiber AFM, XPS, and Raman Spectroscopy, *Applied Surface Science*, 243, 183-198.

[21] **Sonmez, G. and , Sarac, A. S.,** 2003 Structural study of pyrrole-EDOT copolymers on carbon fiber micro-electrodes, *Synthetic Metals*, 135, 459-460.

[22] **Jamal M., Sarac, A. S., and Magner**, **E.**, 2004. Conductive copolymermodified carbon fibre microelectrode: electrode characterization and electrochemical detection of P-aminophenol, Sensors and actuators B-Chemical, 97, 59-66.

[23] **Serantoni, M., Sarac, A. S., and Suddon, D.,** 2005. FIB-SIMS investigation of carbazole-based polymer and coploymers electrocoated onto carbon fibers and an AFM morphological study, *Surface&Coatings Technology,* 194, 36-41.

[24] **Bard, A.J; Faulkner, L. R.** Electrochemicel Methods; Wiley&Sons: New York, 2001; Chapters 3, 5, 7, 10, 13.

[25] **Schmickler W**. Interfacial Electrochemistry; Oxford University Pres: Oxford, 1996.

[26] **Parsons, R.** 1990 The electrical double layer: recent experimental and theoretical developments *Chemical. Reviews*. 90, 813.

[27] **Randles, J. E. B.** 1948 *Trans. Faraday Soc*. 44, 327.

[28] **Pankaj, S.; et al** 1997 *Journal of Electroanalytical Chemistry*. 69,1662.

[29] **Macdonald, J. R.** Impedance Spectroscopy; Wiley- Interscience: New York 1987.

[30] **Sluyters-Rehback, M.; Sluyters, J. H**. 1970. *In Electroanalytical Chemistry*; Bard, A. J., Ed.; Marcel Dekker; New York, Vol. 4.

[31] **De Levie, R.; Husovsky, A. A.** 1969 *Journal of Electroanalytical Chemistry*. 20, 181.

[32] **Armstrong, R. D.; Henderson, M.J**. 1972 *Journal of Electroanalytical Chemistry*. 40, 121

[33] **10- Armstorng, R. D.; Race, W. P.; Thirsk, H. R.** 1974 *Electrochim. Acta*, 19, 215

[34] **S. Kirchmeyer und K. Reuter**, 2005. Scientific importance, properties and growing applications of poly(3,4-ethylenedioxythiophene) *Journal of. Materials. Chemistry*. **15** 2077-2088

[35] **B. Sankaran, J. R. Reynolds**, 1997. High-Contrast Electrochromic Polymers from Alkyl-Derivatized Poly(3,4-ethylenedioxythiophenes) *Macromolecules* **30**, 2582.

[36] **B. Sankaran, J. R. Reynolds**, 1997. High-Contrast Electrochromic Polymers from Alkyl-Derivatized Poly(3,4-ethylenedioxythiophenes) *Macromolecules* **30**, 2582.

[37] **G. Rauchschwalbe, F. Jonas,** 2001. Gallium Complexes in Three-Layer Organic Electroluminescent Devices *Advanced Materials, 1811*

[38] **M. Welsh, A. Kumar, E. W. Meijer, J. R. Reynolds**, 1999. *Advanced Materials*. 11, No. 16 ,1379-1382

[39] **C. L. Gaupp, D. M. Welsh und J. R. Reynolds**, 2002. Poly(ProDOT-Et_2): A High-Contrast, High-Coloration Efficiency Electrochromic Polymer *Macromolecules. Rapid Communications*. **23**, 885-889

[40] **B. C. Thompson, P. Schottland, K. Zong und J. R. Reynolds**, 2000. In Situ Colorimetric Analysis of Electrochromic Polymers and Devices *Chemistry.of Materials*. **12**, 1563-1571

[41] **L. Gaupp, D. M. Welsh, R. D. Rauh und J. R. Reynolds**, 2002. Composite Coloration Efficiency Measurements of Electrochromic Polymers Based on 3,4-Alkylenedioxythiophenes *Chemistry.of Materials* **.** 14, 3964-3970

[42] **A. Argun und J. R. Reynolds**, 2005. Line patterning for flexible and laterally configured electrochromic devices *Journals of. Materials. Chemistry*. **15**, 1793-1800

[43] **H. J**. **Yang, A. J. Bard,** 1992. The Application of Fast Scan Cyclic Voltametry - Mechanistic Study of the Initial-Stage of Electropolymerization of Aniline in Aqueous-Solutions *Journal of Electroanalytical Chemistry*. 339, 423.

[44] **M.Dietrich, J. Heinze, G. Heywang, F. Jonas**, 1994. Electrochemical and Spectroscopic Characterization of Polyalkylenedioxythiophenes *Journal Electroanalytical. Chemistry*., 369 87-92

[45] **By L. 'Bert' Gronendaal, Gianni Zotti, Pierre-Henri Aubert, Shane M. Waybright, and John Reynolds**, *Advanced Materials*

[46] **A. Kumar, D.M. Welsh, M. C. Morvant, F. Piroux, K. A. Abboud, J. R. Reynolds,** 1998. Conducting Poly(3,4-alkylenedioxythiophene) Derivatives as Fast Electrochromics with High-Contrast Ratios *Chemistry of. Materials*. **10**, 896.

[47] **Randriamahazaka H, Plesse C., Teyssie D., Chevrot C.,** 2004. Ions transfer mechanisms during the electrochemical oxidation of poly(3,4-ethylenedioxythiophene) in 1-ethyl-3-methylimidazolium bis((trifluoromethyl)sulfonyl)amide ionic liquid *Electrochemistry communications,* **6,** *299-305*

[48] **Fiordiponti, P. And Pistoia, G.,**1989. An Impedance Study of Polyaniline Films in Aqueous and Organic Solutions, *Electrochimica Acta,* **34**, 215-221.

[49] **Johan Bobacka *, Andrzej Lewenstam, Ari Ivaska**

[50] **C. L. Gaupp, D. M. Welsh und J. R. Reynolds,** 2002. Poly(ProDOT-Et_2): A High-Contrast, High-Coloration Efficiency Electrochromic Polymer *Macromolecules Rapid Communications*. **23**, 885-889

APPENDICES

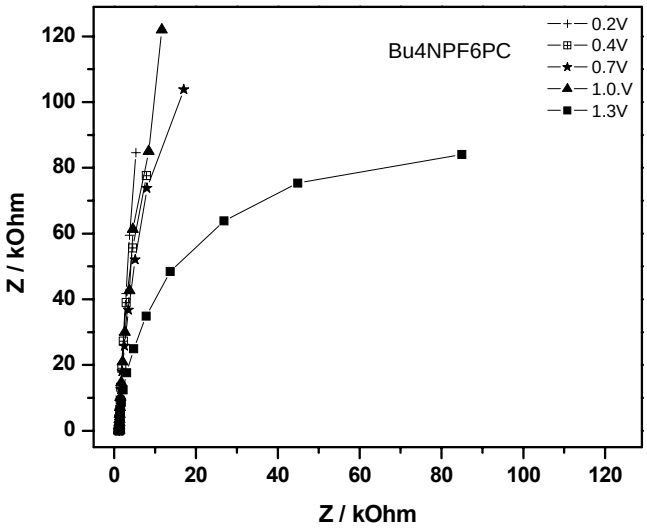

Figure B 1: Nyquist plot at -0.1V to 1.3V for a PProDOT-Me_2 film deposited at 100 mV/s, 20cycle in 0.1 M Bu_4NPF_6/ACN solution and EIS measurements were performed in 0.1 M Bu_4NPF_6/PC solution

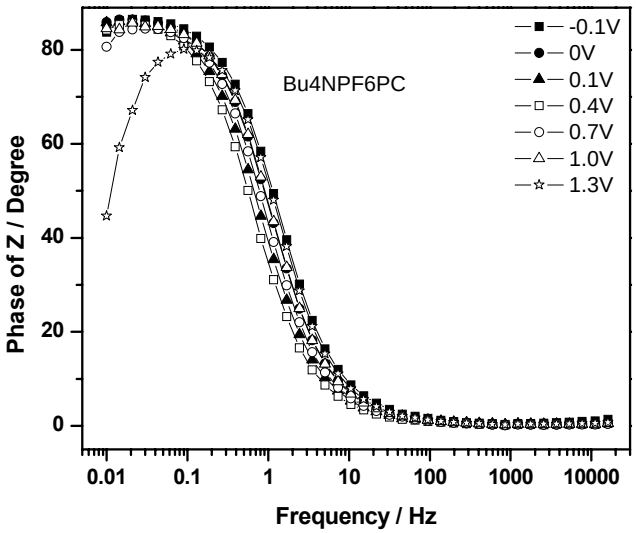

Figure B 2: Bode phase angle at -0.1V to 1.3V for a PProDOT-Me_2 film deposited at 100 mV/s, 20cycle in 0.1 M Bu_4NPF_6/ACN solution and EIS measurements were performed in 0.1 M Bu_4NPF_6/PC solution

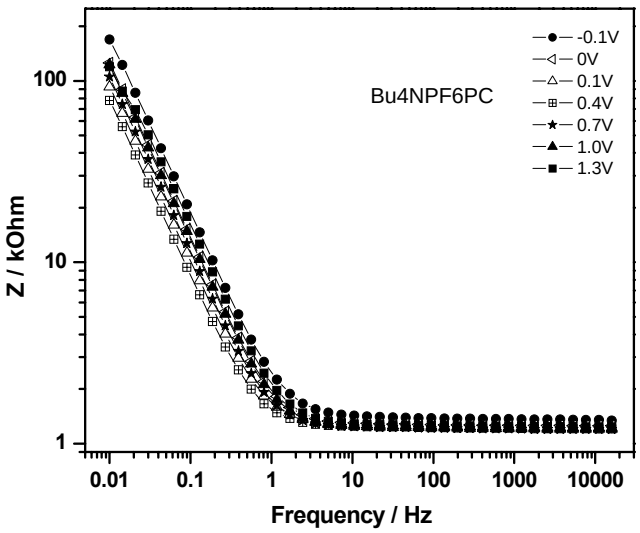

Figure B 3: Bode magnitude of Z at -0.1V to 1.3V for a PProDOT-Me_2 film deposited at 100 mV/s, 20cycle in 0.1 M Bu_4NPF_6/ACN solution and EIS measurements were performed in 0.1 M Bu_4NPF_6/PC solution

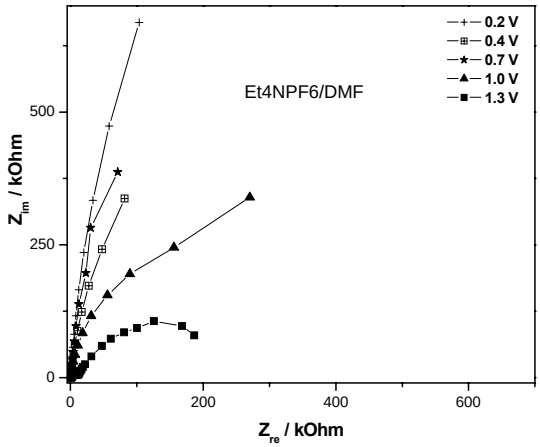

Figure B 4: Nyquist plot at -0.1V to 1.3V for a PProDOT-Me_2 film deposited at 100 mV/s, 20 cycle in 0.1 M Et_4NPF_6/ACN solution and EIS measurements were performed in 0.1 M Et_4NPF_6/DMF solution

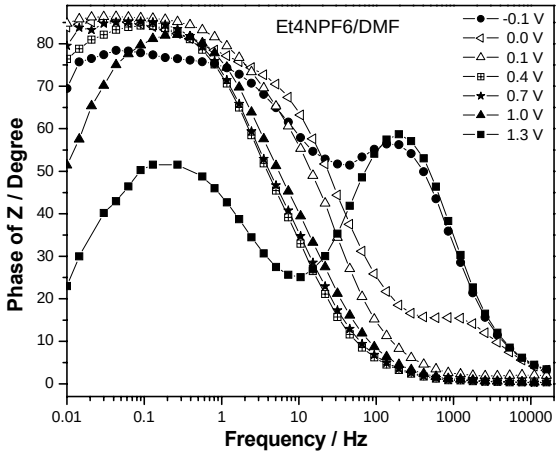

Figure B 5: Bode phase angle at -0.1 V to 1.3 V for a PProDOT-Me_2 film deposited at 100 mV/s, 20 cycle in 0.1 M Et_4NPF_6/ACN solution and EIS measurements were performed in 0.1 M Et_4NPF_6/DMF solution

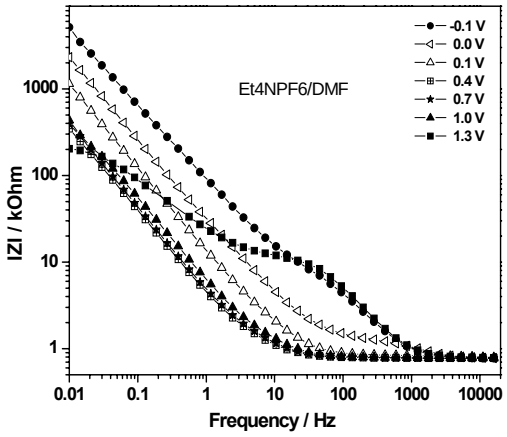

Figure B 6: Bode magnitude of Z at -0.1 V to 1.3 V for a PProDOT-Me_2 film deposited at 100 mV/s, 20 cycle in 0.1 M Et_4NPF_6/ACN solution and EIS measurements were performed in 0.1 M Et_4NPF_6/DMF solution

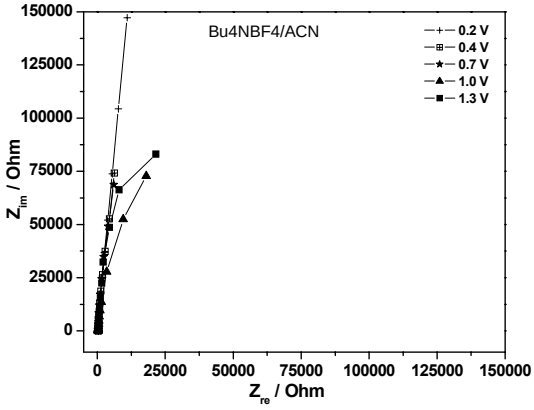

Figure B 7: Nyquist plot at 0.2 V to 1.3 V for a PProDOT-Me_2 film deposited at 100 mV/s, 20 cycle in 0.1 M Bu4NBF4/ACN solution and EIS measurements were performed in 0.1 M Bu_4NBF_4/ACN solution

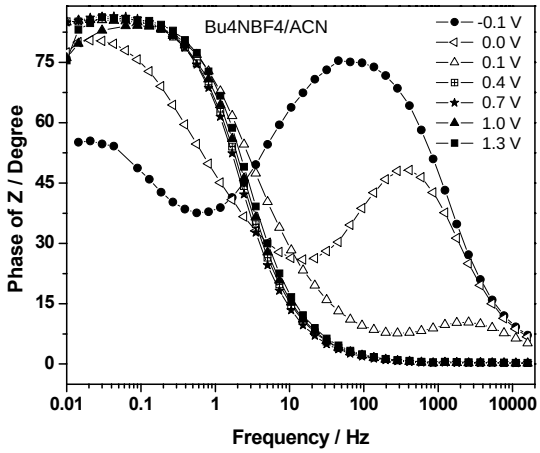

Figure B 8: Bode phase angle plot at -0.1 V to 1.3 V for a PProDOT-Me_2 film deposited at 100 mV/s, 20 cycle in 0.1 M Bu_4NBF_4/ACN solution and EIS measurements were performed in 0.1 M Bu_4NBF_4/ACN solution

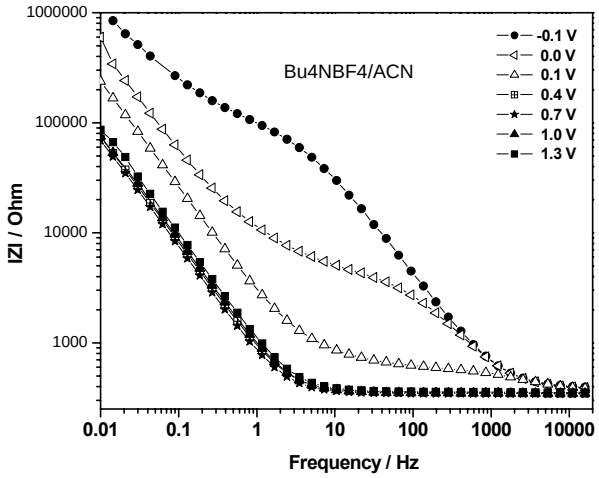

Figure B 9: Bode magnitude of Z at -0.1 V to 1.3 V for a PProDOT-Me_2 film deposited at 100 mV/s, 20 cycle in 0.1 M Bu_4NBF_4/ACN solution and EIS measurements were performed in 0.1 M Bu_4NBF_4/ACN solution

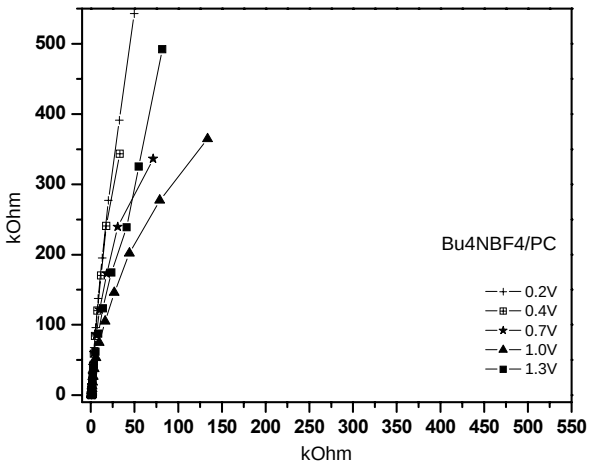

Figure B 10: Nyquist plot at 0.2 V to 1.3 V for a PProDOT-Me_2 film deposited at 100 mV/s, 20 cycle in 0.1 M Bu_4NBF_4/ACN solution and EIS measurements were performed in 0.1 M Bu_4NBF_4/PC solution

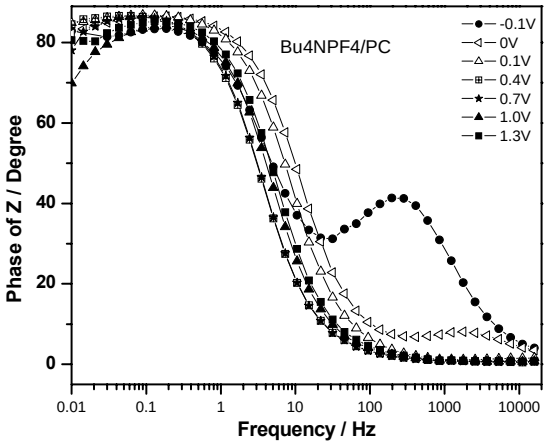

Figure B 11: Bode phase angle plot at 0.2 V to 1.3 V for a PProDOT-Me_2 film deposited at 100 mV/s, 20 cycle in 0.1 M Bu_4NBF_4/ACN solution and EIS measurements were performed in 0.1 M Bu_4NBF_4/PC solution

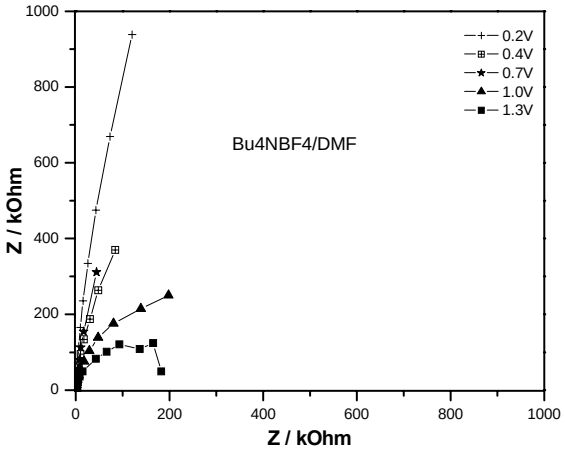

Figure B 12: Nyquist plot at 0.2 V to 1.3 V for a PProDOT-Me_2 film deposited at 100 mV/s, 20 cycle in 0.1 M Bu_4NBF_4/ACN solution and EIS measurements were performed in 0.1 M Bu_4NBF_4/DMF solution

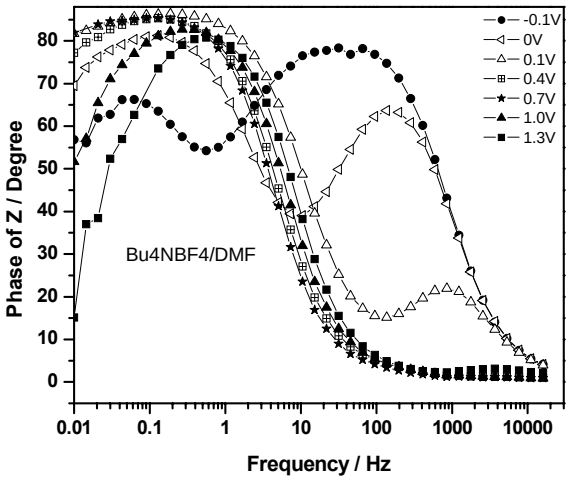

Figure B 13: Bode phase angle plot at -0.1 V to 1.3 V for a PProDOT-Me_2 film deposited at 100 mV/s, 20 cycle in 0.1 M Bu_4NBF_4/ACN solution and EIS measurements were performed in 0.1 M Bu_4NBF_4/DMF solution

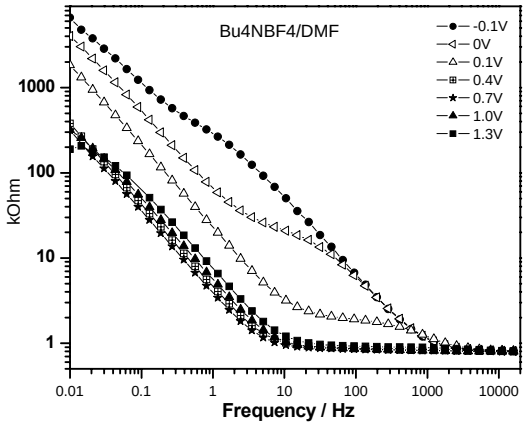

Figure B 14: Bode magnitude of Z plot at 0.2 V to 1.3 V for a PProDOT-Me_2 film deposited at 100 mV/s, 20 cycle in 0.1 M Bu_4NBF_4/ACN solution and EIS measurements were performed in 0.1 M Bu_4NBF_4/DMF solution

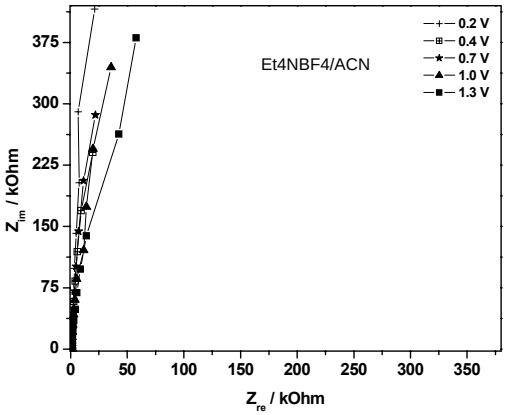

Figure B 15: Nyquist plot at 0.2 V to 1.3 V for a PProDOT-Me_2 film deposited at 100 mV/s, 20 cycle in 0.1 M Et_4NBF_4/ACN solution and EIS measurements were performed in 0.1 M Et_4NBF_4/ACN solution

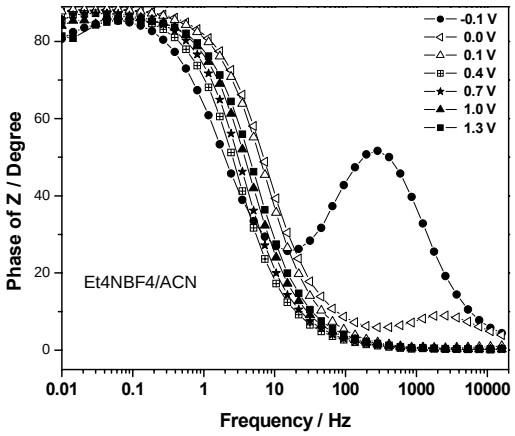

Figure B 16: Bode phase angle plot at 0.2 V to 1.3 V for a PProDOT-Me_2 film deposited at 100 mV/s, 20 cycle in 0.1 M Et_4NBF_4/ACN solution and EIS measurements were performed in 0.1 M Et_4NBF_4/ACN solution

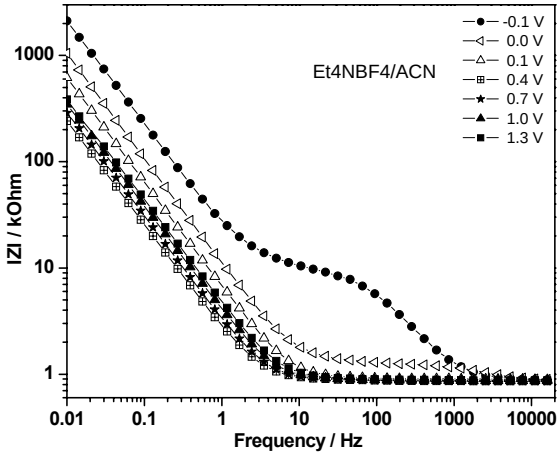

Figure B 17: Bode magnitude of Z plot at -0.1 V to 1.3 V for a PProDOT-Me_2 film deposited at 100 mV/s, 20 cycle in 0.1 M Et_4NBF_4/ACN solution and EIS measurements were performed in 0.1 M Et_4NBF_4/ACN solution

Table A 1: Potential dependence of the parameters calculated from the Model 2 which is given Figure 3.22. at 0.4 V DC potential (different molarities of ProDOT-Me_2 monomer deposited by electrochemically at 100 mV/s, 20cycle in 0.1 M Bu_4NPF_6/ACN solution)

	2mM	5mM	10mM	15mM
R_s / Ohm	1481	1852	455.8	1178
C_{dl} / F	$2.263x10^{-5}$	$1.026x10^{-4}$	$3.496x10^{-4}$	$7.865x10^{-5}$
R_1 / Ohm	649.1	47170	48.59	2752
Q / Y_o/ S s^{-n}	$7.254x10^{-6}$	$4.824x10^{-5}$	$3.321x10^{-4}$	$6.449x10^{-5}$
n	0.9101	0.9664	0.9729	0.9602
R_2 / Ohm	721400	631800	156100	705300
W / Y_o/ S s^{-n}	$8.64x10^{-7}$	$5.434x10^{-6}$	$1.782x10^{-5}$	$5.033x10^{-6}$
Chi Squared	$8.83x10^{-5}$	$4.14x10^{-5}$	$5.10x10^{-5}$	$3.75x10^{-5}$

Table A 2: Dependence of the parameters calculated for PProDOT-Me_2 film deposited at 100 mV/s, 20 cycle from different electrolyte in ACN solution containing 5 mM ProDOT-$(Me)_2$.

	Bu_4NPF_6	Et_4NPF_6	Et_4NBF_4	Bu_4NBF_4
R_s / Ohm	1852	856.3	858	350.6
C_{dl} / F	$1.026x10^{-4}$	$5.59x10^{-5}$	$2.962x10^{-5}$	$1.208x10^{-4}$
R_1 / Ohm	47170	713.5	110.1	155
Q / Y_o/ S s^{-n}	$4.824x10^{-5}$	$7.783x10^{-5}$	$3.168x10^{-5}$	$7.032x10^{-5}$
n	0.9664	0.9666	0.9594	0.9386
R_2 / Ohm	631800	1.473E6	6.238E6	432400
W / Y_o/ S s^{-n}	$5.434x10^{-6}$	$3.176x10^{-6}$	$1.578x10^{-6}$	$3.68x10^{-4}$
Chi Squared	$4.14x10^{-5}$	$9.86x10^{-5}$	$4.98x10^{-5}$	$8.47x10^{-5}$

Table A 3: Dependence of the parameters calculated for PProDOT-Me_2 film (deposited at 100 mV/s, 20 cycle in 0.1 M Bu_4NPF_6/ACN solution) from different solvent containing 5 mM ProDOT-$(Me)_2$.

	ACN	PC	DMF
R_s / Ohm	1852	1211	679.8
C_{dl} / F	$1.026x10^{-4}$	$6.105x10^{-5}$	$5.772x10^{-5}$
R_1 / Ohm	47170	71.59	89.62
Q / Y_o/ S s^{-n}	$4.824x10^{-5}$	$1.276x10^{-4}$	$6.934x10^{-5}$
n	0.9664	0.9753	0.9666
R_2 / Ohm	631800	$1.111x10^{6}$	$1.344x10^{6}$
W / Y_o/ S s^{-n}	$5.434x10^{-6}$	$6.282x10^{-6}$	$6.037x10^{-6}$
Chi Squared	$4.14x10^{-5}$	$6.13x10^{-5}$	$3.40x10^{-5}$

Table A 4: Dependence of the parameters calculated for PProDOT-Me_2 film (deposited at 100 mV/s, 20 cycle in 0.1 M Et_4NPF_6/ACN solution) from different solvent containing 5 mM ProDOT-$(Me)_2$. (0.4V DC potential)

	ACN	PC	DMF
R_s / Ohm	856.3	1140	782.5
C_{dl} / F	$5.59x10^{-5}$	$5.561x10^{-5}$	$2.088x10^{-5}$
R_1 / Ohm	713.5	255	1990
Q / Y_o/ S s^{-n}	$7.783x10^{-5}$	$8.901x10^{-5}$	$1.871x10^{-5}$
n	0.9666	0.9637	0.9315
R_2 / Ohm	$1.473x10^{6}$	$3.019x10^{6}$	$1.516x10^{6}$
W / Y_o/ S s^{-n}	$3.176x10^{-6}$	$1.03x10^{-5}$	$7.882x10^{-6}$
Chi Squared	$9.86x10^{-5}$	$5.91x10^{-5}$	$1.33x10^{-4}$

Table A 5: Dependence of the parameters calculated for PProDOT-Me_2 film (deposited at 100mV/s, 20 cycle in 0.1 M Et_4NBF_4/ACN solution) from different solvent containing 5 mM ProDOT-$(Me)_2$. (0.4V DC potential)

	ACN	PC	DMF
R_s / Ohm	858	859	1052
C_{dl} / F	$2.962x10^{-5}$	$2.55x10^{-5}$	$8.836x10^{-5}$
R_1 / Ohm	110.1	117.9	5102
Q / Y_o/ S s^{-n}	$3.168x10^{-5}$	$2.546x10^{-5}$	$7.418x10^{-5}$
n	0.9594	0.9614	0.9523
R_2 / Ohm	$6.238x10^{6}$	$1.479x10^{7}$	862400
W / Y_o/ S s^{-n}	$1.578x10^{-6}$	$1.24x10^{-7}$	$1.348x10^{-5}$
Chi Squared	$4.98x10^{-5}$	$3.80x10^{-5}$	$2.33x10^{-5}$

Table A 6: Dependence of the parameters calculated for PProDOT-Me_2 film (deposited at 100mV/s, 20 cycle in 0.1 M Bu_4NBF4/ACN solution) from different solvent containing 5 mM ProDOT-$(Me)_2$. (0.4V DC potential)

	ACN	PC	DMF
R_s / Ohm	350.6	1022	813.4
C_{dl} / F	$1.208x10^{-4}$	$1.215x10^{-5}$	$7.825x10^{-6}$
R_1 / Ohm	155	992.5	114.5
Q / Y_o/ S s^{-n}	$7.032x10^{-5}$	$3.005x10^{-5}$	$2.899x10^{-5}$
n	0.9386	0.8	0.9704
R_2 / Ohm	432400	$2.795x10^{6}$	$1.336x10^{8}$
W / Y_o/ S s^{-n}	$3.68x10^{-4}$	$1.098x10^{-6}$	$5.434x10^{-6}$
Chi Squared	$8.47x10^{-5}$	$7.15x10^{-5}$	$1.25x10^{-4}$

Table A 7: Dependence of the parameters calculated for PProDOT-Me_2 film (deposited at 100 mV/s, 20 cycle in 0.1 M Bu_4NPF_6/ACN solution containing 5 mM ProDOT-$(Me)_2$)(0.4V DC potential). EIS masurements were performed in 0.1 M Bu_4 NPF_6/PC

	E=0.2V	E=0.4V	E=0.7V	E=1.0V	E=1.3V
R_s / Ohm	1220	1211	1203	1208	1242
C_{dl} / F	$3.905x10^{-5}$	$6.105x10^{-5}$	$4.976x10^{-5}$	$3.876x10^{-5}$	0.00364
R_1 / Ohm	60.1	71.59	72.07	63.85	69.86
Q / Y_o/ S s^{-n}	$1.365x10^{-4}$	$1.276x10^{-4}$	$8.926x10^{-5}$	$8.007x10^{-5}$	$6.197x10^{-5}$
n	0.9761	0.9753	0.9773	0.9747	0.9771
R_2 / Ohm	$2.5x10^{6}$	$1.111x10^{6}$	653300	840800	184100
W / Y_o/ S s^{-n}	$1.434x10^{-6}$	$6.282x10^{-6}$	$1.139x10^{-5}$	$3.145x10^{-6}$	$5.898x10^{9}$
Chi Squared	$4.603x10^{-5}$	$6.130x10^{-5}$	$6.172x1^{-5}$	$4.281x10^{-5}$	$5.169x10^{-4}$

Table A 8: Dependence of the parameters calculated for PProDOT-Me_2 film (deposited at 100 mV/s, 20 cycle in 0.1 M Bu_4NPF_6/ACN solution containing 5 mM ProDOT-$(Me)_2$)(0.4V DC potential). EIS masurements were performed in 0.1 M Bu_4NPF_6/DMF

	E=0.2V	E=0.4V	E=0.7V	E=1.0V	E=1.3V
R_s / Ohm	685.8	679.8	681.3	683.2	718.9
C_{dl} / F	$2.624x10^{-5}$	$5.772x10^{-5}$	$4.993x10^{-5}$	$3.731x10^{-5}$	$3.286x10^{-7}$
R_1 / Ohm	87.79	89.62	894.1	73.69	2157
Q / Y_o/ S s^{-n}	$2.636x10^{-5}$	$6.934x10^{-5}$	$5.885x10^{-5}$	$4.95x10^{-5}$	$4.691x10^{-5}$
n	0.9624	0.9666	0.8	0.9695	0.8453
R_2 / Ohm	627100	1.344E6	904300	524500	49870
W / Y_o/ S s^{-n}	$8.736x10^{-7}$	$6.037x10^{-6}$	$5.428x10^{-6}$	$1.192x10^{-4}$	$7.051x10^{12}$
Chi Squared	$8.91x10^{-5}$	$3.40x10^{-5}$	$4.46x10^{-5}$	$6.78x10^{-5}$	$1.15x10^{-4}$

Table A 9: Dependence of the Parameters Calculated for PProDOT-Me_2 Film (deposited at 100mV/s, 20 cycle in 0.1 M Et_4NPF_6/ACN solution containing 5 mM ProDOT-$(Me)_2$)(0.4V DC potential). EIS masurements were performed in the same solution.

	E=0.2V	E=0.4V	E=0.7V	E=1.0V	E=1.3V
R_s / Ohm	865.8	856.3	884	882.5	890.4
C_{dl} / F	$3.354x10^{-5}$	$5.59x10^{-5}$	$5.06x10^{-5}$	$4.307x10^{-5}$	$3.765x10^{-5}$
R_1 / Ohm	790.1	713.5	735	705.3	725.5
Q / Y_o/ S s^{-n}	$4.375x10^{-5}$	$7.783x10^{-5}$	$6.993x10^{-5}$	$6.057x10^{-5}$	$5.497x10^{-5}$
n	0.9566	0.9666	0.9746	0.9683	0.9666
R_2 / Ohm	$9.143x10^{6}$	$1.473x10^{6}$	$1.989x10^{7}$	$1.46x10^{6}$	$1.236x10^{6}$
W / Y_o/ S s^{-n}	$9.178x10^{-7}$	$3.176x10^{-6}$	$1.628x10^{-6}$	$4.954x10^{-6}$	$3.727x10^{-6}$
Chi Squared	$9.29x10^{-5}$	$9.87x10^{-5}$	$1.05x10^{-5}$	$8.50x10^{-5}$	$1.13x10^{-4}$

Table A 10: Dependence of the parameters calculated for PProDOT-Me_2 film (deposited at 100 mV/s, 20 cycle in 0.1 M Et_4NBF_4/ACN solution containing 5 mM ProDOT-$(Me)_2$) (0.4V DC potential). EIS masurements were performed in the same solution.

	E=0.2V	E=0.4V	E=0.7V	E=1.0V	E=1.3V
R_s / Ohm	865.2	858	859.5	866.2	875.5
C_{dl} / F	$2.11x10^{-5}$	$2.96x10^{-5}$	$2.54x10^{-5}$	$2.09x10^{-5}$	$1.80x10^{-5}$
R_1 / Ohm	167.4	110.1	109.1	109.9	116
Q / Y_o/ S s^{-n}	$1.53x10^{-5}$	$3.17x10^{-5}$	$2.52x10^{-5}$	$1.97x10^{-5}$	$1.68x10^{-5}$
n	0.9585	0.9594	0.9722	0.9715	0.9638
R_2 / Ohm	$6.89x10^{8}$	$6.24x10^{6}$	$1.16x10^{6}$	$3.16x10^{6}$	$3.54x10^{6}$
W / Y_o/ S s^{-n}	1157	$1.58x10^{-6}$	$8.46x10^{-7}$	$1.30x10^{-6}$	$1.96x10^{-6}$
Chi Squared	$4.66x10^{-5}$	$4.98x10^{-5}$	$5.66x10^{-5}$	$7.05x10^{-5}$	$1.19x10^{-4}$

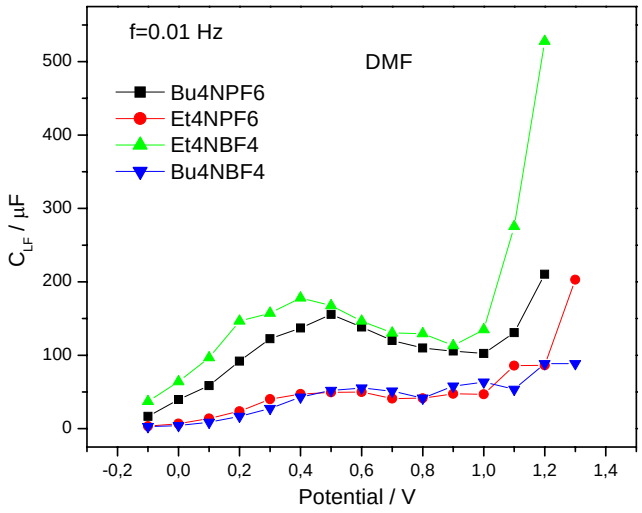

Figure B 18: Variation of low frequency capacitance of the PProDOT-Me_2 film in 10 mHz deposited electrochemically 5mM ProDOT-Me_2 monomer at 100 mV/s, 20 cycle in Bu_4NPF_6/ACN, Et_4NPF_6/ACN, Bu_4NBF_4/ACN, Et_4NBF_4/ACN solutions EIS measurements were performed Bu_4NPF_6/DMF, Et_4NPF_6/DMF, Bu_4NBF_4/DMF, Et_4NBF_4/DMF

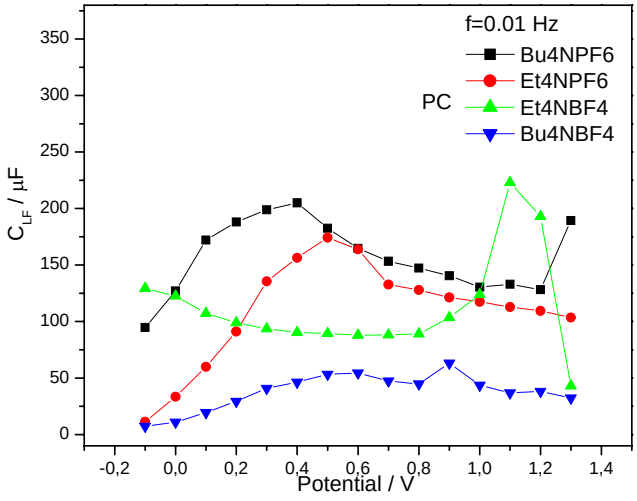

Figure B 19: Variation of low frequency capacitance of the PProDOT-Me_2 film in 10 mHz deposited electrochemically 5mM ProDOT-Me_2 monomer at 100 mV/s, 20 cycle in Bu_4NPF_6/ACN, Et_4NPF_6/ACN, Bu_4NBF_4/ACN, Et_4NBF_4/ACN solutions EIS measurements were performed Bu_4NPF_6/PC, Et_4NPF_6/PC, Bu_4NBF_4/PC, Et_4NBF_4/PC

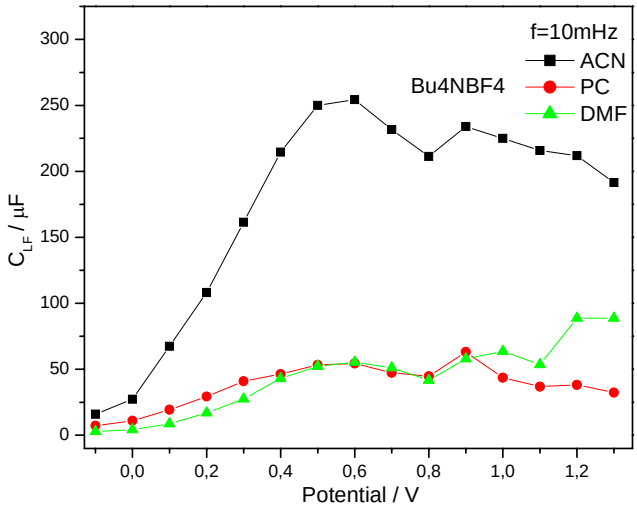

Figure B 20: Variation of low frequency capacitance of the PProDOT-Me_2 film in 10 mHz deposited electrochemically 5mM ProDOT-Me_2 monomer at 100 mV/s, 20 cycle in 0.1 M Bu_4NBF_4/ACN. EIS measurements were performed in 0.1 M Bu_4NBF_4 in different solvent

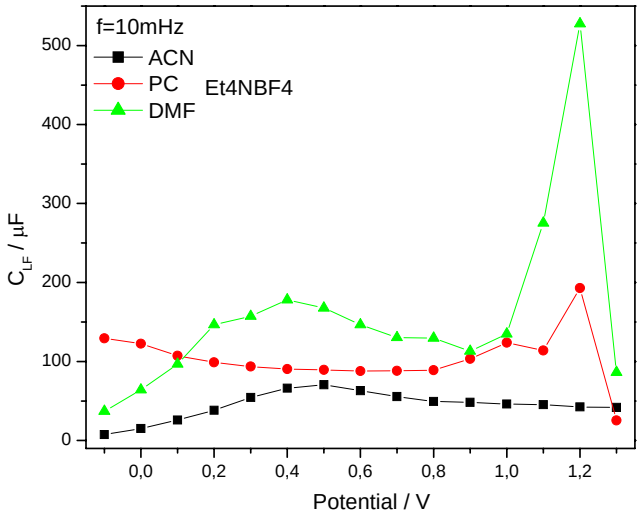

Figure B 21: Variation of low frequency capacitance of the PProDOT-Me_2 film in 10 mHz deposited electrochemically 5mM ProDOT-Me_2 monomer at 100 mV/s, 20 cycle in 0.1 M Et_4NBF_4/ACN. EIS measurements were performed in 0.1 M Bu_4NBF_4 in different solvent

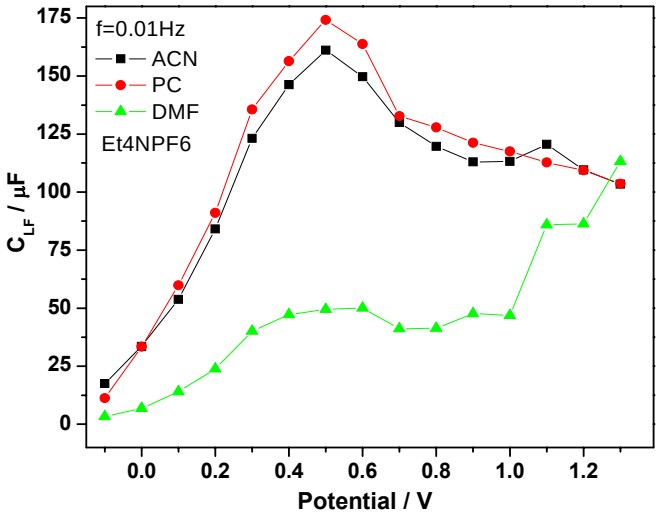

Figure B 22: Variation of low frequency capacitance of the PProDOT-Me_2 film in 10 mHz deposited electrochemically 5mM ProDOT-Me_2 monomer at 100 mV/s, 20 cycle in 0.1 M Et_4NPF_6/ACN. EIS measurements were performed in 0.1 M Bu_4NBF_4 in different solvent

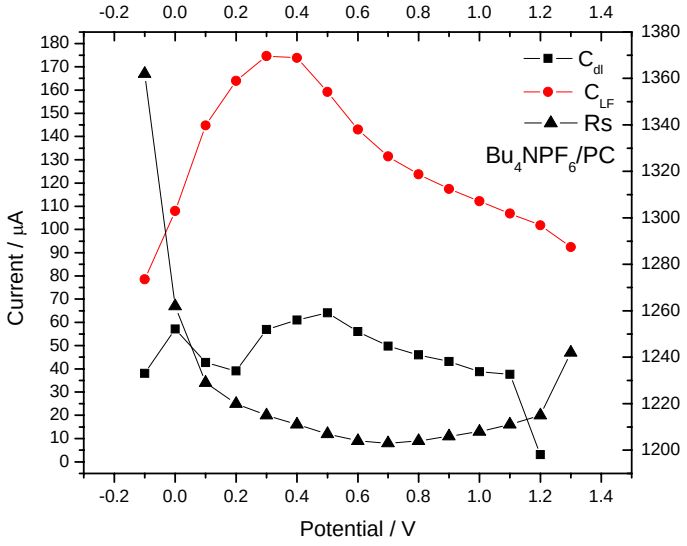

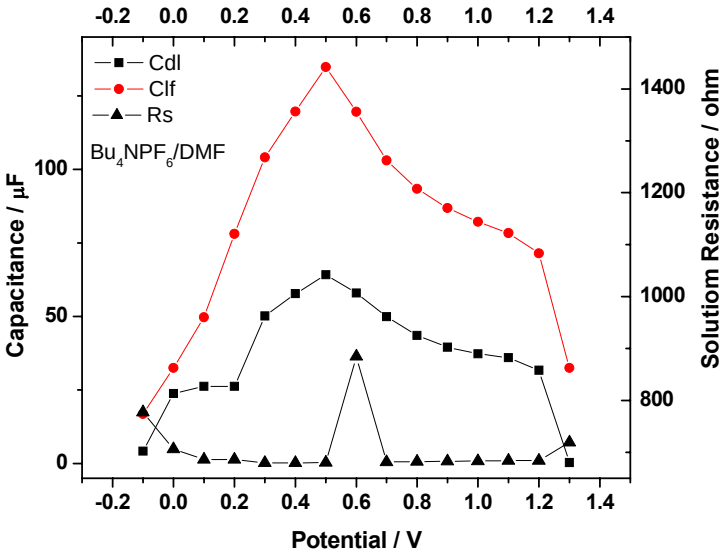

Figure B 23: Variation of the solution resistance, double layer capacitance and low frequency capacitance of the PProDOT-Me_2 film deposited electrochemically 5mM ProDOT-Me_2 monomer at 100 mV/s, 20 cycles in 0.1 M Bu_4NPF_6/ACN solution. EIS measurements were performed **a)** 0.1 M Bu_4NPF_6/PC **b)** 0.1 M Bu_4NPF_6/DMF solution

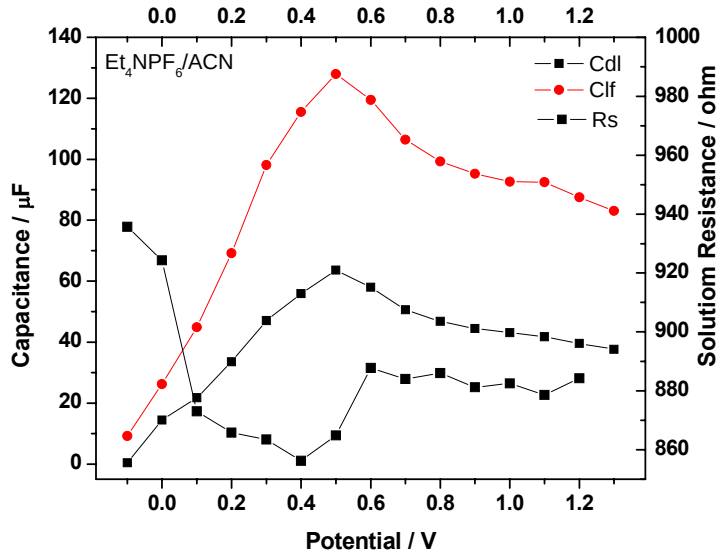

Figure B 24: Variation of the solution resistance, double layer capacitance and low frequency capacitance of the PProDOT-Me_2 film deposited electrochemically 5mM ProDOT-Me_2 monomer at 100 mV/s, 20 cycles in 0.1 M Et_4NPF_6/ACN solution. EIS measurements were performed the same solution

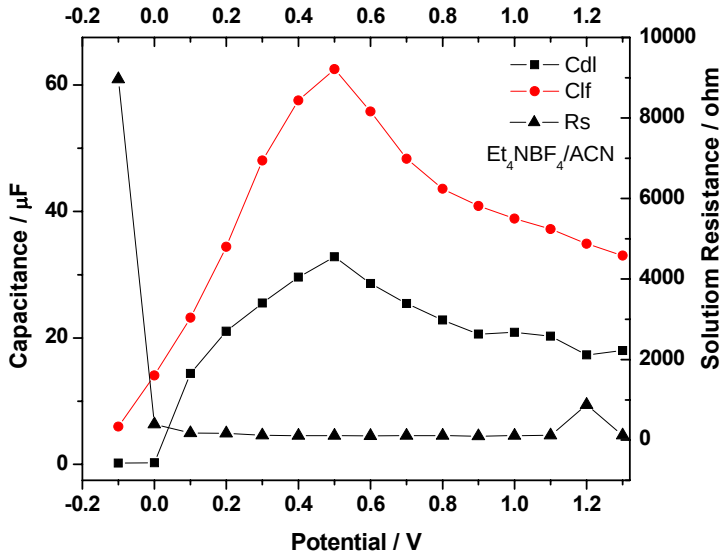

Figure B 25: Variation of the solution resistance, double layer capacitance and low frequency capacitance of the PProDOT-Me_2 film deposited electrochemically 5mM ProDOT-Me_2 monomer at 100 mV/s, 20 cycles in 0.1 M Et_4NBF_4/ACN solution. EIS measurements were performed the same solution

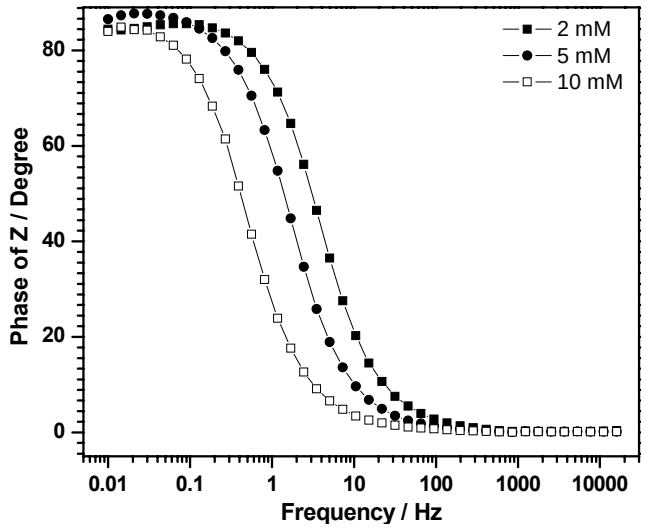

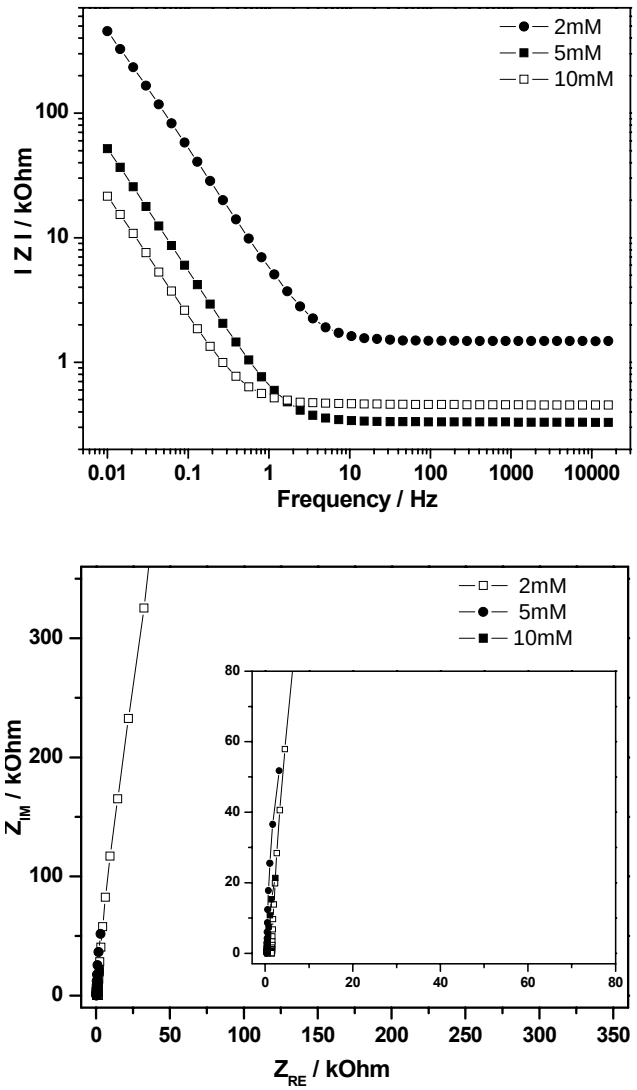

Figure B 26: a) Bode phase angle **b)** Bode magnitude of Z **c)** Nyquist plot of ProDOT-Me_2 film deposited 2 mM, 5mM, 10 mM monomer at 100 mV/s, 30 cycle

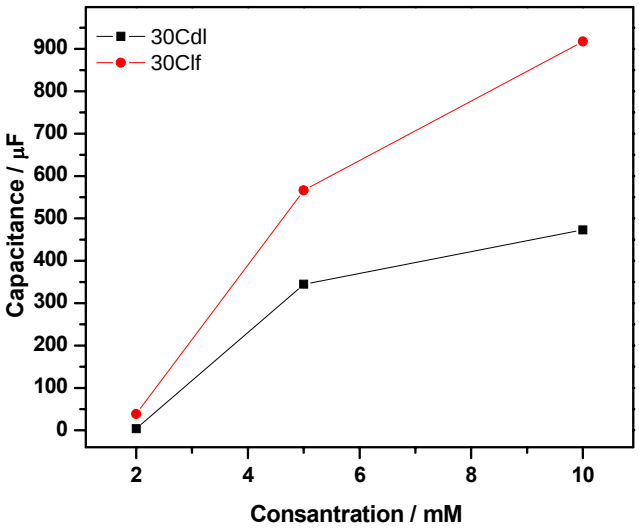

Figure B 27: Variation of capacitance and concentration value of ProDOT-Me_2 film deposited 2 mM, 5mM, 10 mM monomer at 100 mV/s, 30 cycle

BIOGRAPHY

Aslı Gençtürk was born in Tekirdağ in 1981. After finishing primary, secondary and high school in Tekirdağ, she obtained her B.Sc. in Chemistry from Anadolu University in Eskişehir in 2004.

She started her M.Sc. in Polymer Science and Technology at İstanbul Technical University in 2004.